AGGREGATION IN THE SCHELLING MODEL AND INVERTED BIOMASS PYRAMIDS IN ECOSYSTEMS

A Thesis
Presented to
The Academic Faculty

by

Abhinav Singh

In Partial Fulfillment
of the Requirements for the Degree
Doctor of Philosophy in the
School of Physics

Georgia Institute of Technology
Aug 2009

AGGREGATION IN THE SCHELLING MODEL AND INVERTED BIOMASS PYRAMIDS IN ECOSYSTEMS

Approved by:

Professor Howard Weiss,
Committee Chair
School of Mathematics
Georgia Institute of Technology

Professor Predrag Cvitanović
School of Physics
Georgia Institute of Technology

Professor Daniel Goldman
School of Physics
Georgia Institute of Technology

Professor Michael Schatz
School of Physics
Georgia Institute of Technology

Professor Kurt Wiesenfeld
School of Physics
Georgia Institute of Technology

Date Approved: 30 April 2009

To Ram Swarath Singh,

for starting it all.

ACKNOWLEDGEMENTS

I would like to acknowledge the direct and indirect influence of many individuals on this dissertation. The most influential individual was of course my advisor, Prof. Howie Weiss who supported my wanderings. I will always be grateful for his constant support and his encouragement. I can see the influence of my coauthors Dmitri, Hao and Wendy all over this dissertation.

I learnt much from the faculty and students at the fifth floor, some through direct instruction but mostly by example; Predrag with his ready smile and strong sense of humor, Kurt with his calmness and Domenico with his spirited aversion to 'biostuff'. Yamato was my friend, teacher and confessional all in one and I owe him many thanks. Matija Crne and I went on many anthropological adventures, we learnt a lot and drank a little. Mysore, Sagar, Hari, Vivek and Malavika supported this dissertation by talking, listening and most importantly feeding me. Malavika also taught me the tricky art of 'bunnugiri'. My mom made sure that I did not turn out a bum and I am thankful for that. The rest of the family tried to make sense of my research, gave up, but still thought that I was doing something interesting. Kevin, Felicia, Sharon, Lori, Samantha, Judy and the other wonderful staff at Tech went out of their way to help me. Thank you all.

TABLE OF CONTENTS

LIST OF TABLES

LIST OF FIGURES

SUMMARY

When do integrated cities segregate spontaneously and how do we measure segregation? When do inverted biomass pyramids occur in ecosystems and what effect do refuges have on biomass pyramids? We study these questions in this dissertation.

Thomas Schelling proposed a simple spatial model to illustrate how, even with relatively mild assumptions on each individual's nearest neighbor preferences, an integrated city would likely unravel to a segregated city, even if all individuals prefer integration. This agent based lattice model has become quite influential amongst social scientists, demographers, and economists. Aggregation relates to individuals coming together to form groups and Schelling equated global aggregation with segregation. Many authors assumed that the segregation which Schelling observed in simulations on very small cities persists for larger, realistic size cities. We describe how different measures can be used to quantify the segregation and unlock its dependence on city size, disparate neighbor comfortability threshold, and population density. We develop highly efficient simulation algorithms and quantify aggregation in large cities based on thousands of trials. We identify distinct scales of global aggregation. In particular, we show that for the values of disparate neighbor comfortability threshold used by Schelling, the striking global aggregation Schelling observed is strictly a small city phenomenon. We also discover several scaling laws for the aggregation measures. Along the way we prove that in the Schelling model, in the process of evolution, the total perimeter of the interface between the different agents always decreases, which provides a useful analytical tool to study the evolution. We extend our analysis to cities where one category of agents is in a minority. Overall, we find that agents in a minority have fewer opportunities to move to locations where they can be happy

and this leads to a rise in the number of isolated unhappy agents, although in special circumstances we observe the formation of compact segregated minority clusters.

Coral reefs around the world have experienced a dramatic decline during the past 25 years. Overfishing is believed to play a major role. There is significant interest in stabilizing and restoring damaged reefs, and first steps include understanding the functioning of reefs in their natural state and examining the effects of fishing.

The isolated Kingman and Palmyra reefs are believed to provide a baseline for the natural state of coral reefs. At Kingman, it was recently discovered that apex predators constitute 85% of the total fish biomass. This is in sharp contrast to most reefs, where the prey biomass substantially dominates the total fish biomass. The recent study at the two pristine reefs also indicates that the predator:prey fish biomass ratio is an increasing function of reef cover.

Based on these field observations, we model the fish biomass structure at a pristine coral reef. We introduce a new refuge based mechanism for predator-prey interaction with an explicit dependence on refuge size. Since the prey hide from predators in the coral, predators do not have access to all the prey and interactions between predators and prey are rare. Therefore, the fundamental assumption of Lotka-Volterra model that predators and prey are well-mixed does not approximate the situation at Kingman. Our refuge based model does not assume mass action interaction between predators and prey and may provide a new mechanism in ecology to produce inverted biomass pyramids. Our model yields both the inverted biomass pyramid and the increasing dependence of the predator:prey biomass ratio on reef cover.

We add various forms of fishing to our model, and show that sufficiently high fishing pressure with quite general types of fishing transforms the inverted biomass pyramid to be bottom heavy. We also show that prey fishing alone has the same effect.

Refuges protect prey from predators and diminish the food supply of predators

in coral reefs, but affect the feeding habits of predators in other ecosystems in more complex ways. Current models in the ecological literature incorporate the role of refuges in an ad-hoc manner and are not rooted in the refuge mediated behavior of predators and prey. Based on evidence from previous field studies, we generalize the classical predator-prey models to incorporate three possible effects of refuges on the feeding habits of predators. We show that refuges can facilitate inverted biomass pyramids but can also discourage them. We also show that immigrating prey unequivocally support the existence of inverted biomass pyramids.

CHAPTER I

SCHELLING MODEL

1.1 Introduction

Thomas Schelling developed an influential space-time model which demonstrated that cities can self-segregate even when individuals have no segregationist tendencies [70, 72, 71, 73]. He famously discovered this phenomenon by setting up an 8 by 8 checkerboard as a city, pennies and nickels as the two types of residents of the city and used a very simple rule to determine the movement of a resident. We shall hereby refer to the residents of a city as 'agents'. The rule states that an agent will be considered 'happy' if it is surrounded by a minimum number of agent of its own type, e.g., a nickel would like to be surrounded by at least 3 other nickels. If an agent is not happy in its current location it will move to another location where it can be happy.

Schelling tracked the evolution of these 'cities' by physically setting up a checkerboard and moving pennies and nickels by hand. We can do better because we have powerful computers. He saw that integrated cities quickly became massively segregated. Scientists accepted that massive segregation would occur in a city subject to these simple rules. We show that he was *incorrect*. As an example, consider Figure 1.1. Figure 1.1a shows a typical result from Schelling's simulation of a city of size 8×8. Figure 1.1b shows the result of a city of size 100×100. It is visually obvious that the 8×8 city is massively segregated while the 100×100 city is not.

Currently, there is a spirited discussion in the sociological literature on the validity of Schelling-type models to describe actual segregation, with arguments both for (e.g., [85, 24]), and against (e.g., [49, 46]), and a few authors used and extended the

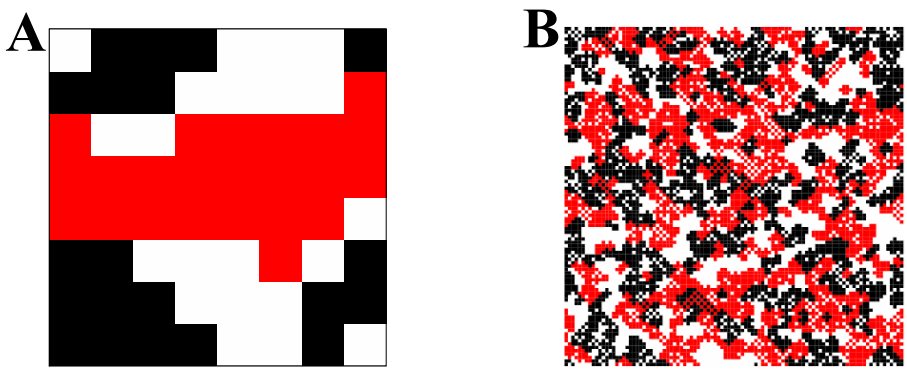

Figure 1.1: **A**: A simulation of Schelling's original model with $N = 8$; **B**: Our simulation with $N = 100$.

Schelling model to address actual population data [11, 5, 3, 67, 12]. Although, a qualitative analysis of the Schelling model based on visual inspection is important and intuitively appealing, we also need to quantitatively analyze the Schelling model. Few examples of quantitative analyses of such models [63], [24], and [28] exist in the current literature and a comprehensive quantitative analysis of the Schelling model is missing.

We quantitatively analyze the Schelling model by first breaking down the visual phenomenon of aggregation into a number of objective aggregation indices. We then develop efficient algorithms that enable us to speedily simulate the Schelling model thousands of times in a short period of time. We finally use our aggregation indices to characterize the final states of the Schelling model. There are an equal number of the two types of agents (pennies and nickels) in the classical Schelling model. In Chapter 2, I extend this analysis to a city where nickels are in a minority.

1.2 Schelling Model

We formalize the description of the Schelling model by considering it as a discrete spatially extended dynamical system. Therefore, there are two aspects to the description of the model. First, we specify the initial condition of the system. This corresponds

to specifying the initial distribution of agents in a city. Second, we specify the rule for the evolution of the dynamical system. This means specifying the rule by which individuals move from one location to another.

Consider a square which is divided into $N \times N$ squares forming a lattice with periodic boundary conditions. Each square is either occupied by an agent or empty. We label the two types of agents as R and B. Before we specify initial condition of the system and the rule for the movement of an agent we need to define two technical terms:-

- **Neighborhood**. We introduce the notion of the neighborhood of an agent. Consider an agent located at (i, j). Its neighborhood is given by the locations $\bigcup_{k=-1}^{k=1} \bigcup_{l=-1}^{l=1} (i+k, j+l)/(i, j)$ which we can visualize as the square surrounding the agent. The neighborhood consists of 8 locations all of which may not be occupied by agents and is known as the Moore neighborhood in the literature. Figure 1.2 illustrates the concept of the neighborhood. Consider the R agent at the center of the 7×7 city. Its neighborhood consists of 2 R agents, 2 empty locations and 4 B agents.

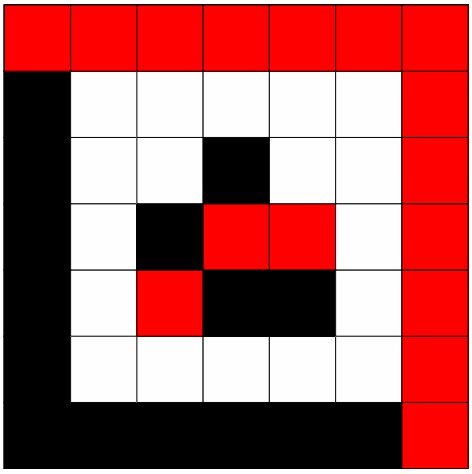

Figure 1.2: 8-point Moore neighborhood.

- **Happiness**. Each agent is characterized by its 'happiness'. This characteristic is binary in nature; it has two numerical values 0 and 1 which we shall hereby refer to as unhappy and happy respectively. The happiness of the agent is determined by its neighbors. Each agent is happy if and only if it is surrounded by a minimum number of neighbors of its own type. This minimum number is called the neighbor comfort threshold T. If an agent is unhappy it moves to an empty location where it will be happy. The neighbor comfort threshold can range from 0 to 8, but for the purpose of our simulations, we restrict T to be in the range of 3-5.

1.2.1 Initial configuration

We represent the Schelling city as a matrix. Each location in the city is represented by the co-ordinates (i, j) and each agent in the city is denoted the variable $x(i, j)$. An R agent is represented by 1, a B agent by -1 and an empty location is denoted by 0.

We specify the initial configuration of the Schelling model by the following variables.

- *Size of the city.* The city is modeled as an $N \times N$ lattice with periodic boundary conditions. This means that $x(i, j) = x(i \ mod \ N, j \ mod \ N)$.

- *Vacancy ratio v.* The vacancy ratio v is the fraction of locations in the city which are empty. The vacancy ratio v takes values from the set {v=0.02, 0.6, 0.10, 0.15, 0.20, 0.24, 0.28, 0.33}.

- *Relative concentration of R and B agents r.* The concentration of R agents can be a variable fraction of the total number of agents. The fraction is drawn from the set {r=0.5, 0.6, 0.7, 0.8, 0.9}.

- *Initial spatial distribution.*The agents are distributed in two possible ways. The

first method is called a 'checkerboard' configuration where R and B agents are found in alternating locations in the horizontal and vertical directions. The second method is to randomly distribute the agents within the the lattice.

- *Perturbations: Number and size.* Consider a square of given size anywhere within the lattice. Now shuffle the locations of the agents within this square. This constitutes a single perturbation. The size of the square within which we shuffle the location of the agents is the size of the perturbation. The notion of perturbations makes sense only if we choose to initially set up the city in a checkerboard configuration.

We first choose the size of the city and then decide if we want to set up the city as checkerboard or randomly distribute the agents. We then perturb the city and finally empty the appropriate number of locations in the city.

1.2.2 Evolution

The state of the system changes by repeatedly moving a single unhappy agent to a favorable location. We first randomly find an unhappy R agent. It then moves to a location where it shall be happy, which is again randomly chosen. We then repeat this procedure for an agent of type B. Together this constitutes a cycle. Our algorithm closely follows Schelling's original algorithm [70] and later used in [64, 3].

An exception is made for the case where the neighbor comfort threshold T has been set to 5. In this situation we allow unhappy R and B agents to switch locations if it makes both agents happy.

1.2.3 Halt

This is a computational aspect of the model. We need to specify a method for stopping the program. If an R agent cannot find a favorable location then we try to find a suitable location for an unhappy B agent and vice versa. This algorithm terminates

in one of the two conditions: there are no unhappy agents in the lattice or no unhappy agent can find a suitable location.

1.3 Schelling's segregation is a small city phenomenon

I briefly summarize how Schelling simulated his model. He filled a checkerboard with pennies and nickels on alternate locations. He then removed one-third of the pennies and nickels, thus creating a large number of empty locations [73]. According to his rule, a penny was 'happy' if it was surrounded by at least 3 other pennies in its neighborhood and similarly for nickels. If a penny was unhappy, it moved to a location where it could be happy. He then did the same for a nickel and then repeated the process. He stopped when there were no unhappy pennies or nickels or there were no locations where unhappy pennies and nickels could be happy. A typical final state of his checkerboard can be seen in Figure 1.1(a).

The size of Schelling's checkerboard was 8×8. One-third of the locations were empty. This turns out to be crucial to the segregation that Schelling observed. It is even more interesting to note that Schelling required pennies to be surrounded by 3 other pennies to be happy. What happens if pennies need 4 other pennies to be happy? What about 5? We answer these questions in the following sections. As it turns out, the minimum number of agents of similar type which an agent needs to be happy has a dramatic effect on aggregation patterns.

We investigate whether the global aggregation that Schelling observed for very small lattices persists for larger lattices. In Fig 1.1**B**, we present a characteristic final state for our simulations with city size $N = 100$. Comparing Figs 1.1**A** and 1.1**B**, one can see a striking qualitative difference between the two final states. While there is some local aggregation in the final state with $N = 100$, there is no global aggregation. By viewing the plots of this and other final states, one immediately sees that the global aggregation that Schelling observed is a small lattice phenomenon.

To quantify the difference in aggregation between a small city ($N = 8$) and a larger city ($N = 100$) we use a combination of two aggregation measures: the number of clusters in the final state of the model and the normalized average size of individual clusters. We determine the normalized average size of a cluster by dividing the average size of a cluster by the total number of agents in the city. The latter determines the proportion of a city covered by an individual cluster and provides a way to compare aggregation across cities of different sizes. Figure 1.3 shows the mean values of these two aggregation measures in the final states of cities of two sizes ($N = 8$ and 100). We compute the mean values of the two measures based on 100 trials for each choice of the vacancy ratio v and neighbor comfort threshold $T = 3$. We observe that the normalized average size of a cluster in the large city is smaller than one in a small city. This implies that an individual cluster in a large city covers a smaller proportion of the city as compared to a cluster in a smaller city. Most final states of the small city are segregated into two clusters for all choices of the vacancy ratio while the number of clusters in the large city increases from 22 for a city with 24% empty locations to 55 for a city with 33% empty locations. As we move from a small city to a large one, the relative size of a cluster in the final state decreases and the number of clusters increases. This shows that the large scale global aggregation observed by Schelling is strictly a small city phenomenon and does not occur for larger cities.

1.4 Measures of aggregation

The term 'segregation' denotes primarily a visual impression of the final state of the model such as in Figure 1.4.

Is the city in Figure 1.5(a) segregated? How about the city in Figure 1.5(b)? It seems that the city in Figure 1.5(a) is more segregated but can we go beyond the judgement of the eye?

One of our main tasks is to develop a set of aggregation indices which can put the

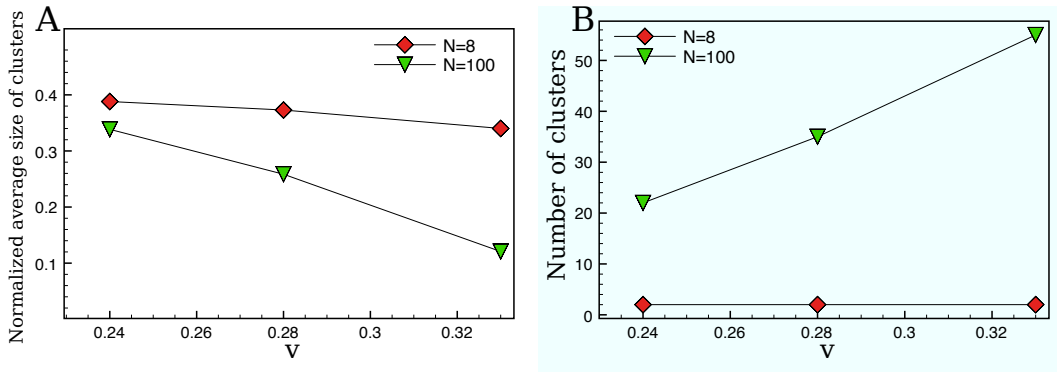

Figure 1.3: Aggregation measures to distinguish between a small city ($N = 8$) and a large city ($N = 100$) for constant neighbor comfort threshold $T = 3$ and different values of vacancy ratio v. **A**: Normalized average size of an individual cluster. **B**: Number of clusters in the final state of a city.

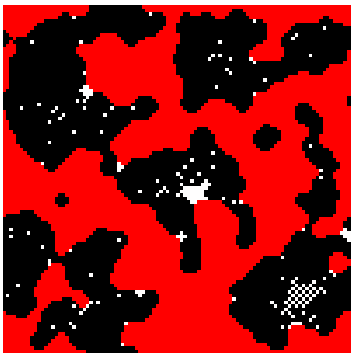

Figure 1.4: Segregation in the Schelling Model.

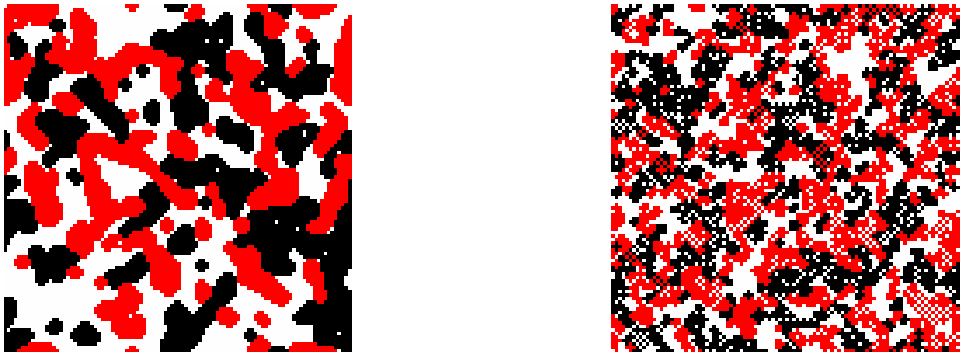

(a) (b)

Figure 1.5: Two cities.

idea of segregation on a firm, objective setting. This has been a subject of intense study by sociologists and demographers over the years. The notion of aggregation can be broken down into a number of different ideas which are known in the literature as evenness, exposure, centrality, concentration and clustering [22, 50, 51]. We shall focus on the notions of exposure and clustering as they are most suited to the present model. Exposure relates to the degree of contact between agents of different kinds and clustering relates to the degree of contiguity among agents of one kind.

1.4.1 Clustering

A cluster is defined as the set of locations which can be traversed by a set of steps where one meets only agents of one type. A step is a movement from any location in the lattice to a location in its '8-point neighborhood'. There are three aspects to the description of clusters in a city: the number of clusters, size of the clusters, and the scale of the clusters. No single property is sufficient by itself to provide a complete description of clustering in a city, but we can gain a comprehensive understanding of clustering by considering them in tandem.

1.4.1.1 Number of clusters, N_c

Measuring the number of clusters is a powerful index of aggregation. Figure 1.6 shows the final states for two cities. City (a) is more segregated than city (b), the former has only five clusters while city (b) has many more. However, simply comparing the number of clusters can be misleading. The number of clusters N_c is a useful index of aggregation when the clusters in the city are compact, a property satisfied by both cities in Figure 1.6.

When the clusters are not compact, the number of clusters do not provide a good measure of aggregation. Consider Figure 1.7. The figure on the left is a typical final state for a city of size N=100, neighbor comfort threshold T=5 and vacancy ratio v=0.28 and the second is a final state for a city with N=100, T=4 and v=0.02. The

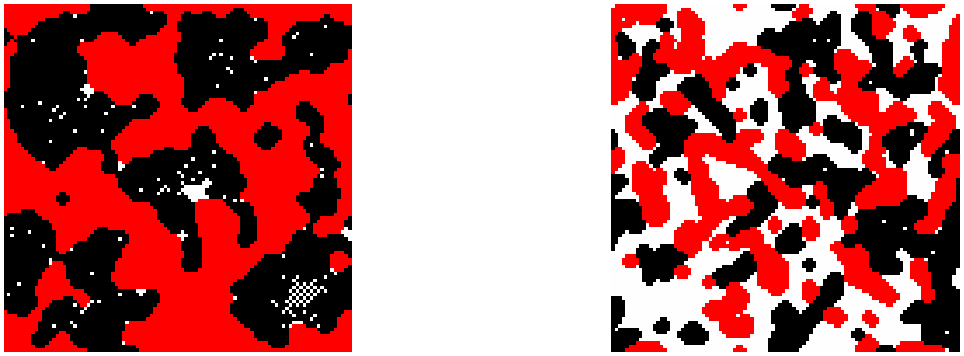

(a) (b)

Figure 1.6: (a) Final state for N=100, T=4, v=0.02 (b) Final state for N=100, T=4, v=0.33.

final state of the city in (a) contains far larger number of clusters than (b), because it contains a large number of 'singletons', isolated agents which cannot move to any other location where they can be happy.

(a) (b)

Figure 1.7: (a) Final state for N=100, T=5, v=0.28 (b) Final state for N=100, T=4, v=0.02.

1.4.1.2 Size of a cluster

The size of a cluster provides a natural measure of aggregation, but must be used with care. As an extreme example, compare the two situations in Figure 1.8. Figure 1.8(a)

shows a city in the state of a pristine checkerboard and (b) shows a final state with all R agents clustered in the form of a rectangle in the center of the lattice while all the other locations are occupied by B agents. In both situations, there is only one R and B cluster, but it is obvious that the city in (b) is maximally segregated while the city in (a) is maximally integrated.

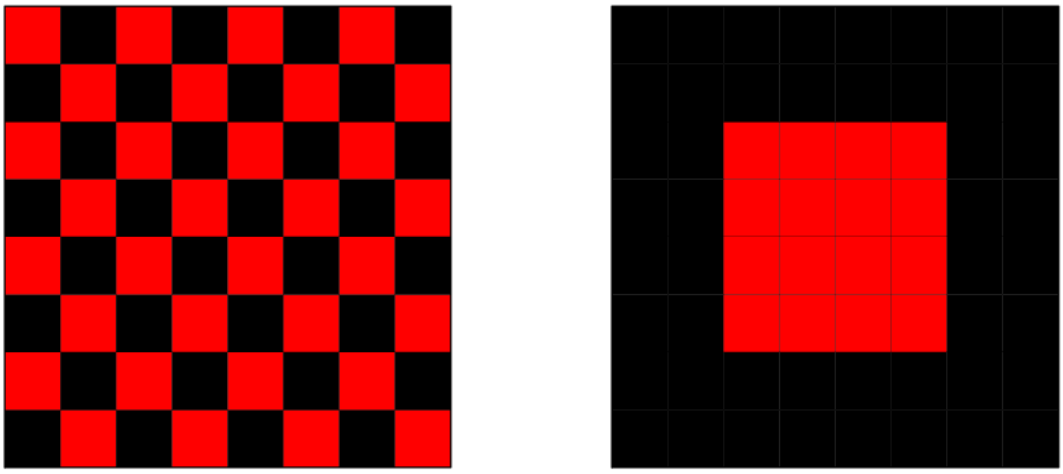

(a) (b)

Figure 1.8: (a) Checkerboard configuration (b) An example of extreme aggregation.

1.4.1.3 Maximum length of a cluster L

We also use the notion of the maximum length of a cluster denoted by the symbol L. The maximum length of a cluster is the length of a rectangle which can enclose a cluster. We assume here that the longer side of the rectangle represents the length of the rectangle.

Figure 1.9 illustrates the use of this index. The city consists of two clusters: one R cluster and one B cluster (note the periodic boundary conditions). A rectangle of size 3×5 can completely enclose the B cluster while we need a 4×6 rectangle to enclose the R cluster. Therefore, the maximum length of a cluster L is 6.

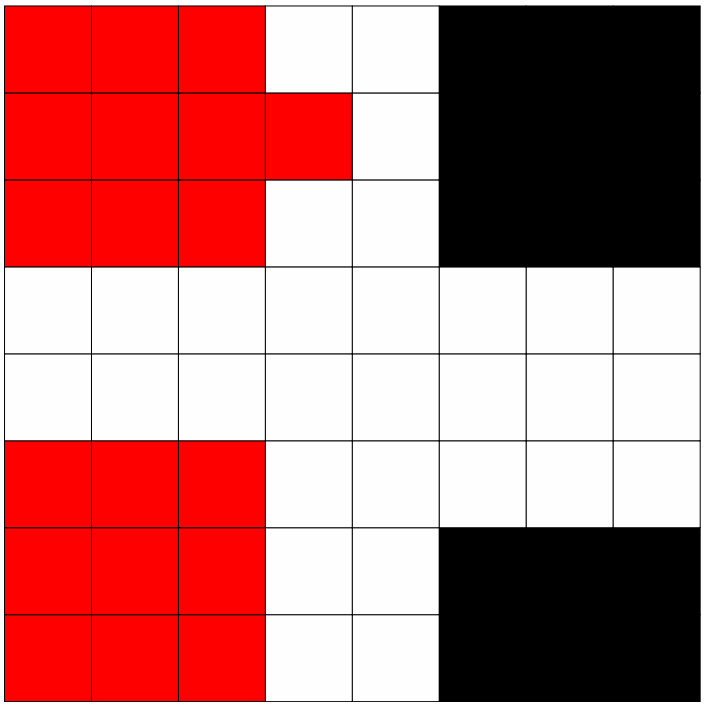

Figure 1.9: A hypothetical final state of a 8 x 8 city in an Schelling model. Note that there is only one R and one B cluster due to the periodic boundary conditions. The maximum length of a cluster L here is 6.

The maximum length L provides a measure of the **scale** of aggregation. The maximum length of a cluster L in the figure 1.9 is comparable to the size of the city (N=8), suggesting the aggregation occurs on a macroscale in this case. As with other indices, one must be careful, the scale of aggregation may occur on a macroscale but aggregation may still overall be less intense. Figure 1.8 is a good example of this phenomenon. The checkerboard is the least segregated configuration of the city but the maximum length of the cluster is 100 since it consists of only two clusters. The index L is useful when we refer to situations where the clusters are compact such as Figure 1.8(b). The exposure indices in the next section provide ways to estimate if the clusters are compact or sparse.

1.4.2 Exposure

An exposure index measures the interaction of an agent to dissimilar agents locally within its neighborhood. We use three exposure indices in this manuscript.

1.4.2.1 Agents completely surrounded by like neighbors

The number of agents which are completely surrounded by agents of the same type provides an indicator of the 'exposure' of agents. Figure 1.8 illustrates the use of this index. In Figure 1.8(a), each agent is surrounded by four agents of similar type and four agents of a different type; thus no agent is isolated. On the other hand, in Figure 1.8(b), all agents except ones on the interface of clusters are completely surrounded by eight agents of similar type. Thus they are completely isolated. A larger number of such agents denotes a more aggregated state. It also gives us an additional piece of information. It provides an indicator of the compactness of clusters. Consider Figure 1.10. Figure 1.10(a) shows a typical final state for a city with T=3, N=100 and v=0.33. We observe that the city is segregated, but the clusters are sparse and are not compact. This is reflected in the number of agents which are surrounded by eight similar neighbors; a mere 2% of the agents. Howevere in Figure 1.10(b),

40% of the agents are surrounded by eight similar neighbors, indicating a presence of compact clusters and greater aggregation.

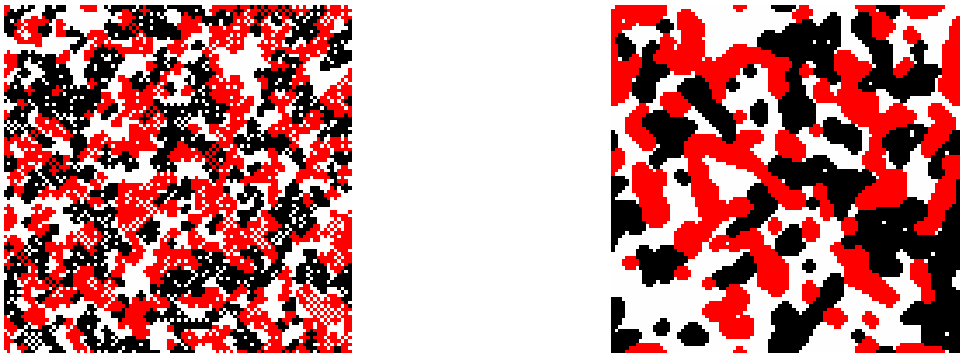

(a) (b)

Figure 1.10: (a) Final state for N=100, T=3, v=0.33 (b) Final state for N=100, T=4, v=0.33.

1.4.2.2 Unlike:like ratio u/l

A more nuanced exposure index is the average ratio of unlike to like neighbors surrounding each agent in the lattice. If an agent is completely surrounded by unlike neighbors, u/l is set to 8. In Figure 1.8(a), u/l would be 1, and in Figure 1.8(b) it would be closer to zero. A lower unlike:like ratio indicates a more aggregated final state. The average ratio of unlike to like neighbors is a useful index but does not provide a full picture. It hides a lot of information which is encoded in the variance and higher moments, thus must be used in conjunction with other indices to provide a complete picture.

1.4.2.3 Perimeter P

The perimeter P is a method of capturing the interface of clusters and is our most important index to measure exposure.

Consider the neighborhood of an agent located at (i, j). Measure the number of unlike neighbors and vacant locations in its neighborhood and denote them by $q(i, j)$

and $w(i,j)$ respectively. Let $S(i,j) = q(i,j) + w(i,j)/2$. This denotes a measure of the local boundary around an agent. The perimeter P is equal to the sum of the local boundaries of each agent ($P = \sum_{i,j}^{N} S(i,j)$) and provides a measure of the total interface. Demographically, the adjusted perimeter, $p = P/N^2$, is the average number of contacts an agent has with the opposite kind or with vacant sites and is closely connected to exposure indices in the sociological literature [50].

The perimeter P serves a dual function, it not only provides a useful index of estimating the exposure of agents but also serves as analytical tool to characterize the dynamics of the model. Since the Schelling model is a dynamical system with many degrees of freedom, there is no apriori reason to assume that it will not show periodic orbits, chaotic trajectories or other kinds of interesting dynamical behavior. We show that these possibilities do not occur and the system always reaches an equilibrium. We show that the perimeter $P = \sum_{i,j}^{N} S(i,j)$ forms a Lyapunov function for the system which decreases with each step in the evolution of the Schelling model.

Consider a legal switch for an R agent which moves from location 1 to 2. Let R_1, B_1, V_1 be the number of R agents, B agents and empty locations in the neighborhood of location 1. Correspondingly let R_2, B_2, V_2 be the number of R agents, B agents and empty locations in the neighborhood of location 2. Since this is a legal movement $R_2 > R_1$. Also consider that

$$R_1 + B_1 + V_1 = R_2 + B_2 + V_2 = 8.$$

The contribution of the R agent and its neighborhood to the Lyapunov function is given by

$$P_{initial} = 2B_1 + V_1 + B_2 + R_2$$

$$P_{final} = 2B_2 + V_2 + B_1 + R_1.$$

The change in the Lyapunov function is given by

$$\begin{aligned} P_{final} - P_{initial} &= B_2 + V_2 - R_2 - B_1 - V_1 + R_1 \\ &= 8 - 2R_2 - (8 - 2R_1) \\ &= 2(R_1 - R_2) < 0. \end{aligned}$$

Similarly, if there is a switch between R and B agents, we have

$$P_{final} - P_{initial} = 2\,(R_2 - R_1) + 2\,(B_1 - B_2) < 0.$$

Since P decreases by at least 2 on every switch and P cannot be negative, there can only be finitely many moves before the algorithm halts.

1.5 Simulations

We are the first to quantify aggregation in a large city based on a large number of simulations. We develop highly efficient algorithms to simulate the model and quantify the aggregation. We currently need approximately one minute to run a single simulation for a city of size $N = 100$ and we ran more then nine thousand simulations for this manuscript. We achieve this boost in speed by coming up with innovative ways to determine the happiness of each agent and to find a suitable location for an unhappy agent. We exploit the ability of modern software packages like Numpy [58] to efficiently manipulate matrices; we can now compute properties of all agents in a city simultaneously thus escaping the slow process of dealing with each agent individually. The speed at which we find an unhappy agent in the city and a suitable location for it determines the speed of the simulation. Naively looking at each agent in the city to determine if it is unhappy and testing each empty location to determine if it is a suitable location for an unhappy agent, makes the simulation much slower. A much more efficient approach is to construct matrices highlighting the unhappy agents in the city and suitable locations for unhappy agents. The unhappiness of an agent and the suitability of a location are both based on the number of similar neighbors in the

neighborhood of a given location. As an example of the efficiency gained by matrix methods, we outline the steps to determine the number of R agents surrounding each agent in the city simultaneously. In our 'city matrix', an R agent is represented by 1, a B agent by -1 and an empty location by 0. Therefore, the problem of determining the number of surrounding R agents reduces to adding up the 1's in the neighborhood of each agent and ignoring the -1's. We ignore the -1's by simply finding the absolute value of each element in the city matrix, this converts the -1's into 1's but leaves the 1's and 0's unchanged. We call this modified matrix as the 'absolute value matrix'. When we add the city matrix and the absolute value matrix, all the -1's are gone and the sum of all the elements gives the number of R agents in the 8-point neighborhood. Similar methods can be used to speed up the process of finding suitable locations for unhappy agents and computing aggregation measures. Refer to Appendix B for more details.

We ran the program 100 times for different choices of the size of the city N, neighbor comfort threshold T, vacancy ratio v, concentration of R agents and initial spatial distribution given below.

- N=50, 100, 200
- v={ 0.02, 0.06 ,0.10, 0.15, 0.20, 0.24, 0.28, 0.33 }
- T= {3,4,5}
- r = {0.5, 0.6, 0.7, 0.8, 0.9}
- Checkerboard settting

The large number of trials enable us to compute accurate statistics for the aggregation measures. The Central limit theorem provides confidence about the mean values of all the aggregation measures.

1.6 Aggregation

Before we commence a quantitative analysis, it is useful to have a look at some of the typical final states for the Schelling model as shown in Figures 1.12, 1.13 and 1.14. We will refer to these figures frequently as they help in developing an intuitive feel for the various indices of aggregation.

We also use the aggregation indices that we have developed to characterize the final states and these results are summarized in Figure 1.11. In the following subsections, we will study and interpret this figure in detail.

1.6.1 Dependence on vacancy ratio

1.6.1.1 $T = 3$: sparse clusters

Figure 1.12 shows the typical final states for a city of size $N = 100$, neighbor comfort threshold $T = 3$ and different choices of vacancy ratio v. In particular, Figure 1.12**H** shows the typical final state of a city with 33% empty locations. While the typical final state of Schelling's original city of size N=8 and 33% empty locations (Figure 1.1**A**), consists of two large, compact R and B clusters, the N=100 city is broken up into many small, sparse clusters.

Figure 1.12 shows that the final states closely resemble a checkerboard when the vacancy ratio is low and distinct clusters emerge only when $v \geq 0.24$. Even the distinct clusters are sparse and retain remnants of the checkerboard structure. This is no accident but a direct result of the checkerboard structure of the initial state of the city. Each agent has 4 neighbors of its own type in a checkerboard and is happy. Even more, each agent has one spare neighbor. Therefore, the checkerboard is not only stable, but super-stable. A large deviation from the checkerboard is therefore needed before the checkerboard structure can be broken.

Our aggregation indices indicate the sparseness of clusters and persistence of

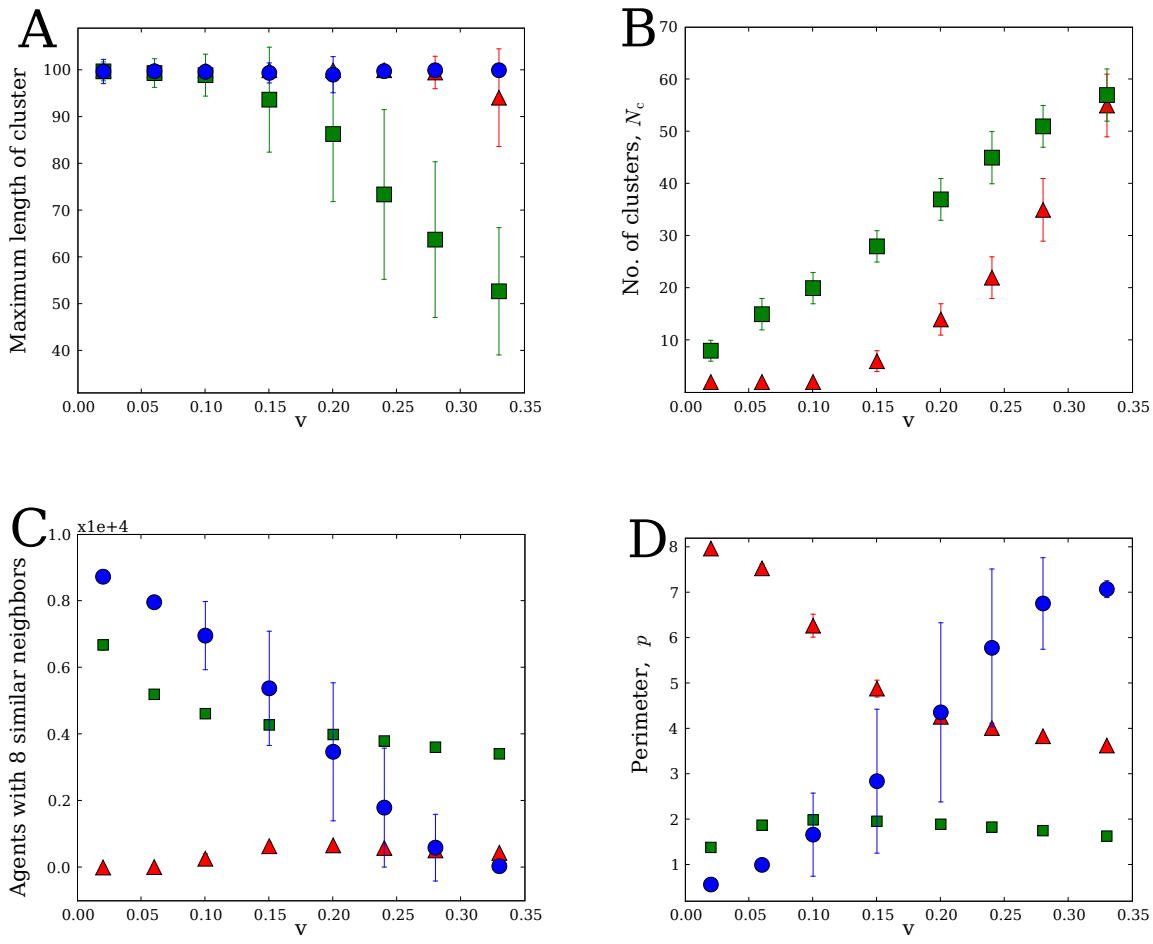

Figure 1.11: Statistics of four key measures of aggregation of final states for $T = 3$ (red triangles), $T = 4$ (green squares), and $T = 5$ (blue circles) for different v: **A** The scale of aggregation L; **B** The number of clusters N_C; **C** The number of agents with eight like nearest neighbors N_0; **D** Normalized perimeter p.

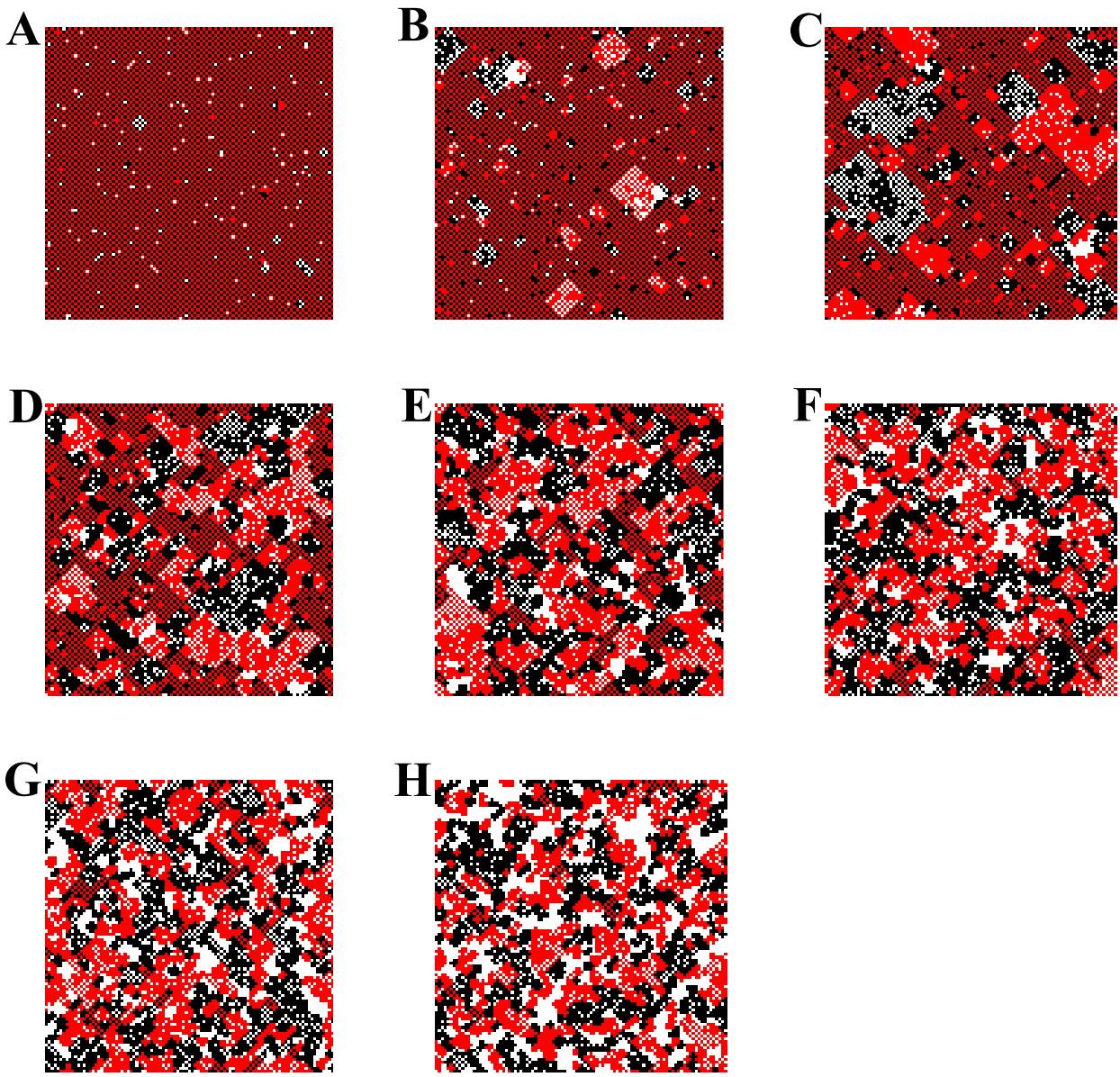

Figure 1.12: Characteristic final states for $T = 3$ for different v: **A**: $v = 2\%$, **B**: $v = 6\%$, **C**: $v = 10\%$, **D**: $v = 15\%$, **E**: $v = 20\%$, **F**: $v = 24\%$, **G**: $v = 28\%$, **H**: $v = 33\%$.

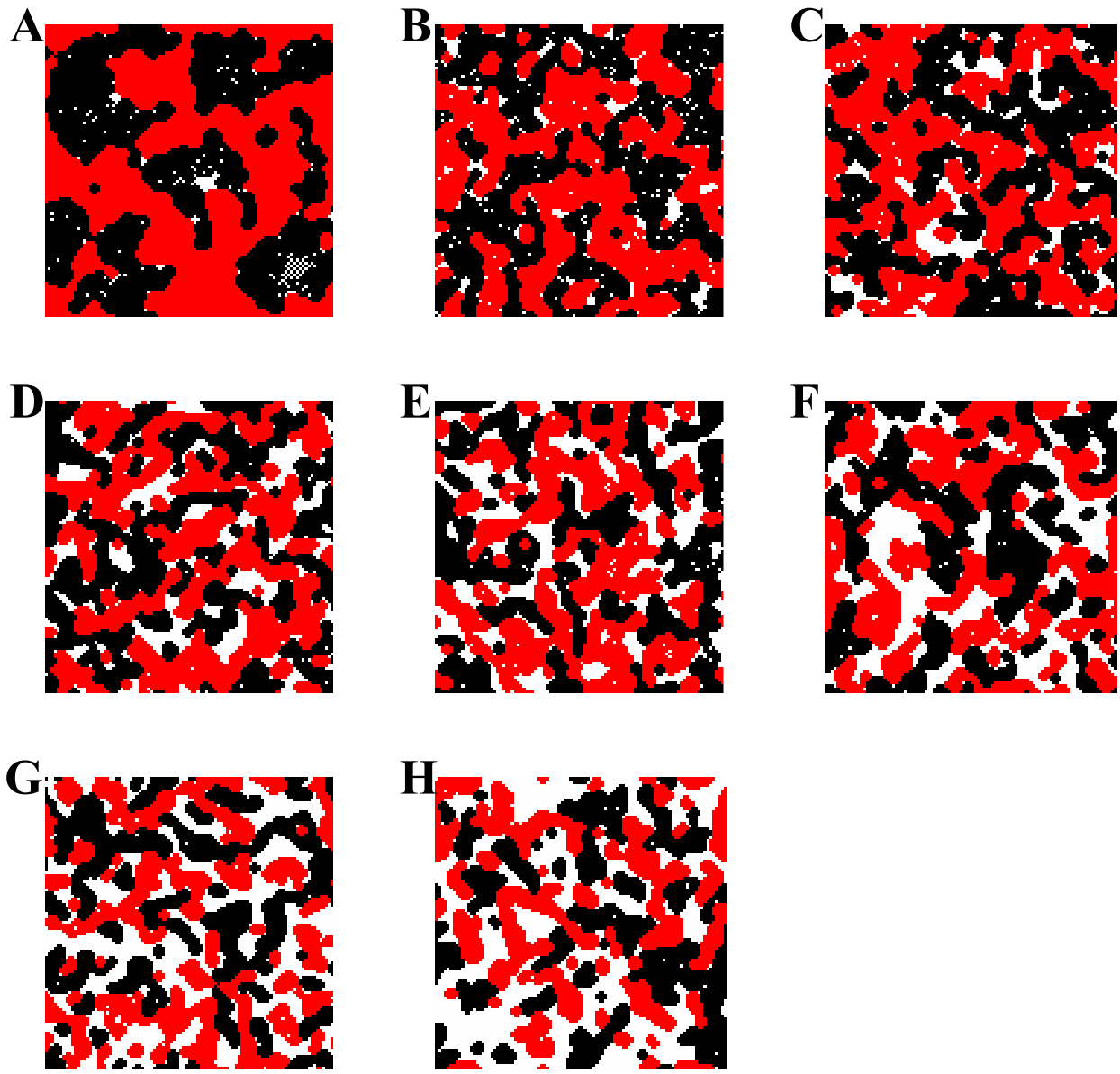

Figure 1.13: Characteristic final states for $T = 4$ for different v: **A**: $v = 2\%$, **B**: $v = 6\%$, **C**: $v = 10\%$, **D**: $v = 15\%$, **E**: $v = 20\%$, **F**: $v = 24\%$, **G**: $v = 28\%$, **H**: $v = 33\%$.

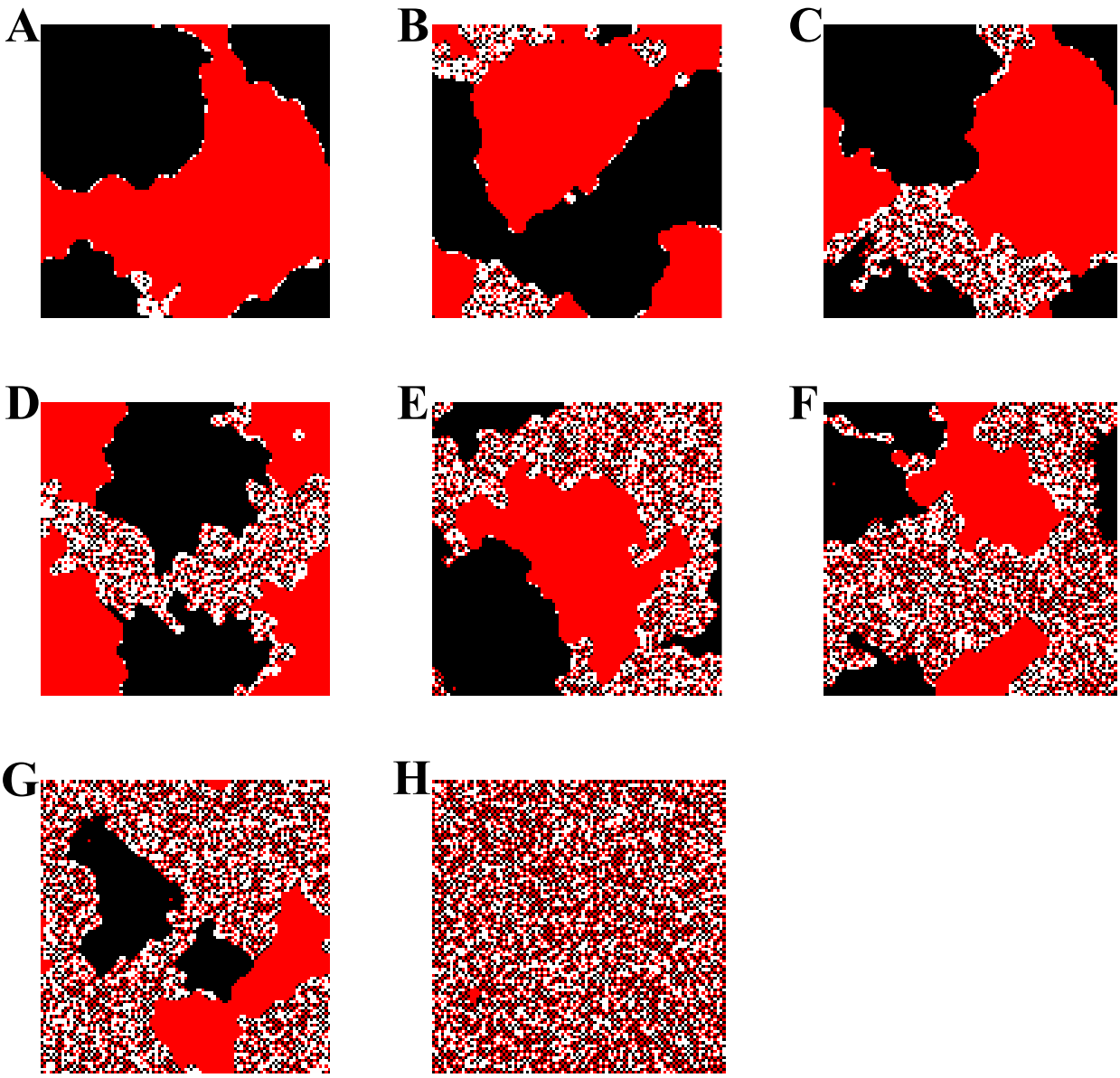

Figure 1.14: Characteristic final states for $T = 5$ for different v: **A**: $v = 2\%$, **B**: $v = 6\%$, **C**: $v = 10\%$, **D**: $v = 15\%$, **E**: $v = 20\%$, **F**: $v = 24\%$, **G**: $v = 28\%$, **H**: $v = 33\%$.

the checkerboard structure. Almost no agents are completely surrounded by similar agents, demonstrating a lack of isolated agents. The normalized perimeter of a checkerboard is 8 and the normalized perimeter of a maximally aggregated city is approximately zero. We plot the normalized perimeter in Figure 1.11**D**, the red triangles refer to the city with neighbor comfort threshold T=3. The normalized perimeter p is almost 8 for a city with 2% empty locations showing a close match with the checkerboard configuration. As the number of empty locations increases, the perimeter p decreases, indicating that the checkerboard patterns slowly goes away. When the city has 33% empty locations, the perimeter of the city is approximately 4, indicating that the city is not maximally segregated and the agents have contacts with 1-2 dissimilar agents.

Note that the checkerboard structure consists of one R and one B cluster. As the vacancy ratio v increases, the checkerboard structure withers away and the number of clusters in the final states, N_C, increases (Fig. 1.11**B**). The numbers of clusters is almost a cubic function of the vacancy ratio. The value for the slope in Fig. 1.11**B** corresponding to $T = 3$ is 2.86 and the value 3 is well within the error bars.

1.6.1.2 $T = 4$:compact clusters and mesoscale aggregation

Figure 1.13 shows the typical final states for a city of size $N = 100$, neighbor comfort threshold $T = 4$ and different choices of vacancy ratio v. A quick comparison of Figure 1.13 and Figure 1.12 shows that aggregation patterns change dramatically with the change in the neighbor comfort threshold. As agents now need 4 similar neighbors to be happy, the super-stability of the checkerboard is gone and this leads to the rise of compact clusters.

Almost 40% of agents are completely surrounded by 8 similar neighbors (Fig 1.11**C**) for $T = 4$, only 10% of agents in a $T = 3$ city are ever surrounded by 8 other similar neighbors. The normalized perimeter p is always less than 2 in a city with $T = 4$,

indicating that agents are surrounded by at most 1 dissimilar neighbor and the empty locations form patches of their own. Unlike final states in a city with $T = 3$, R and B clusters are compact when $T = 4$.

The maximum length of a cluster L defines the scale of the aggregation in the city. It is almost 100 when the city has 2% empty locations and matches the size of the city but declines to almost half of the city size when the city has 33% empty locations. This shows that the scale of the aggregation changes from macroscale to mesoscale with an increase in the number of empty locations.

The number of clusters in the final state of cities for $T = 4$ is an increasing function of the vacancy ratio. In fact, the number of clusters increases almost linearly with an increase in the number of empty locations. The value for the slope in Fig. 1.11**B** corresponding to $T = 4$ is 0.89 and the value 1 is well within the error bars. When we combine the information from the two indicators: maximum length L and the number of clusters N_C, we conclude that in a city with $T = 4$, aggregation is a decreasing function of vacancy ratio. This is directly opposite to the aggregation pattern in a city with $T = 3$, where aggregation is an increasing function of vacancy ratio.

In conclusion, an increase in the number of empty locations has dramatically different effects on aggregation in cities with $T = 3$ and $T = 4$. *Empty locations promote aggregation when* $T = 3$ *but inhibit aggregation when* $T = 4$.

1.6.1.3 $T = 5$: isolated unhappy agents

Figure 1.14 shows the typical final states for a city of size $N = 100$, neighbor comfort threshold $T = 5$ and different choices of vacancy ratio v. The final states of a city with $T = 5$ are marked by a huge increase in the number of unhappy agents.

When an agent requires 5 similar agents in its neighborhood to be happy, the normal rules of movement present very few such opportunities. Therefore we relax the rules and allow agents to swap positions if this increases the happiness of both

agents (similar to the selection algorithms in [63, 83, 86]). Despite this, one observes massive isolation amongst the agents. This isolation increases as as the number of empty locations increases.

Figure 1.15 shows two aggregation measures especially suited for a $T = 5$ city. Figure 1.15**A** shows the number of unhappy agents as a function of the vacancy ratio. When $T = 5$, we observe unhappy agents in the final state of the city for the first time (theoretically they might occur for $T = 3$ and $T = 4$, but they are extremely unlikely). The number of unhappy agents is surprisingly linearly dependent on the number of empty locations. Figure 1.15**B** shows the mean value of the size of the largest cluster for a given vacancy ratio v. When the vacancy ratio v is low, the final state is dominated by a 2 large clusters and few singletons. As the number of empty locations increases, the large clusters decrease in size, the number of singletons increases and at last there are no large compact clusters when the city has 33% empty locations.

The number of agents completely surrounded by 8 like neighbors is a monotonically decreasing function of the number of empty locations. The perimeter increases monotonically showing that isolation increases as the number of empty locations increases. The number of clusters is not a meaningful quantity for quantifying the aggregation in this case beacuse the singletons completely distort the picture even for the case of $v = 0.02$.

1.7 Dependence on city size

The aggregation patterns change dramatically when the city increases from a city of size $N = 8$ to $N = 100$. It is interesting to determine if the patterns in aggregation changes if the size of the city further increases. Therefore we ran simulations for cities with $N = 50, 100$ and 200. One can see some typical final states for $N = 50$ and $N = 200$ in Figure 1.16 and 1.17 .

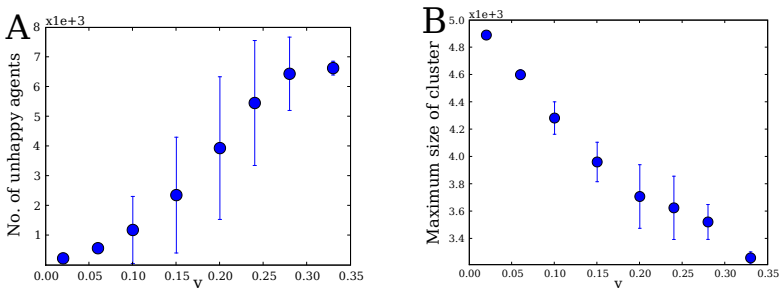

Figure 1.15: Statistics of the final states with neighbor comfort threshold $T = 5$: **A**: The average number of unhappy agents in final states; **B**: The average number of the agents in the two big clusters.

A useful way to determine aggregation patterns is to look at Figure 1.18 where we compare indices for the three city sizes. An important feature of these indices is that they have been normalized by the number of locations in the cities. We can immediately see that there is very little difference in the indices across the cities. This shows that no new qualitative patterns are observed as the size of cities varies and indicates a proportionality between segregation indices and size of cities.

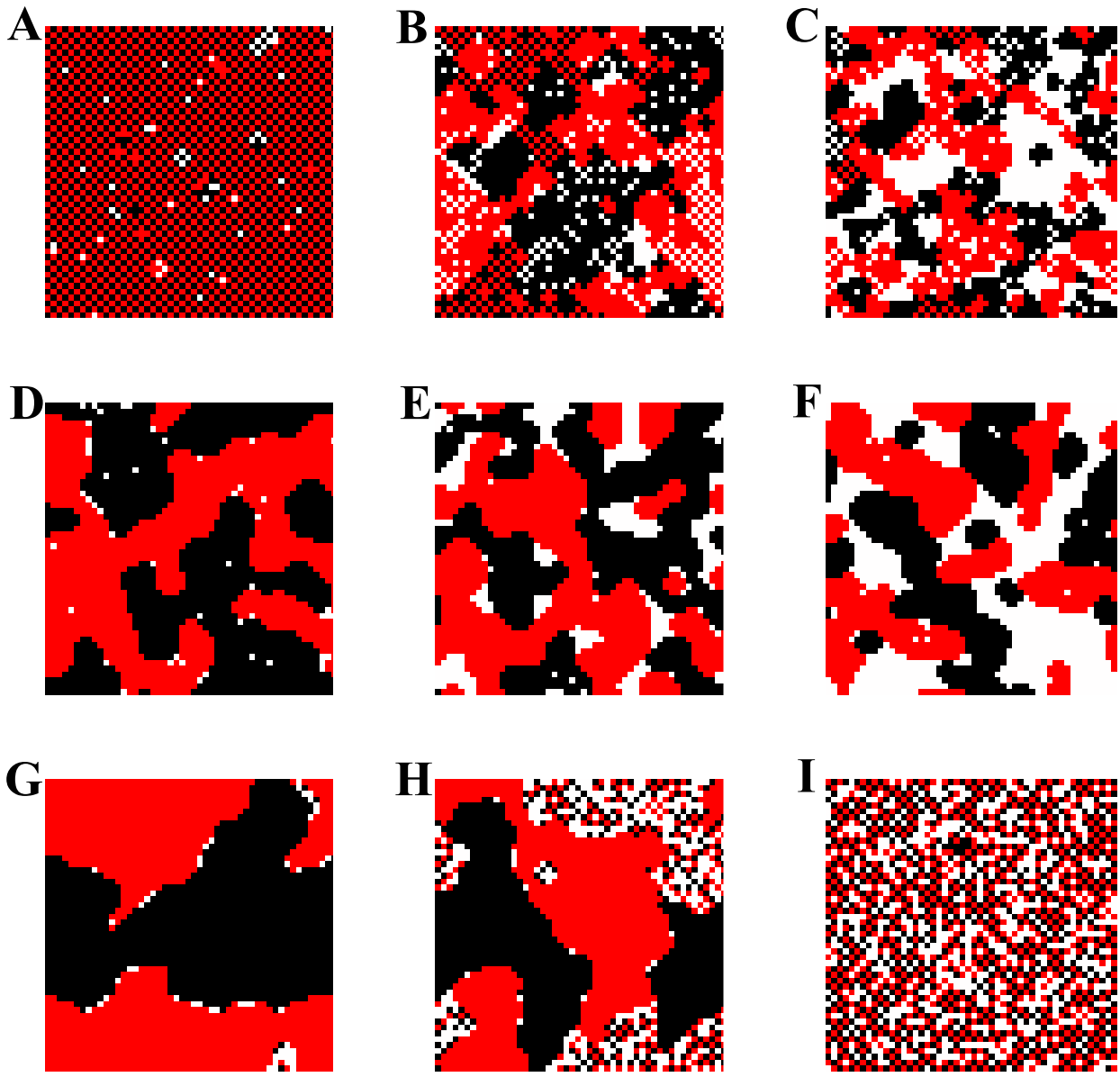

Figure 1.16: Characteristic final states for $N = 50$ and different values of T and v: **A**: $T = 3$, $v = 2\%$, **B**: $T = 3$, $v = 15\%$, **C**: $T = 3$, $v = 33\%$, **D**: $T = 4$, $v = 2\%$, **E**: $T = 4$, $v = 15\%$, **F**: $T = 4$, $v = 33\%$, **G**: $T = 5$, $v = 2\%$, **H**: $T = 5$, $v = 15\%$, **I**: $T = 5$, $v = 33\%$.

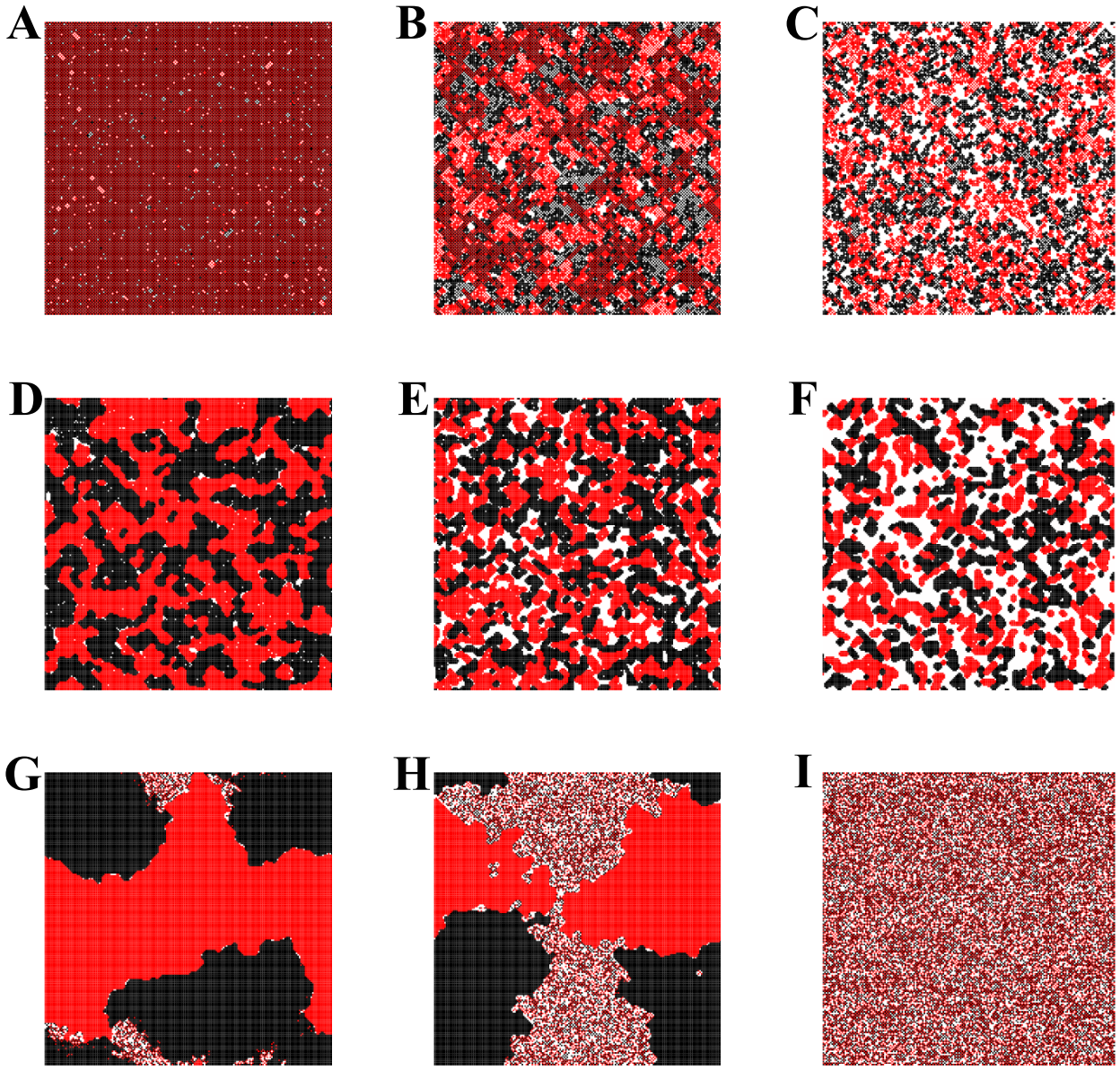

Figure 1.17: Characteristic final states for $N = 200$ and different values of T and v: **A**: $T = 3$, $v = 2\%$, **B**: $T = 3$, $v = 15\%$, **C**: $T = 3$, $v = 33\%$, **D**: $T = 4$, $v = 2\%$, **E**: $T = 4$, $v = 15\%$, **F**: $T = 4$, $v = 33\%$, **G**: $T = 5$, $v = 2\%$, **H**: $T = 5$, $v = 15\%$, **I**: $T = 5$, $v = 33\%$.

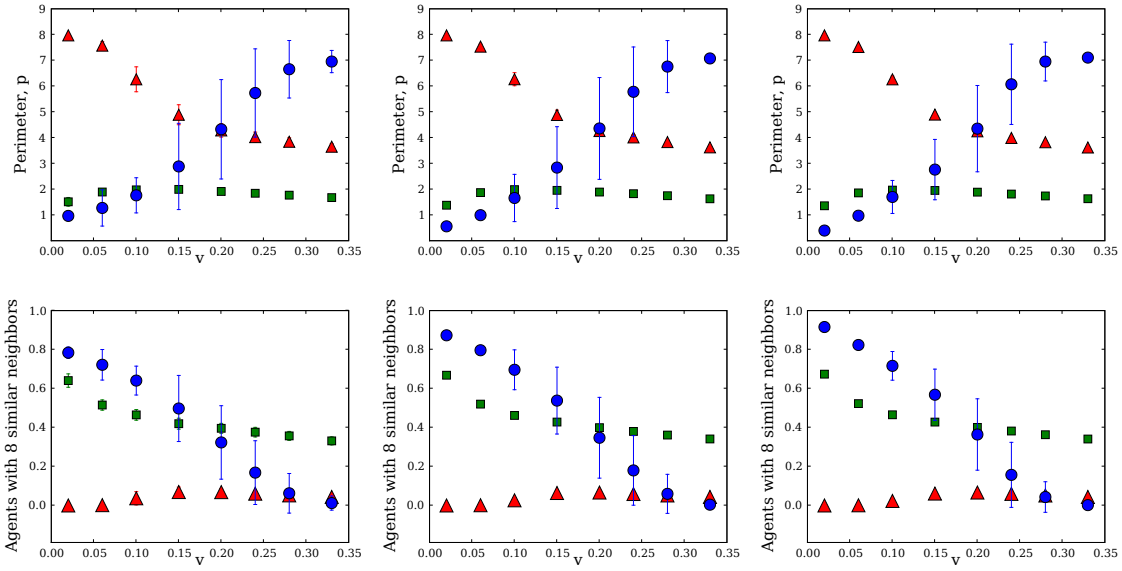

Figure 1.18: Characteristic values of the perimeter (top row) and the number of agents with only like neighbors (bottom row) for $N = 50$ (left column), $N = 100$ (middle column), and $N = 200$ (right column); in every fame, $T = 3$ (red triangles), $T = 4$ (green squares), and $T = 5$ (blue circles).

CHAPTER II

MINORITIES

2.1 Questions

We chase the natural questions: Do aggregation patterns qualitatively change if one type of agent is in a minority? Is there a difference in the aggregation patterns of the majority and minority agents? The short answer is yes. Overall, being in a minority limits the opportunity for B agents to become happy and leads to the rise of isolated unhappy B agents. But we also occasionally observe the formation of intensely aggregated minority clusters.

2.2 Aggregation dependence on neighbor comfort threshold T

The relative concentration of R agents in the city is denoted by r. If $r = 0.6$, this means that 60% of agents in the city are R agents. We divide our analysis into two parts. We first determine aggregation in a city where B agents are in a small majority ($r = 0.6$). We quantify the difference in aggregation of R and B agents. Then we determine the effects of further decreasing the percentage of B agents in a city ($r = 0.7$). Figure 2.1 and Figure 2.2 plot the aggregation indices of R and B agents for different neighbor comfort threshold T and vacancy ratio v in a city with 60% R agents.

2.2.1 $T = 3$

Figure 2.3 shows the typical final states for a city of size $N = 100$ with 60% R agent concentration and neighbor comfort threshold $T = 3$. The aggregation in this city is different from a city where the agents are equally concentrated and B agents lead the

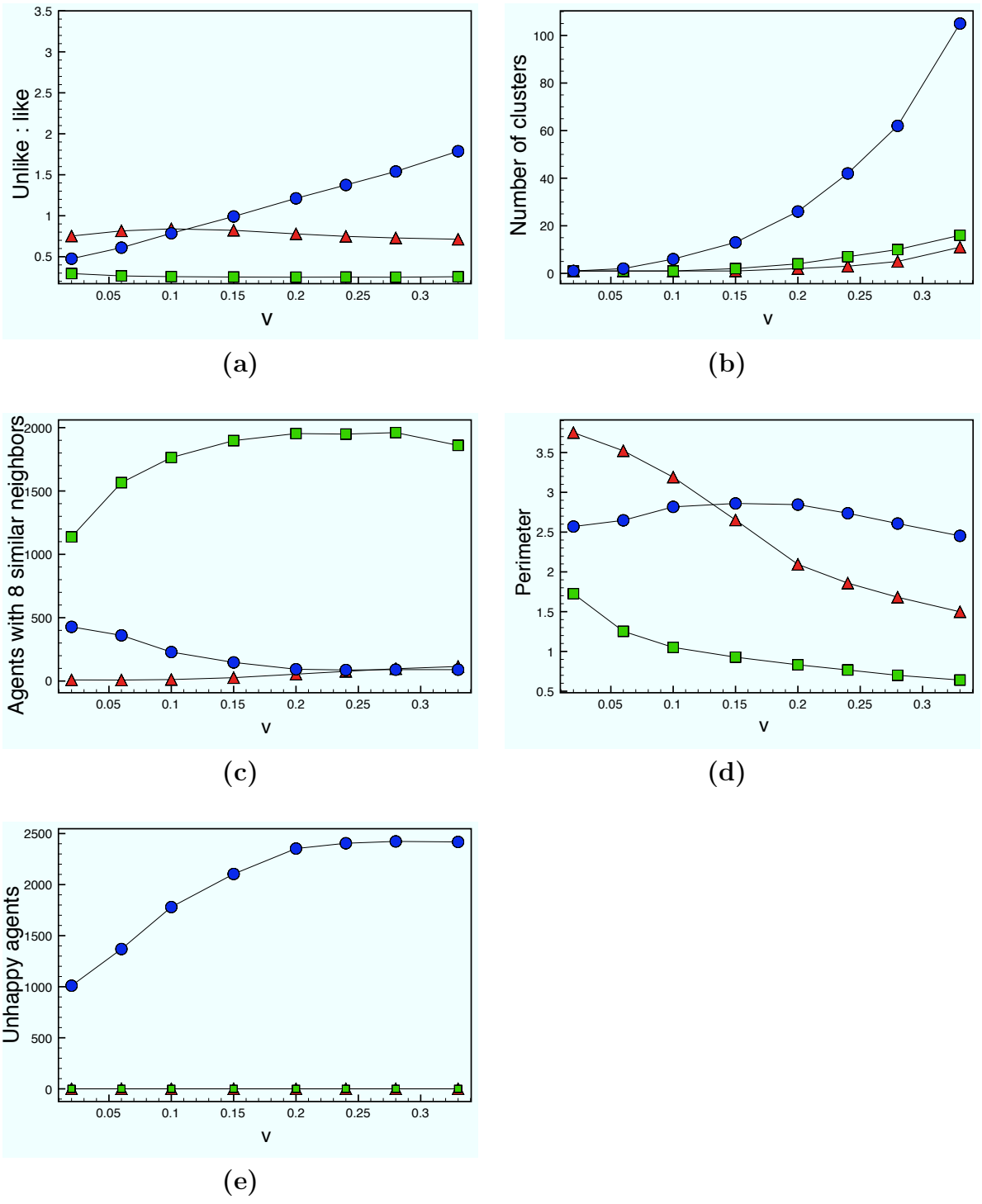

Figure 2.1: Statistics of five key measures of aggregation of final states for R agents for $T = 3$ (red triangles), $T = 4$ (green squares), and $T = 5$ (blue circles) for different v : **(a)** The exposure measured by the unlike:like neighbors ratio; **(b)** The number of clusters N_C; **(c)** The number of agents with eight like nearest neighbors N_0; **(d)** Normalized perimeter p; **(e)** No. of unhappy agents. Concentration of R agents: 60%.

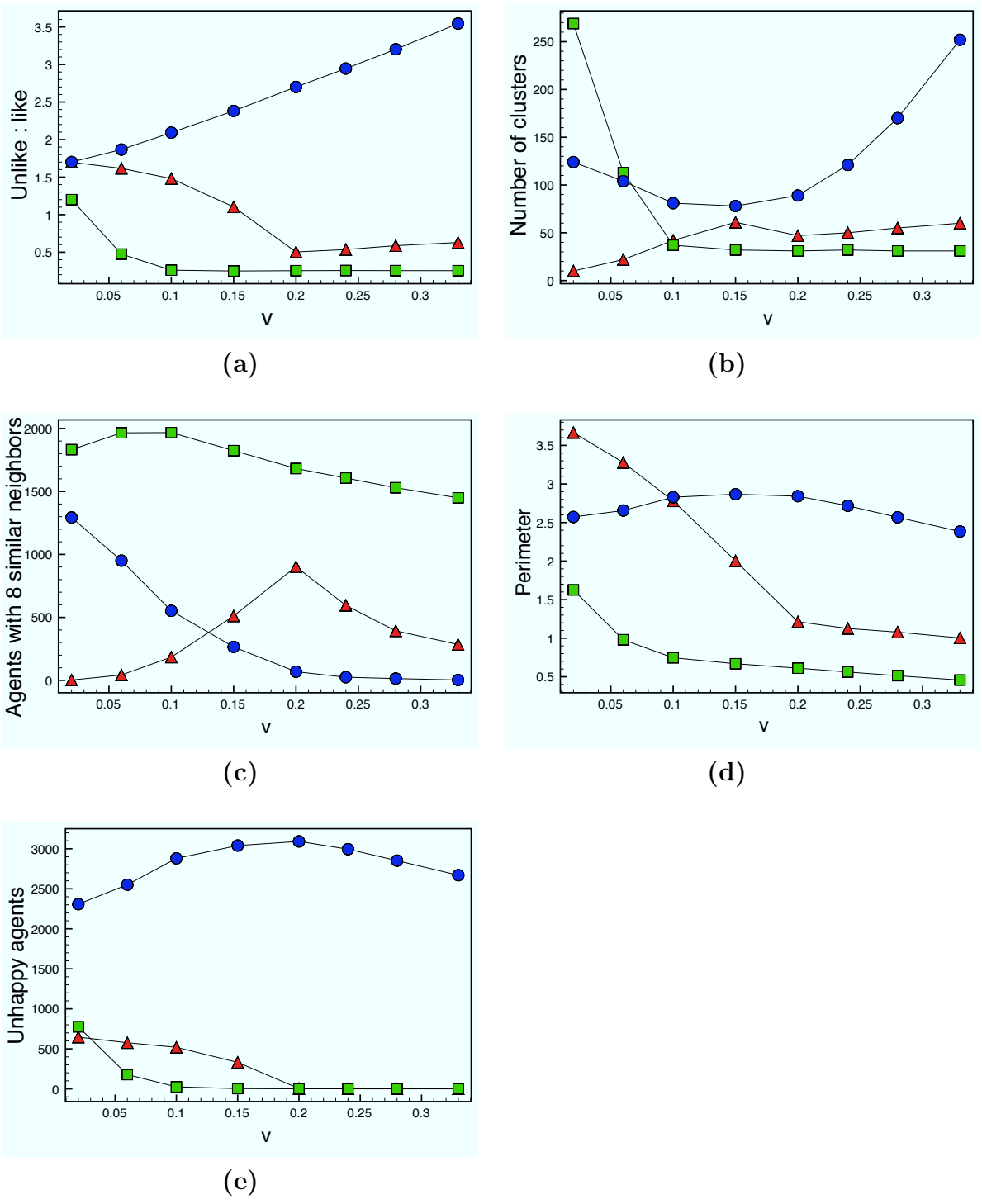

Figure 2.2: Statistics of five key measures of aggregation of final states for B agents for $T = 3$ (red triangles), $T = 4$ (green squares), and $T = 5$ (blue circles) for different v: **(a)** The exposure measured by the unlike:like neighbors ratio; **(b)** The number of clusters N_C; **(c)** The number of agents with eight like nearest neighbors N_0; **(d)** Normalized perimeter p; **(e)** No. of unhappy agents. Concentration of R agents: 60%.

deviation from the classical Schelling city. In the classical Schelling city, when the neighbor comfort threshold $T = 3$, the checkerboard structure provides super stability and is very persistent. In a city with minorities, the checkerboard pattern of the initial state breaks up much more easily, as the minority B agents are unhappy and need to move to become happy. Therefore, the aggregation patterns of the R and B agents are different. In particular, *B agents form compact clusters, while the R agents do not*. The difference is particularly striking when the vacancy ratio $v = 0.15, 0.2, 0.24$. We also observe that when the vacancy ratio $v \leqslant 0.2$, most B clusters are marked by the absence of surrounding empty locations and are mostly surrounded by R agents.

The initial checkerboard configuration provides an advantage to R agents. The checkerboard pattern provides super stability since there is a spare neighbor in the perfect checkerboard. R agents rarely need to move and there are almost no unhappy R agents for any choice of the vacancy ratio v. Therefore, the clusters of R agents remain sparse and on the whole, the aggregation of R agents resembles a city where the agents are equally concentrated ($r = 0.5$).

Each of these observations are supported by the aggregation measures. Figure 2.2 shows that B agents are unhappy when the vacancy ratio $v = 0.2, 0.6$. The B agents remain unhappy since empty suitable locations are scarce. When the number of empty locations increases, B agents gain mobility and the unhappy agents disappear. The presence of compact B clusters is indicated by the marked increase in the number of B agents completely surrounded by other B agents. As the R agents do not move and retain the checkerboard structure while B agents move to become happy, B agents end up forming many more clusters as compared to R agents. When B agents start forming compact clusters, the unlike:like ratio for B agents falls down dramatically and is significantly higher than that of R agents.

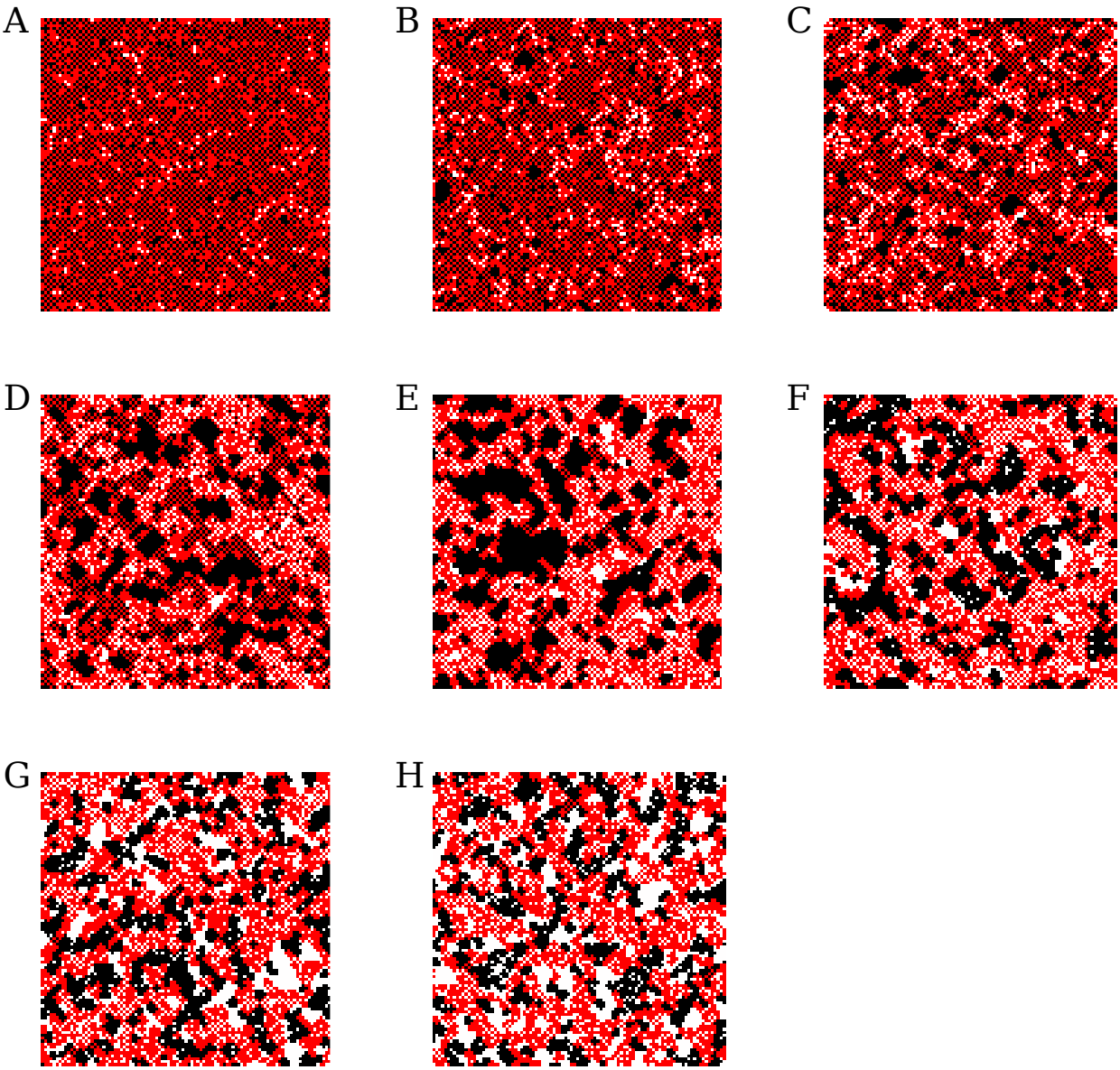

Figure 2.3: Characteristic final states for $r = 0.6$ and $T = 3$ for different v: **A**: $v = 2\%$, **B**: $v = 6\%$, **C**: $v = 10\%$, **D**: $v = 15\%$, **E**: $v = 20\%$, **F**: $v = 24\%$, **G**: $v = 28\%$, **H**: $v = 33\%$.

2.2.2 $T = 4$

Figure 2.4 shows the typical final states for a city of size $N = 100$ with with 60% R agent concentration and neighbor comfort threshold $T = 4$. The B agents are at a tremendous disadvantage due their relatively lower concentration. The most prominent observation is the presence of a number of isolated B agents when the vacancy ratio is low. The aggregation measures reflect this observation. There are a large number of unhappy B agents and the unlike:like ratio of B agents is much higher than that of R agents.

The number of B agent clusters is massively higher than R agent clusters when the vacancy ratio is low ($v \leq 0.1$), isolated B agents are the cause of this massive difference. But even when the there are considerable number of empty locations in the city, B agents continue to form more clusters than R agents. When $v \geq 0.15$, the number of B clusters remains roughly constant but the number of B agents in the city decreases, therefore the size of the B clusters decreases.

Just like cities with equal R and B agent concentration and $T = 4$, there are almost no remnants of the checkerboard pattern. Both the R and B clusters are compact. The unlike:like ratio of a checkerboard is 1. The unlike:like ratio of R and B clusters is usually below that of of a checkerboard, the only exceptions are cities with small number of vacancies which have a large number of completely isolated B agents. As soon as there are enough vacancies so that B agents can move around, the isolated B agents disappear and the cities become divided into a large number of aggregated compact R and B clusters.

As in the case of $T = 3$, when the vacancy ratio is high, the final states of cities with $T = 4$ resemble the final states of classical Schelling cities with equal R and B agent concentration.

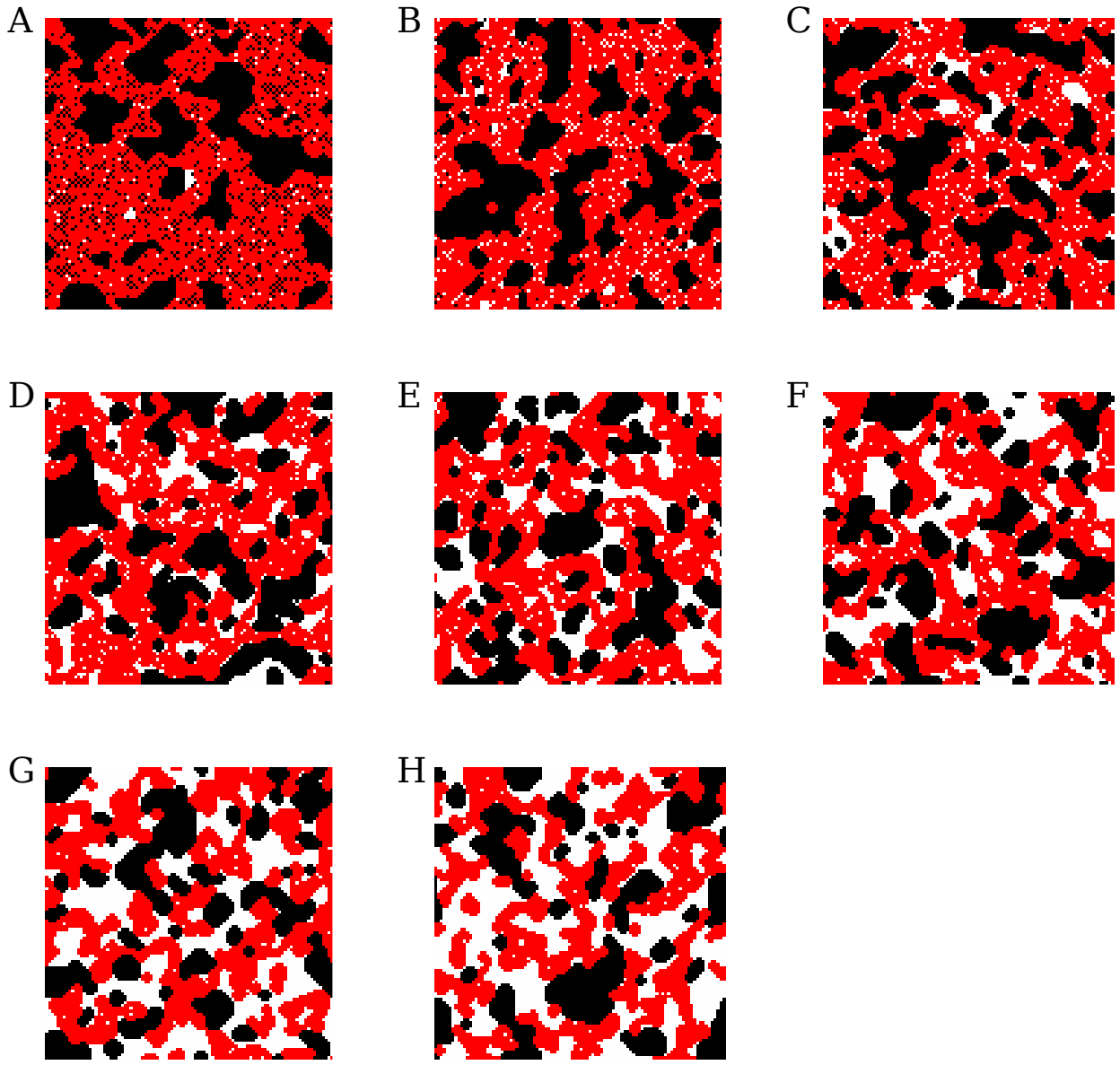

Figure 2.4: Characteristic final states for $r = 0.6$ and $T = 4$ for different v: **A**: $v = 2\%$, **B**: $v = 6\%$, **C**: $v = 10\%$, **D**: $v = 15\%$, **E**: $v = 20\%$, **F**: $v = 24\%$, **G**: $v = 28\%$, **H**: $v = 33\%$.

2.2.3 $T = 5$

Figure 2.5 shows the typical final states for a city of size $N = 100$ with 60% R agent concentration and neighbor comfort threshold $T = 5$. We can readily observe that the aggregation patterns of R and B agents are markedly different. We note the appearance of large compact B clusters for low vacancy ratios and their disappearance with an increase in vacancy ratios. The number of B agents completely surrounded by other B agents records this phenomenon. The number of B agents completely surrounded by 8 B agents diminishes rapidly with an increase in vacancy ratio. The number of B clusters also decreases initially, but then rapidly increases as large compact B clusters rarely occur and the clusters become sparse.

The number of unhappy B agents is a complicated measure which is affected by two trends. First, as compact clusters go away, the number of unhappy B agents decreases. Then the total number of B agents decreases, thus the number of unhappy agents decreases along with it.

The aggregation patterns of R agents are complicated. For low vacancy ratios, there are few R clusters but they are spotted with B agents, thus R clusters have fewer agents completely surrounded by 8 other R agents. However the unlike:like ratio of R agents consistently remains lower than B agents. As a combination of these two opposing trends, the adjusted perimeters of R and B agents are remarkably similar. The number of R clusters is an increasing function of vacancy ratio, B clusters always outnumber R clusters.

However, the most surprising observation is that the unlike:like ratio for both R and B agents is remarkably linearly dependent on the vacancy ratio.

2.2.4 Concentration of R agents = 70%

Figure 2.6 and Figure 2.7 quantify the aggregation of R and B agents for different neighbor comfort threshold T and vacancy ratio v in a city with 70% R agents.

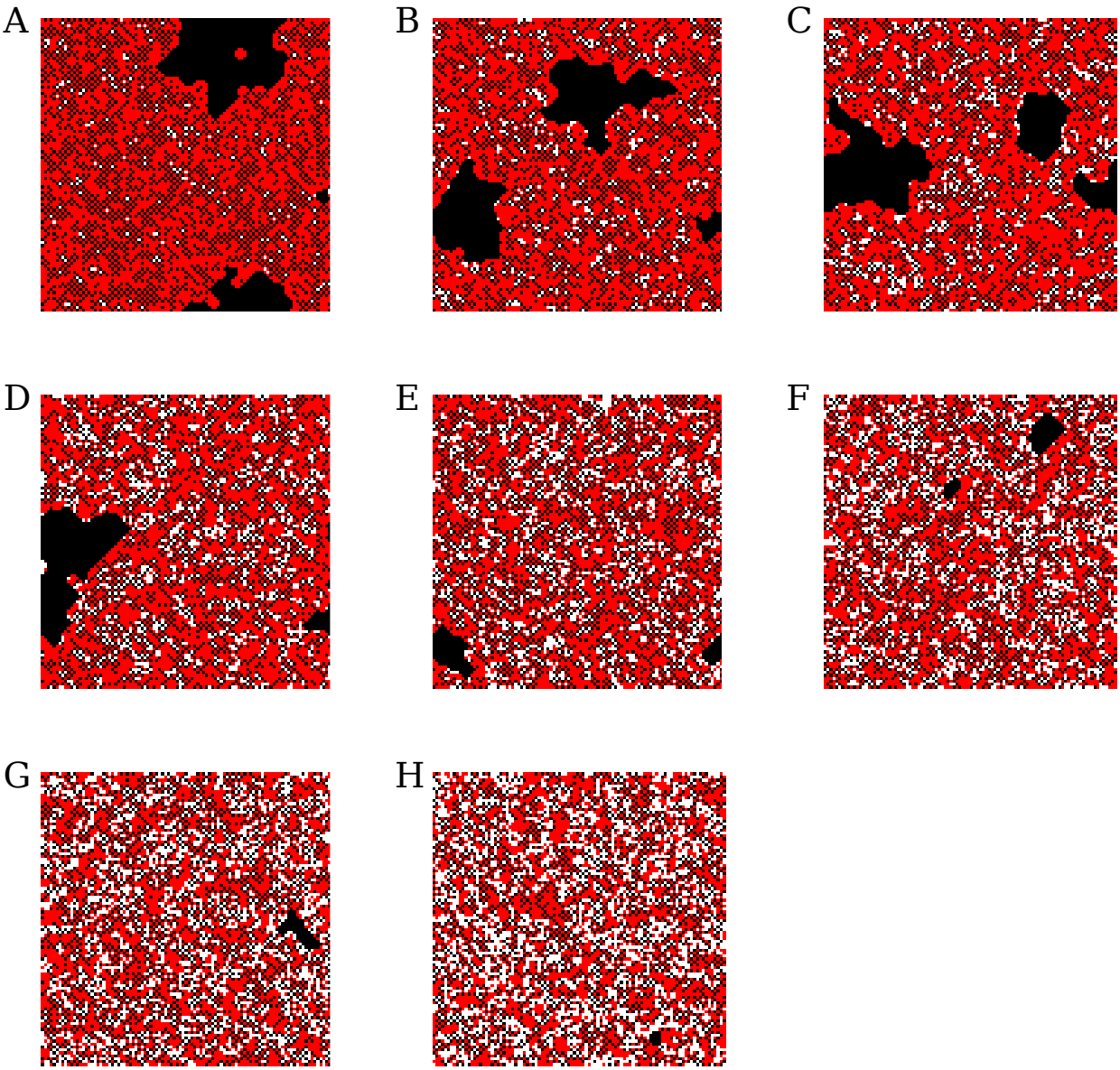

Figure 2.5: Characteristic final states for $r = 0.6$ and $T = 5$ for different v: **A**: $v = 2\%$, **B**: $v = 6\%$, **C**: $v = 10\%$, **D**: $v = 15\%$, **E**: $v = 20\%$, **F**: $v = 24\%$, **G**: $v = 28\%$, **H**: $v = 33\%$.

Figure 2.8, 2.9 and 2.10 show the typical final states in a city of size $N = 100$ for different neighbor comfort threshold T.

With a further decrease in the concentration of B agents, we do not observe a qualitative change in the aggregation patterns. The number of compact B clusters further decreases. The number of unhappy B agents and isolated B agents further increases. Overall, being in a minority reduces opportunities for B agents to move around and find a suitable location where they can be happy. It is interesting to note that often there are empty locations where no individual B agent would be happy, but a group of B agents could be happy, if they were to move together.

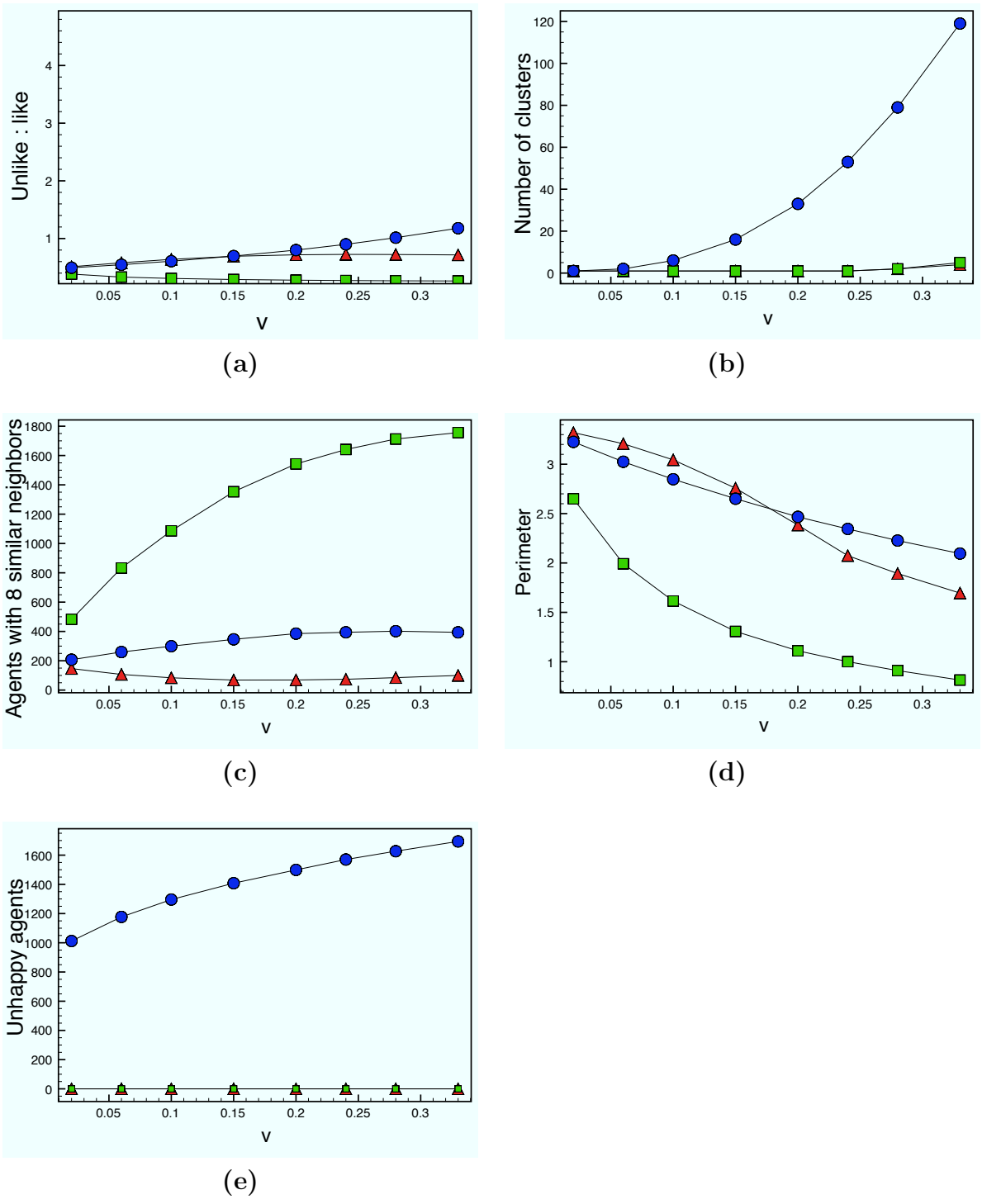

Figure 2.6: Statistics of five key measures of aggregation of final states for R agents for $T = 3$ (red triangles), $T = 4$ (green squares), and $T = 5$ (blue circles) for different v : **(a)** The exposure measured by the unlike:like neighbors ratio; **(b)** The number of clusters N_C; **(c)** The number of agents with eight like nearest neighbors N_0; **(d)** Normalized perimeter p; **(e)** No. of unhappy agents. Concentration of R agents: 70%.

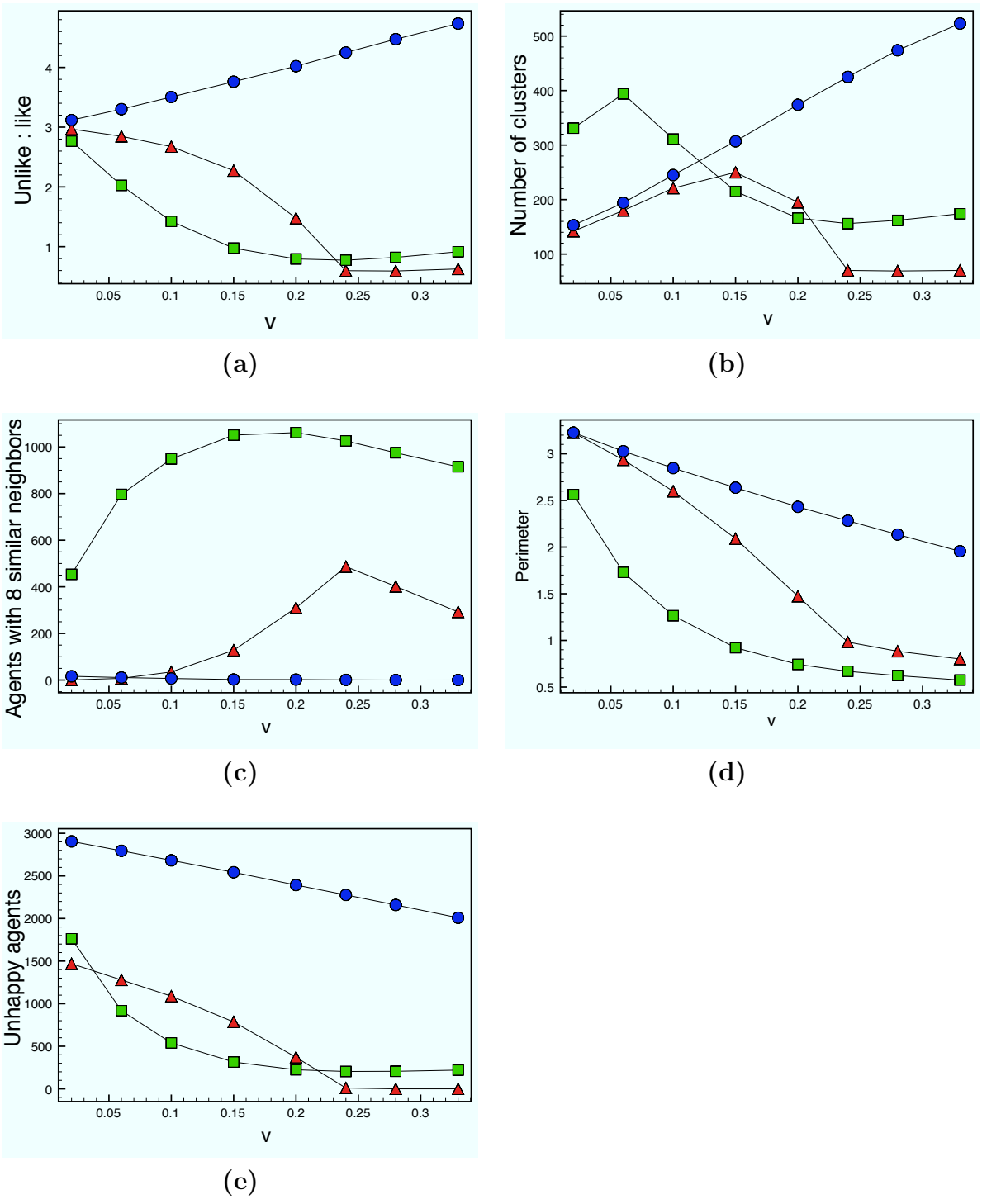

Figure 2.7: Statistics of five key measures of aggregation of final states for B agents for $T = 3$ (red triangles), $T = 4$ (green squares), and $T = 5$ (blue circles) for different v: **(a)** The exposure measured by the unlike:like neighbors ratio; **(b)** The number of clusters N_C; **(c)** The number of agents with eight like nearest neighbors N_0; **(d)** Normalized perimeter p; **(e)** No. of unhappy agents. Concentration of R agents: 70%.

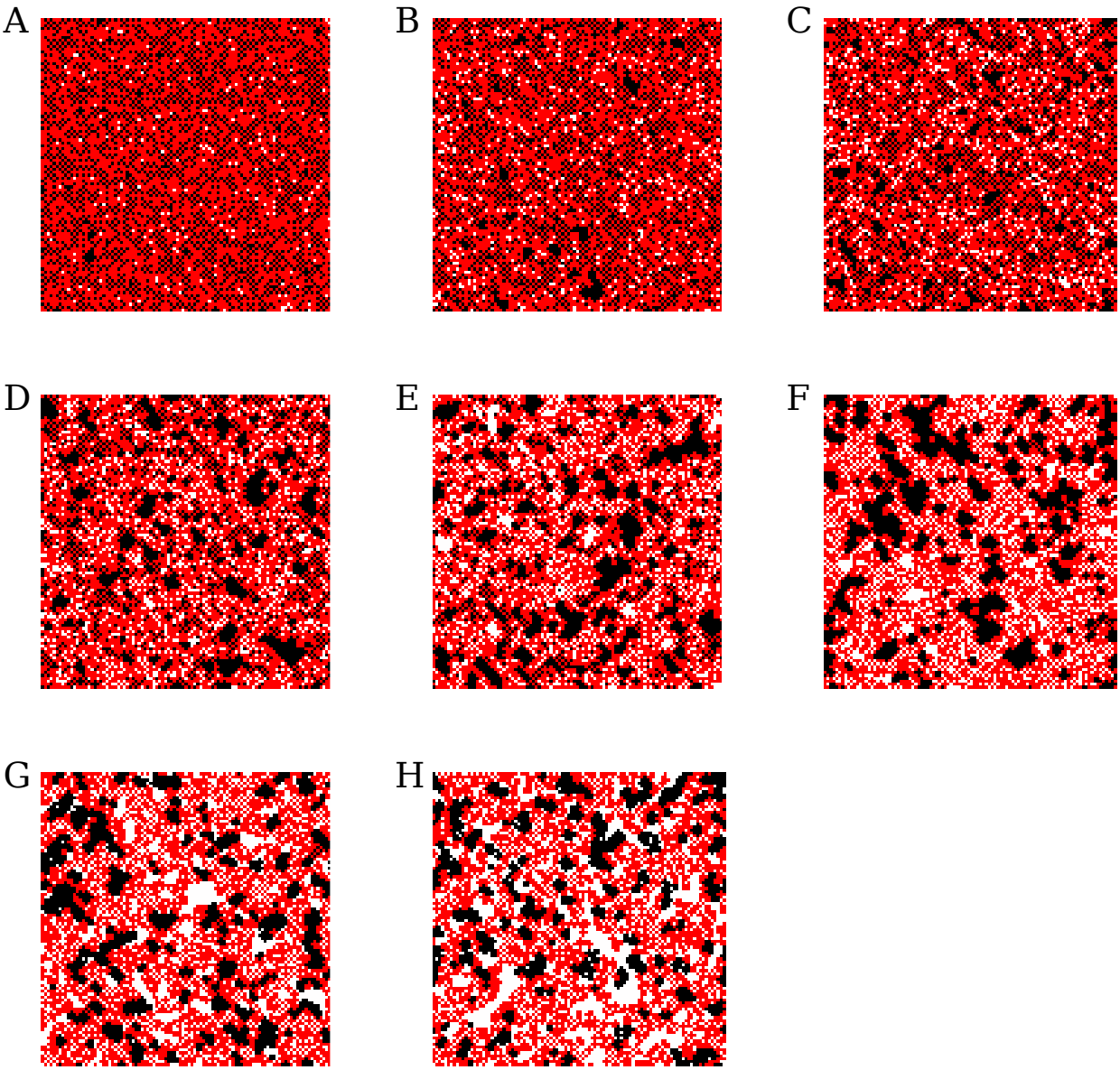

Figure 2.8: Characteristic final states for $r = 0.7$ and $T = 3$ for different v: **A**: $v = 2\%$, **B**: $v = 6\%$, **C**: $v = 10\%$, **D**: $v = 15\%$, **E**: $v = 20\%$, **F**: $v = 24\%$, **G**: $v = 28\%$, **H**: $v = 33\%$.

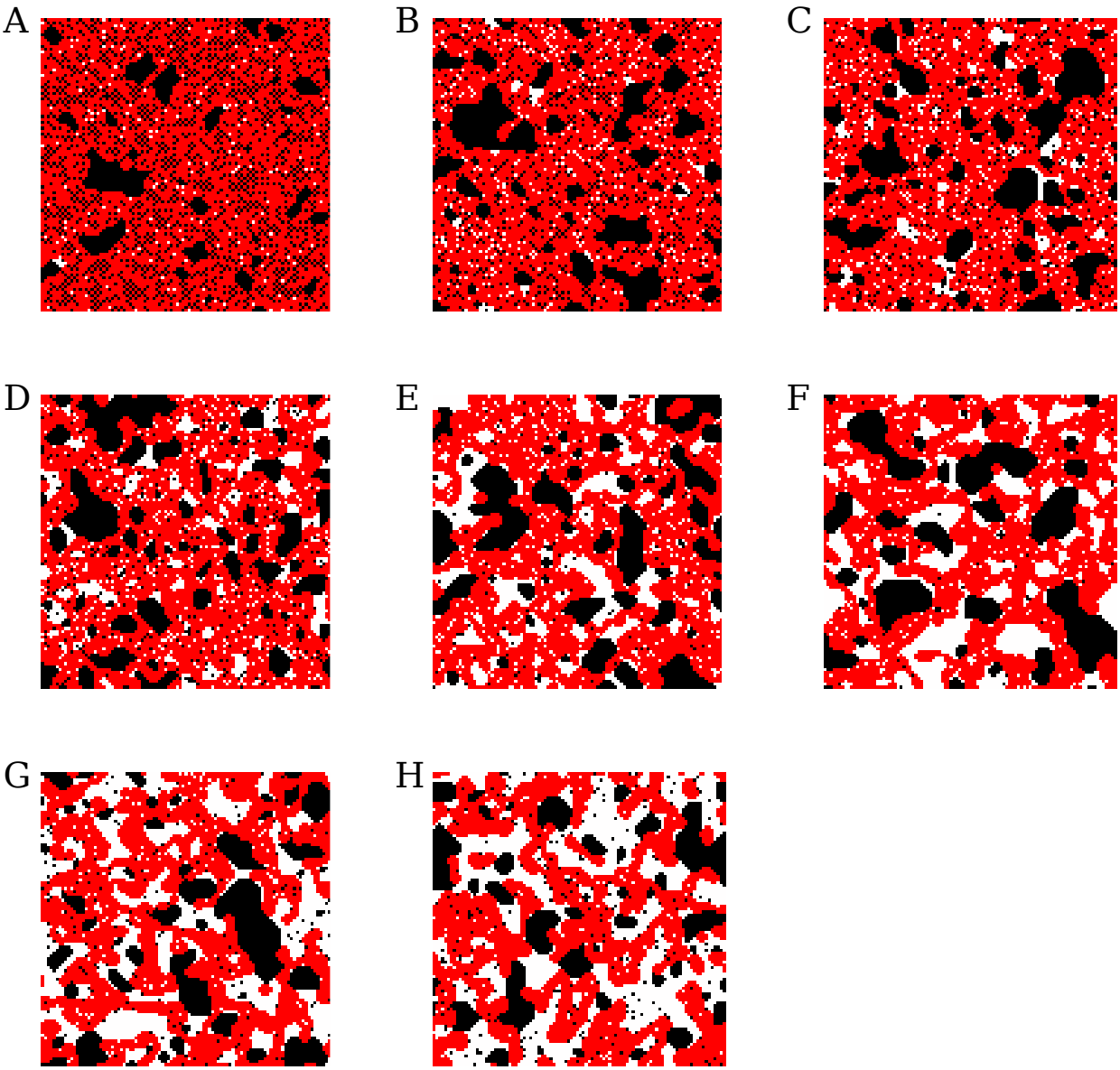

Figure 2.9: Characteristic final states for $r = 0.7$ and $T = 4$ for different v: **A**: $v = 2\%$, **B**: $v = 6\%$, **C**: $v = 10\%$, **D**: $v = 15\%$, **E**: $v = 20\%$, **F**: $v = 24\%$, **G**: $v = 28\%$, **H**: $v = 33\%$.

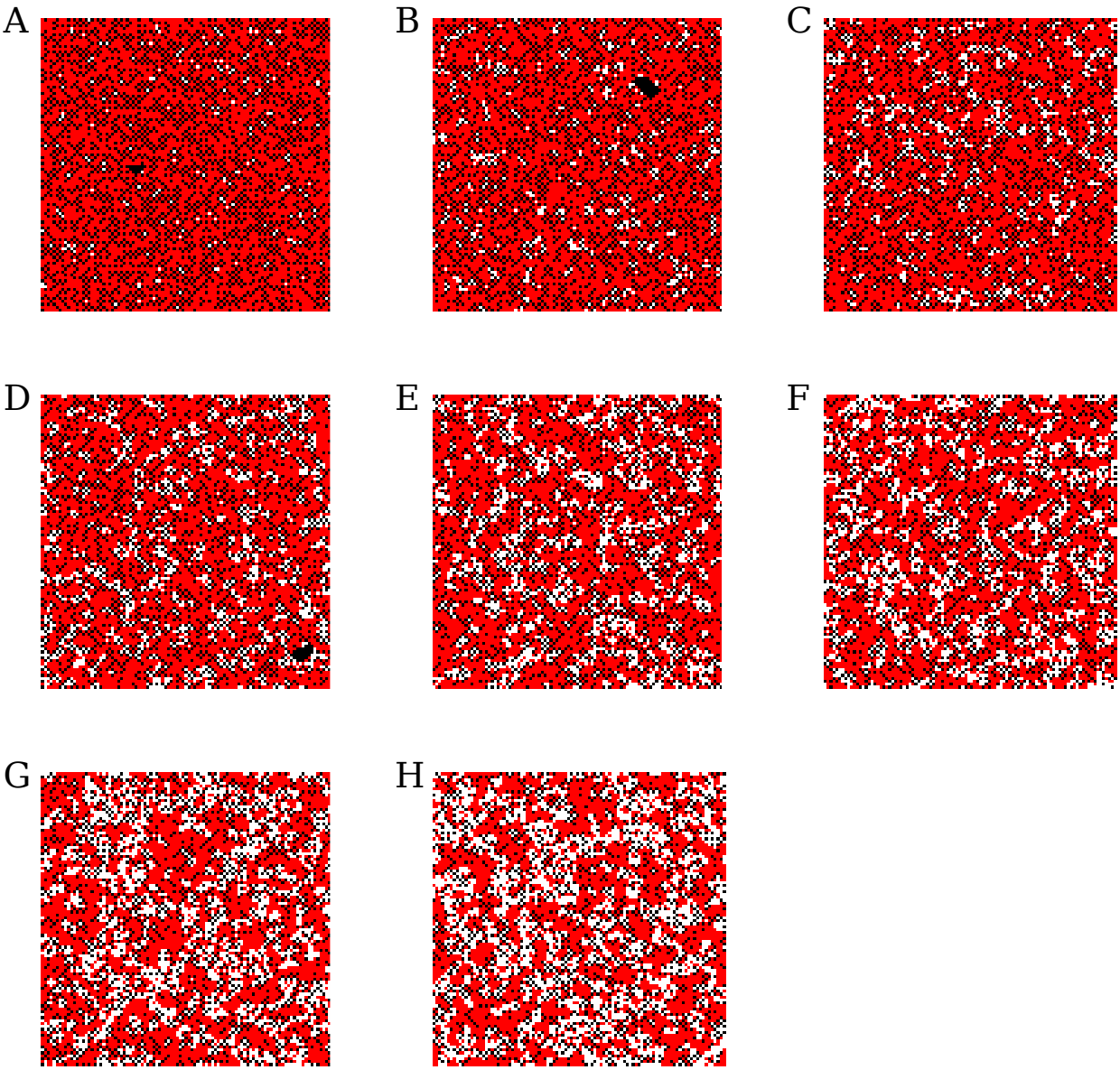

Figure 2.10: Characteristic final states for $r = 0.7$ and $T = 5$ for different v: **A**: $v = 2\%$, **B**: $v = 6\%$, **C**: $v = 10\%$, **D**: $v = 15\%$, **E**: $v = 20\%$, **F**: $v = 24\%$, **G**: $v = 28\%$, **H**: $v = 33\%$.

CHAPTER III

INVERTED BIOMASS PYRAMIDS AND REFUGES

3.1 Biomass Pyramids

A trophic pyramid is a hierarchical graphical representation of trophic levels in an ecosystem. A trophic level is a collection of organisms which consume organisms from the trophic level right below and are consumed by next higher trophic level. Figure 3.1 shows a typical trophic pyramid. There are two types of trophic pyramids: energy pyramids and biomass pyramids. Energy pyramids illustrate the energy flow in an ecosystem while the biomass pyramid illustrates the distribution of biomass between different trophic levels in an ecosystem [56, 66, 19]. In a typical ecosystem, only 10% of energy from a lower trophic level is available to a higher trophic level, the rest is devoted to metabolic processes [61]. Therefore, energy pyramids are always base heavy and narrow at the top.

A typical biomass pyramid is similar to an energy pyramid; a lower trophic level is heavier than a higher trophic level [17]. Base heavy biomass pyramids are usually found in terrestrial ecosystems like grasslands and forests. In special circumstances, we find inverted biomass pyramids where a light lower trophic level supports a heavier higher trophic level. Inverted biomass pyramids (IBP) have been found in freshwater planktons [56, 19, 54], marine planktons [6, 27] and recently in marine coral reefs [25, 69]. IBPs are rare and have received little attention in the ecological literature. We seek to answer the question: *when do inverted biomass pyramids occur and what effect do refuges have on biomass pyramids?*

Biologists suspect that IBPs occur in an ecosystem when the autotrophs (prey) reproduces at a high rate or the heterotrophs (predators) have a low turnover rate [56,

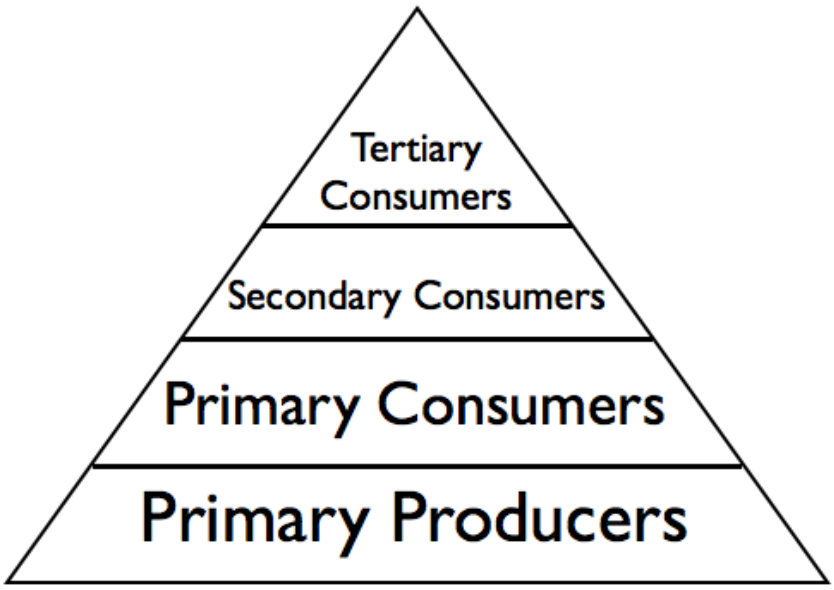

Figure 3.1: The typical biomass pyramid. The primary producers do not depend on other species in the ecosystem and survive on their own. The primary consumers feed upon the primary producers, the secondary consumers eat the primary consumers and the tertiary consumers feed upon the secondary consumers.

10, 19]. A prominent ecologist also believes that immigration of autotrophs may also influence the occurrence of IBPs [31]. The intuition of ecologists provides an essential component of the answer but it is incomplete. It excludes the role played by other environmental factors in mediating the interaction between predators and prey, specifically refuges.

Animals take refuge from predators in a variety of natural ecosystems [14, 75] such as burrows [13],trees [21] , cliff faces [4], thick vegetation [8] or rock talus [36]. Recently, scientists found inverted biomass pyramids in isolated marine coral reef ecosystem where coral reefs provide refuge for small prey fish [25, 69]. Refuges modulate predator-prey interaction in ecosystems in complex ways. Refuges provide a place for the prey to hide and can reduce the food available for predators. Our model of coral reefs is an example of such a situation. But refuges may also provide a place for prey to multiply safely. If the refuge is a suitable environment for prey to multiply safely, the refuge may end up increasing the food supply of predators overriding the protective aspect of the refuges. The structure of the biomass pyramid acutely depends on the role played by the refuge in directing the interaction between predators and prey.

We develop a general theory of biomass pyramids in the framework of predator-prey dynamics. The classical Lotka-Volterra model is our starting point, it is a useful model which confirms the intuition of ecologists about inverted pyramids [47, 81]. But the Lotka-Volterra model makes strong simplistic assumptions about the interaction between predators and prey. It assumes that predators and prey are well mixed in ecosystems, an assumption strongly violated in ecosystems where prey hide in refuges. We make our model more realistic by incorporating the effects of refuges on the interaction between predators and prey and derive the conditions under which the biomass pyramid is inverted. As the refuge can affect the feeding behavior of predators in different ways, our results show that refuges may facilitate or discourage

the existence of inverted biomass pyramids. On the other hand, the influence of immigrating prey is unequivocal, they support inverted biomass pyramids.

3.2 Lotka-Volterra model

The classical Lotka-Volterra model describes the interaction of a predators and prey species governed by the equations provided below. Although simplistic in its assumptions about the behavior of prey and predators, it has served as a useful framework in mathematical ecology for over 80 years. It assumes that the prey grow exponentially, predators die a at a constant rate, natural death of prey can be ignored and most importantly that predators and prey are well mixed. The simple Lotka-Volterra model contains important hints about the conditions which lead to an inverted biomass pyramid.

$$\frac{dx}{dt} = ax - bxy, \tag{3.1}$$

$$\frac{dy}{dt} = cbxy - dy, \tag{3.2}$$

where

x : prey biomass density, y : predator biomass density,

a : prey growth rate, b : per capita predation rate,

c : biomass conversion efficiency, d : predator death rate.

The interior equilibrium point $(x^*, y^*) = \left(\frac{d}{cb}, \frac{a}{b}\right)$ is neutrally stable (a center), at which the predator:prey biomass ratio is

$$\frac{y^*}{x^*} = \frac{ac}{d}. \tag{3.3}$$

The biomass pyramid is inverted when the biomass ratio is greater than 1. In context of the Lotka-Volterra model, an IBP occurs if and only if $ac > d$. This result

provides a mathematical foundation for the intuition of biologists that IBPs occur when a fast reproducing prey meets a slowly dying predator. But the result also shows that the role of the biomass conversion efficiency cannot be ignored.

The classical model assumes that the prey biomass available to the predators increases linearly. This is not realistic, the prey biomass available to predators is usually a nonlinear function of the prey biomass [35, 34]. We incorporate this assumption in the equation below.

$$\frac{dx}{dt} = ax - bf(x)y, \tag{3.4}$$

$$\frac{dy}{dt} = bcf(x)y - dy, \tag{3.5}$$

where $f(x)$ is the predation response function. It is continuously differentiable and strictly increasing. At the interior equilibrium point $(\hat{x}, \hat{y})$, the ratio $\hat{y}/\hat{x} = a/f(\hat{x})$, where $f(\hat{x}) = d/bc$. Thus the predator:prey biomass ratio is

$$\frac{\hat{y}}{\hat{x}} = \frac{ac}{d}. \tag{3.6}$$

The predation response function is unspecified and can model many different types of interactions between predators and prey. However, the conditions necessary for the the existence of an inverted biomass pyramid do not change and an IBP continues to occur when $ac > d$. It completely ignores the exact form of the functional response. But the condition $ac > d$ is no longer sufficient. The stability of the interior equilibrium point is now tied to the exact form of the functional response $f(x)$. As long as the equilibrium point is stable, an inverted biomass pyramid continues to occur when $ac > d$.

We now refine the assumptions made by the the Lotka-Volterra model about the interaction of predators and prey. First, the prey grow exponentially in the absence of predators. This is realistic only for low values of prey biomass. Second, the system is

closed. There is no immigration or emigration of prey or predators. Most importantly, the Lotka- Volterra model assumes that the predators and prey are well mixed. All prey biomass is equally available to the predators and predators consume a fixed percentage of the available prey. This is the *central* assumption in the model about the interaction between prey and predators and is not supported by evidence in most ecosystems. We refine each of these three assumptions in turn and determine the effect on the biomass pyramid.

The exponential growth of prey in absence of predators is realistic only for small values of prey biomass. As the prey biomass increases, intra-species competition for resources limits the growth of prey. The logistic function models this phenomena much better, the prey grow exponentially for low values values of prey biomass but slow down with an increase in biomass. The following equations incorporate logistic prey growth into the preceding predator-prey model.

$$\frac{dx}{dt} = ax\left(1 - \frac{x}{K}\right) - bf(x)y, \tag{3.7}$$

$$\frac{dy}{dt} = bcf(x)y - dy, \tag{3.8}$$

where K is the prey carrying capacity. The prey carrying capacity is the maximum prey biomass that can be sustained in an environment in the absence of predators.

The biomass ratio at the interior equilibrium point $(\tilde{x}, \tilde{y})$ is

$$\frac{\tilde{y}}{\tilde{x}} = \frac{ac}{d}\left[1 - \frac{f^{-1}(d/bc)}{K}\right]. \tag{3.9}$$

The addition of the logistic growth to the model changes the condition for the existence of an inverted biomass pyramid. An IBP will now occur only if $(ac/d)[1 - f^{-1}(d/c)/K] > 1$. The old condition $ac > d$ is no longer sufficient to produce an inverted biomass pyramid. Ecologically, this means that an inverted biomass pyramid may not occur even if an ecosystem has a fast growing prey and a slowly dying

predator. Unlike before, the exact form of the functional response $f(x)$ and the prey carrying capacity K now crucially influence the existence of the inverted biomass pyramid. In particular, an increase in the prey carrying capacity K supports an inverted biomass pyramid.

The prey biomass at equilibrium $\tilde{x} = f^{-1}(d/bc)$ and the predator biomass $\tilde{y} = \frac{ac}{d}\tilde{x}\left[1 - \frac{f^{-1}(d/bc)}{K}\right]$. As before, the predation functional response $f(x)$ is a strictly increasing function, thus the inverse function f^{-1} and the interior equilibrium point definitely exists as long as $f^{-1}(d/bc) < K$.

The prey biomass at equilibrium only depends on the biomass conversion efficiency c and the predator death rate d, and is independent of the prey growth rate a or the prey carrying capacity K. On the other hand, the predator biomass crucially depends on the the prey growth rate a or the prey carrying capacity K. A fast growing prey can provide more food to the predators and a large carrying capacity makes sure that the prey are growing rapidly without competing with each other for resources.

Our model still assumes that predators and prey are well mixed and refuges are not mentioned. The introduction of refuges sharply attacks this assumption and directly influences the occurrence of inverted biomass pyramids as we will show in the next section.

3.3 Refuges

Ecological modelers have studied the effect of refuges in the past by expanding the functional form of the predation response to include the effects of refuges. We introduce the concept of refuge size, the maximum prey biomass that can persist inside the refuge.

For example, the Holling Type III is one pre-existing model of a refuge at low prey population density [55]; the functional form is given by $f(x, n) = \frac{x^2}{n+x^2}$. Another method used by ecologists is to simply multiply $f(x)$ by $1 - r$ where $0 \leq r \leq 1$ serves

as a proxy for the refuge size [52, 74, 30, 39, 37, 45, 43]. However, these models of refuges suffer from two defects. First, the switch point of the predation response, the point where the predation rate rapidly starts increasing depends on the proxy refuge size and the half saturation constant. We prefer the functional form to be of the sort where the switch point depends solely on the refuge size. Second, predation response functions like Holling Type III were derived from specific ecological principles and describe a certain feeding pattern of predators. They have a clear mechanistic basis which does not include refuges. No model in the current ecological literature includes a refuge that is based on direct mechanistic principles.

We introduce a family of predator-prey models which include refuges explicitly and provide a direct relation between the functional form of the predation response and the feeding behavior of predators. We call these the **Refuge-modulated predator-prey (RPP) models**. In our models, the switch point of the predation rate depends solely on the refuge size. There are three classes of RPP models- Type I, II and III. Each type is associated with a different effect of the refuge size on the feeding rate of predators.

3.3.1 Refuge-modulated predator-prey (RPP) models

The equations describing RPP models are given below:

$$\frac{dx}{dt} = ax\left(1-\frac{x}{K}\right) - bf(x,r)y, \tag{3.10}$$

$$\frac{dy}{dt} = bcf(x,r)y - dy, \tag{3.11}$$

where r is the refuge size.

The function $f(x,r)$ is the refuge-dependent predation response. The refuge can affect the feeding behavior of predators in complex ways and the precise form of the predation response will reflect the effect of the refuge size on the feeding behavior of predators. For a given refuge size r, the function $f(x,r)$ is a monotonically increasing function. Therefore its inverse f_r^{-1} exists. The RPP model has 3 equilibrium points:

(0,0), (K,0) and the interior equilibrium point $(\bar{x}, \bar{y})$. The prey biomass at the interior equilibrium point is $\bar{x} = f_r^{-1}(d/bc)$ and the biomass ratio is

$$\frac{\bar{y}}{\bar{x}} = \frac{ac}{d}\left[1 - \frac{f_r^{-1}(d/bc)}{K}\right]. \tag{3.12}$$

The functional form of the biomass ratio is similar to the case of well mixed populations but the biomass ratio is now crucially dependent on the refuge size, it is no longer sufficient that $ac > d$ for an IBP to occur.

We have only placed minimal restrictions on the form of the predation response function and have not specified it with precision. The effect of the refuge size on the biomass ratio cannot be determined without specifying the predation response function. We refine our model by proposing three possible precise predation response functions based on ecological considerations.

3.4 RPP Type I

If the prey species hide in refuges for extended periods of time, opting for security and do not venture out to find food, a refuge would limit the prey available to to predators [62, 29, 65]. Consequently, the feeding rate of predators would be inversely correlated with the refuge size. We chose the following function as the predation response as it explicitly takes into account the role of the refuge. This function is a generalization of the predation function used to model the fish biomass structure at coral reefs.

$$f(x, r) = \frac{1}{1 + \beta e^{-\xi(x-r)}}. \tag{3.13}$$

The parameters β, ξ, r regulate the properties of the function $f(x, r)$. The parameter β determines the minimum possible predation rate. Consider the situation when there is no prey, x=0. The predation rate is now $\frac{b}{1+\beta}$. The minimum predation rate is very small, $\beta >> 1$ as in the absence of the main prey, predators switch to temporary alternative food supply. The refuge size r determines the switch point of

the predation rate. As the prey biomass approaches the refuge size, the predation rate rapidly increases. The rate of increase in the predation rate is reflected in the slope of the function and is controlled by the parameter ξ.

We are mainly concerned with the biomass ratio at the interior equilibrium point . The prey biomass at the interior equilibrium is $\bar{x} = f_r^{-1}(d/bc) = r-(1/\xi)\ln[(1/\beta)(bc/d-1)]$ and the predator biomass is $\bar{y} = a\bar{x}(1-\frac{\bar{x}}{K})/bf(\bar{x},r)$. The interior equilibrium points exists only when $bc > d$. This has a direct ecological interpretation, the product of the b and c represents the maximum prey biomass which is converted into predator biomass and d represents the rate at which predator biomass is lost. If the rate of replenishment is less than the loss rate, then situation is unsustainable and no equilibrium is possible.

3.5 RPP Type II

This model assumes that there is no effect of the refuge on the feeding behavior of predators, i.e. the function $f(x,r)$ is actually independent of the refuge size r. We chose the function:

$$f(x,r) = \frac{1}{1+\beta e^{-\xi x}}. \tag{3.14}$$

The parameters β, ξ play the same role as in the Type I model, β controls the minimum predation rate and ξ controls the slope of the sigmoid function.

3.6 RPP Type III

We hypothesize that refuges can sometimes aid the feeding habits of predators. When sufficient food is available in the refuge, prey can multiply within the refuge. Soon, the prey will be limited by the total resources available within the refuge and some prey will have to emigrate. The number of emigrating prey will positively depend on the refuge size and the emigrating prey will provide food to the predators. Elks in the Yellowstone demonstrate this kind of behavior. Elk refuge provide protection

and food to elk during winter (97% of elk survive [48]). The survivors emigrate out of the refuge and are a source of food for predators in the Yellowstone National Park and surrounding areas [76].

We use the following function to represent this feeding behavior:

$$f(x,r) = \frac{1}{1+\beta e^{-\xi(x+r)}}. \tag{3.15}$$

The predation function is similar to the Type I predation function but we interpret the terms differently. We divide the prey biomass into two categories: variable x represents the prey biomass inside the refuge and r represents the prey biomass outside the refuge. We implicitly assume that predators feed on the prey available inside and outside the refuge.

The prey biomass at the interior equilibrium point is $\bar{x} = f_r^{-1}(d/bc) = -r + (1/\xi)\ln[\beta d/(bc-d)] > 0$. As in Type I, the interior equilibrium point exists only when $bc > d$. However, the refuge size also determines the existence of an equilibrium point, there is an upper threshold for the refuge size. The maximum possible refuge size $\bar{r} = (1/\xi)\ln[\beta d/(bc-d)] > 0$ given that $bc > d$.

The three RPP type models share some common features. We assume a small predation response even when there are no prey, i.e. $f(0,r) > 0$. This is reasonable since predators switch to temporary alternative prey when the primary prey is not available [82, 57, 41, 23]. Mathematically, this can lead to negative prey biomass which is ecologically meaningless. Therefore we associate a negative prey biomass with the extinction of prey. Of course, we can fine tune the minimum predation rate according to the ecosystem at hand by changing β. We note again that the switch point of the predation response function, the point where the predation rapidly increases depends solely on the refuge size, a key strength of our model.

3.7 Dependence of biomass ratio on the refuge size

The three RPP models correspond to three possible effects of the refuge size on the feeding habits of predators. There is a close connection between the feeding habits of predators and the biomass ratio, therefore the refuge size can have three possible effects on the biomass ratio.

The biomass ratio for all three RPP type models is given by the general expression

$$\frac{\bar{y}}{\bar{x}} = \frac{ac}{d}\left[1 - \frac{f_r^{-1}(d/bc)}{K}\right]. \tag{3.16}$$

When $\frac{ac}{d}\left[1 - \frac{f_r^{-1}(d/bc)}{K}\right] > 1$, the biomass pyramid is inverted else it is standard.

For a RPP Type I model, $f_r^{-1}(d/bc) = r + (1/\xi)\ln[\beta d/(bc-d)]$. The inverse is an increasing function of the refuge size. Therefore, the biomass ratio is a decreasing function of the refuge size. Ecologically, a larger refuge size means a much larger space for the prey to hide and much fewer prey available to the predators. There the *refuge size is inversely correlated with the biomass ratio.*

For the RPP Type II model, the inverse of the predators response function is independent of the refuge size. As the refuge size has no effect on the feeding habits of predators, the refuge size has no effect on the biomass ratio.

For the RPP Type III model, $f_r^{-1}(d/bc) = r + (1/\xi)\ln[\beta d/(bc-d)]$. The inverse is an decreasing function of the refuge size. Therefore, the biomass ratio is an increasing function of the refuge size. In an RPP Type III model, the refuge provides a place for prey to grow, multiply and also provides a feeding ground for predators, thus the *refuge size is positively correlated with the biomass ratio.*

Figure 3.2 summarizes the effect of effect of refuges on the biomass ratio in the three RPP models.

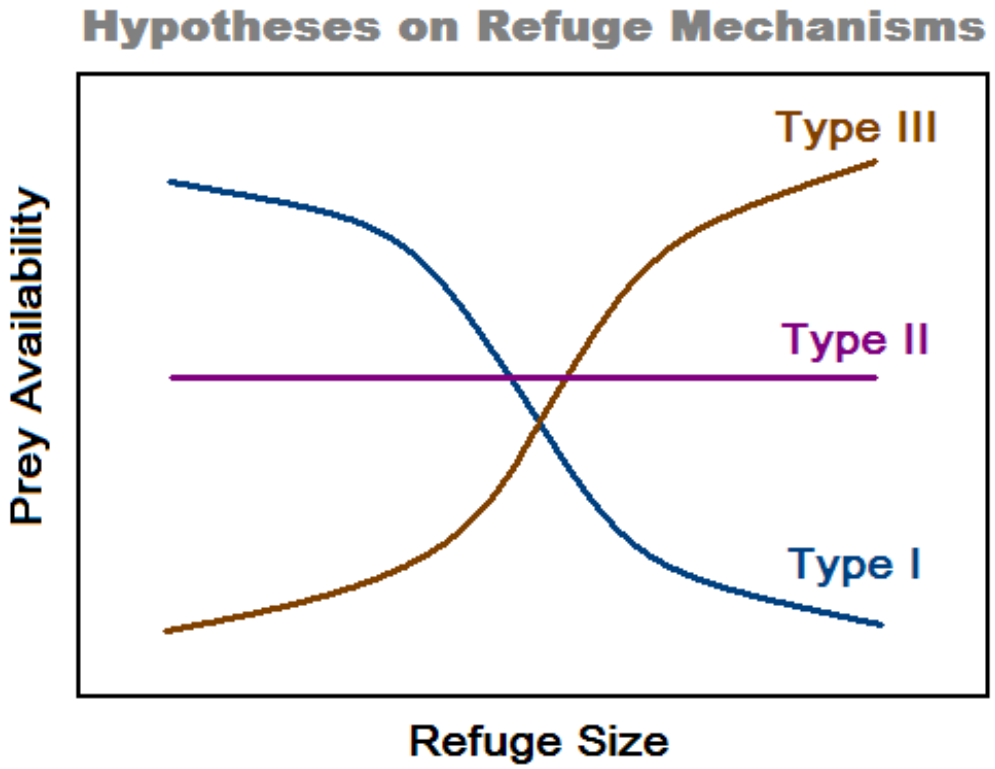

Figure 3.2: Three biological hypotheses for the effects of the refuge size on the prey availability for predators. Type I: the prey available for predators is a decreasing function of the refuge size, because the refuge provides places for prey to hide from predators. Type II: the prey available for predators is independent of the refuge size in the sense of density (per unit area), because in a number of cases prey biomass is proportional to the refuge size. Type III: the prey available for predators is an increasing function of the refuge size, because the refuge both provides prey to predators and stores prey for latter consumption by predators.

3.8 Immigration

Reef ecologists observe significant immigration of prey fish in a North Carolina coral reef and believe that this may have significant effect on the biomass pyramid [31]. We consider two possible effects of immigration: immigrating prey fish adapt to the local environment and stay permanently or they move on after a temporary period during which some of them are food for predators. We build these two possibilities into the Lotka-Volterra model for purposes of pedagogical clarity but we obtain qualitatively similar results for the RPP models.

3.8.1 Prey are permanent residents

$$\frac{dx}{dt} = ax - bxy + \theta, \tag{3.17}$$

$$\frac{dy}{dt} = cbxy - dy; \tag{3.18}$$

where θ models immigration.

The biomass ratio at the interior equilibrium point $(\tilde{x}, \tilde{y})$ is

$$\frac{\tilde{y}}{\tilde{x}} = \frac{ac}{d} + \theta\frac{c^2b}{d^2}. \tag{3.19}$$

The biomass ratio at the interior equilibrium point in the classical Lotka-Volterra model without immigration is ac/d. When we incorporate the effect of immigrating prey which settle down at the ecosystem, the biomass ratio increases.

3.8.2 Prey are temporary aliens

In this model, the prey only stay temporarily and contribute to the food supply for the predators but do not add anything to the prey biomass.

$$\frac{dx}{dt} = ax - bxy, \tag{3.20}$$

$$\frac{dy}{dt} = cb(x + \hat{\theta})y - dy; \tag{3.21}$$

where $\hat{\theta}$ models the food supplied to the predators by the temporary visiting prey.

The biomass ratio at the interior equilibrium point $(\hat{x}, \hat{y})$ is

$$\frac{\hat{y}}{\hat{x}} = \frac{ac}{d - \hat{\theta}cb}. \tag{3.22}$$

The temporary prey again boost the biomass ratio as compared to the classical Lotka-Volterra model. We find qualitatively similar results for the RPP model. To conclude, *immigrant prey increase the possibility of the inverted biomass pyramid.*

3.9 Discussion

Our RPP models are based on a set of simplifying assumptions. We only model the interaction between two trophic levels in a trophic pyramid and do not discuss intra-trophic predation, predators who eat species at multiple trophic levels. The addition of these would change the precise conditions under which an inverted biomass pyramid would occur.

Our models also suffer from a mathematical defect, it is not first quadrant invariant. It could be made invariant if the predation response function satisfied some conditions: (i)$f(x, r)$ is continuously differentiable in x and r (ii) $f(0, r)$ =0 (iii) $\partial f/\partial x > 0$; (iv) $\partial^2 f/\partial x^2 < 0$ for sufficiently large x; (v) the refuge size r solely determines the shift of the predation curve. We are currently unable to find a closed-form expression for such a function.

The current RPP models divide the influence of refuges into three distinctly separate categories: Type I, II and III. These three categories represent only three points on a spectrum of possibilities, at one end Type I inhibits the food supply of predators, while Type III increases the food supply of predators and Type II is right in the middle. We can represent every possibility on the spectrum by expanding the RPP models through the equations below.

$$f(x, r) = \frac{1}{1 + \beta e^{-\xi(x+\eta r)}}, \tag{3.23}$$

where $-1 \leq \eta \leq 1$.

When $-1 \leq \eta < 0$, the model is close to RPP Type I, close to RPP Type III when $0 < \eta \leq 1$ and is RPP Type II when $\eta = 0$.

CHAPTER IV

CORAL REEFS

4.1 Introduction

Coral reef ecosystems around the world are under threat from global warming, rising acidity of ocean waters, local effects of overfishing, pollution, diseases and shoreline development [2, 38, 60, 33, 40]. There is significant interest in stabilizing and restoring damaged reefs, and first steps include understanding the functioning of reefs in their natural state and examining the effects of fishing. Some reef ecologists believe that the isolated Kingman and Palmyra reefs represent the natural state of coral reefs [42], and thus provide a baseline for natural reefs. The coral cover at these two pristine reefs is far more extensive and healthier than at conventional reefs; these reefs seem to be resilient to ocean warming and rising acidity [68].

At Kingman, it was recently discovered that apex predators constitute 85% of the total fish biomass [68, 20]. This is in sharp contrast to most reefs, where the prey biomass substantially dominates the total fish biomass [68]. Thus the biomass pyramid is dramatically inverted at Kingman. Figure 4.1(a) from Kingman shows apex predators such as sharks, jacks and snappers roaming the reef while smaller prey are hiding in the coral. Figure 4.1(b) shows Tabuarean, a conventional reef where fishing is practiced: small prey fish are abundant and apex predators are rare.

We aim to answer the questions: *why do inverted pyramids occur at pristine coral reefs and why do they become non-inverted at conventional reefs?*

We build a model which explicitly incorporates a 'prey refuge' where the refuge size influences predator hunting patterns (predation response). With realistic parameter values, our consumer-resource model with refuge yields an inverted biomass

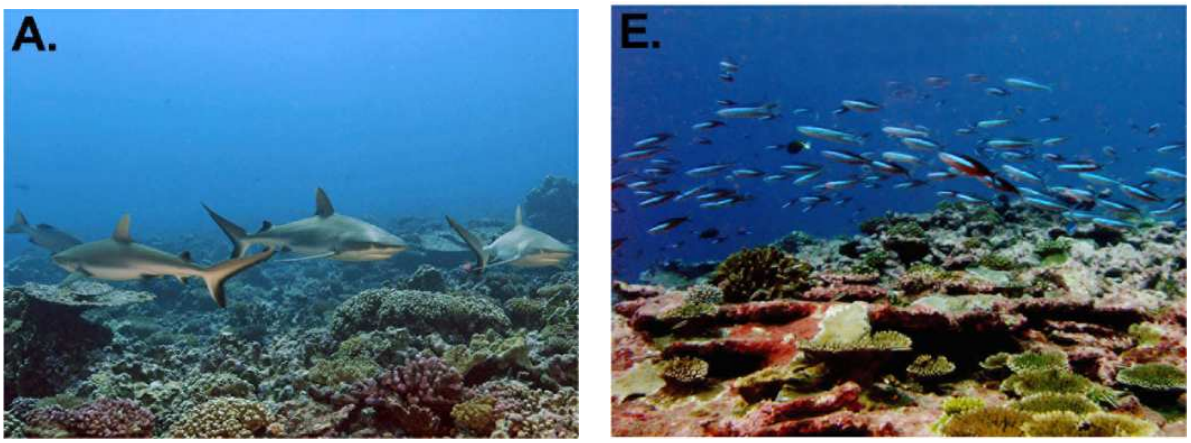

(a) (b)

Figure 4.1: Comparison of situations at Kingman , a pristine coral reef and Tabuarean, a conventional reef where fishing is practiced [68].

pyramid. We believe that refuges provide a general new mechanism in ecology to create an inverted biomass pyramid, that does not require mass action interactions between predators and prey.

At the pristine reefs, the investigators speared many predators and almost always found their stomaches nearly empty [59]. Therefore, we believe that evolution favors predators having higher biomass conversion efficiency. An increase in coral cover may provide prey with more hiding spaces, making them harder to catch, and forcing only the more efficient predators to survive. We discuss the additional consequences of assuming that predators at coral reefs with larger benthic coral cover were selected for higher biomass conversion efficiency. In this case, we find that the predator-prey biomass ratio is an increasing function of coral cover; this is supported by data from Kingman and Palmyra [68].

Overfishing is believed to play a major role in reef degradation, but few mechanisms are understood. We add various forms of fishing to our model, and show that sufficiently high fishing pressure, for quite general types of fishing, transforms the inverted biomass pyramid to be bottom heavy. We also show that prey fishing alone has the same effect.

4.2 Derivation of the Model

Guided by field observations at pristine Kingman and Palmyra coral reefs, we derive a model for the biomass of coral reef fishes using a pair of differential equations.

Following Sandin et al [68], we classify reef fishes as prey or predators. Prey fish eat plankton and algae and hide from predators in coral holes [59, 68, 32, 7]. We assume that prey biomass grows logistically and (per capita predator) predation rate depends on prey biomass and availability of coral holes to hide. Predators grow by eating prey fish and die a natural death at pristine reefs.

Prey fish find 'refuge' in coral holes and rarely venture out of the holes at Kingman [59]. Therefore, the availability of hiding space for prey in coral holes affects predator hunting patterns and thus the biomass pyramid. We define the 'refuge size' as the maximum prey biomass which can sustainably hide in coral holes, i.e. the coral-specific prey carrying capacity in presence of predators [16]. We distinguish the refuge size from the prey carrying capacity in absence of predators (K); the prey will not be forced to stay inside the holes when the predators are absent and the reef can support a much greater prey biomass. We assume that the refuge size is an increasing function of coral cover at pristine reefs. The equations describing such a community are

$$\dot{x} = ax\left(1 - \frac{x}{K}\right) - bf(x,r)y, \tag{4.1}$$

$$\dot{y} = cbf(x,r)y - dy. \tag{4.2}$$

x : prey biomass density (kg/m^2),

y : predator biomass density (kg/m^2),

a : prey growth rate (/day),

b : maximum predation rate: maximum prey biomass,
hunted per kg of predator biomass (/day),

K : prey carrying capacity in absence of predators (kg/m^2),

r : refuge size (kg/m^2),

$f(x,r)$: predation response,

c : biomass conversion efficiency,

d : predator death rate (/day).

The estimated annual mortality rates of small reef fish can be as high as 5-6 [44, 84], suggesting that in the absence of predation, prey fish can double in 2-3 months. Therefore, we estimated the prey growth rate, a=0.0048/day. Predator death rate (d=0.0005/day) was estimated using the equation: d = -ln (0.01)/longevity [53], with the estimated longevity for grey reef shark of 25 years [26]. We set prey carrying capacity at K=1 kg/m^2, roughly seven times the maximum prey biomass measured at Kingman reef [20]. We set the biomass conversion efficiency (c) to 0.15, a reasonable estimate given that conversion efficiencies are higher in marine versus terrestrial environments [1]. Predation rates of 12% predator body weight per day have been documented for smaller sedentary predators [80], suggesting that rates for active predators would be higher. We therefore set the maximum predation, b=0.8/day.

The predation response function $f(x, r)$ should have the following properties. It should be a monotonically increasing function of prey biomass. When the prey biomass is less than the refuge size, it should be small. When prey biomass approaches refuge size, it should rapidly increase and approach a constant as prey biomass greatly exceeds the refuge size; thus forming an S shaped curve. Since corals limit the food supply of predators, RPP Type I predation response is the appropriate response function. The predation function

$$f(x, r) = \frac{1}{1 + e^{-10(x-r).}} \tag{4.3}$$

Figure 4.2 is a plot of $f(x, r)$ for fixed refuge size of 2 kg/m^2.

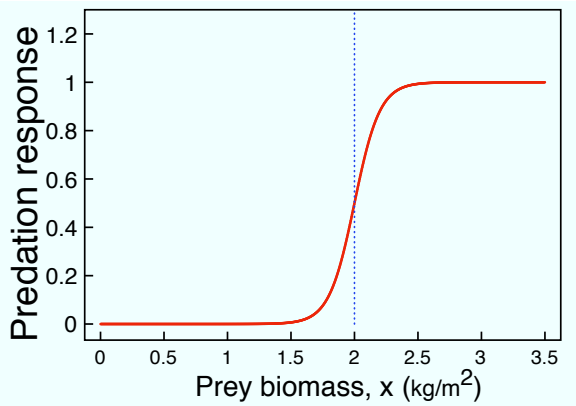

Figure 4.2: Predation function $f(x, r)$ vs biomass of prey for fixed refuge size $r =$ 2 kg/m^2.

4.3 Results

The model has three equilibrium points. The unstable equilibrium point, $x = 0,\ y = 0$ corresponds to a reef with no fish. The equilibrium point $x = K,\ y = 0$ corresponds to the absence of predators and is rarely seen in reefs. The third and the most interesting

equilibrium point, which we call the interior equilibrium point is

$$x^*(r) = r - \frac{1}{10}\ln\left(\frac{bc}{d} - 1\right), \tag{4.4}$$

$$y^*(r) = \frac{ac}{d}x^*\left(1 - \frac{x^*}{K}\right). \tag{4.5}$$

This equilibrium point is locally attractive for the refuge size between 0.6-0.85 kg/m^2. The predator-prey biomass ratio at the third equilibrium point is

$$\frac{y^*(r)}{x^*(r)} = \frac{ac}{d}\left(1 + \frac{1}{10K}\ln(\frac{bc}{d} - 1) - \frac{r}{K}\right). \tag{4.6}$$

As$\frac{1}{10K}\ln(\frac{bc}{d} - 1) > 0$,

$$\frac{y^*(r)}{x^*(r)} \geq \frac{ac}{d}\left(1 + \frac{1}{10K}\ln(\frac{bc}{d} - 1) - \frac{0.85}{K}\right) \geq 1.004 \tag{4.7}$$

when $\quad 0.65 \leq r \leq 0.85.$

Therefore the biomass pyramid is *inverted* for all refuge sizes between 0.65 and 0.85 kg/m^2. As an example, the biomass ratio is 1.22 at a coral reef with a refuge size of 0.7 kg/m^2.

4.4 Effects of Fishing

It is believed that fishing can dramatically change the biomass ratio; the fish biomass pyramid becomes bottom heavy at reefs with fishing [68, 40]. We add fishing to our model and show that sufficiently high fishing pressure will destroy the inverted pyramid. Destruction of the inverted pyramid in presence of predator fishing is direct, but we show that prey fishing alone will also destroy the inverted biomass pyramid.

As an illustrative example, we assume that predator fishing rate is proportional to the predator biomass and prey fishing is similar to predator hunting. We understand that this is not the only form of prey fishing and thus we further show that our results

are qualitatively robust to changes in forms of prey fishing. The model equations incorporating fishing are

$$\dot{x} = ax\left(1-\frac{x}{K}\right) - b\frac{y}{1+e^{-10(x-r)}} - b\frac{q}{1+e^{-10(x-r)}} \tag{4.8}$$

$$\dot{y} = cb\frac{y}{1+e^{-10(x-r)}} - dy - ly. \tag{4.9}$$

The prey and predator biomass at the interior equilibrium point are

$$\tilde{x}(r,l) = r - \frac{1}{10}\ln\left(\frac{bc}{(d+l)} - 1\right), \tag{4.10}$$

$$\tilde{y}(r,l) = \frac{ac}{(d+l)}\tilde{x}(r,l)\left(1-\frac{\tilde{x}(r,l)}{K}\right) - q. \tag{4.11}$$

The new predator-prey biomass ratio at the interior equilibrium point is

$$\frac{\tilde{y}(r,l)}{\tilde{x}(r,l)} = \frac{ac}{d+l}\left(1-\frac{\tilde{x}(r,l)}{K}\right) - \frac{q}{\tilde{x}(r,l)}, \tag{4.12}$$

$$\text{with} \quad \tilde{x}(r,l) = r - \frac{1}{10}\ln\left(\frac{bc}{(d+l)} - 1\right). \tag{4.13}$$

We plot the predator-prey biomass ratio for various refuge sizes and fishing rates in Figure 4.3.

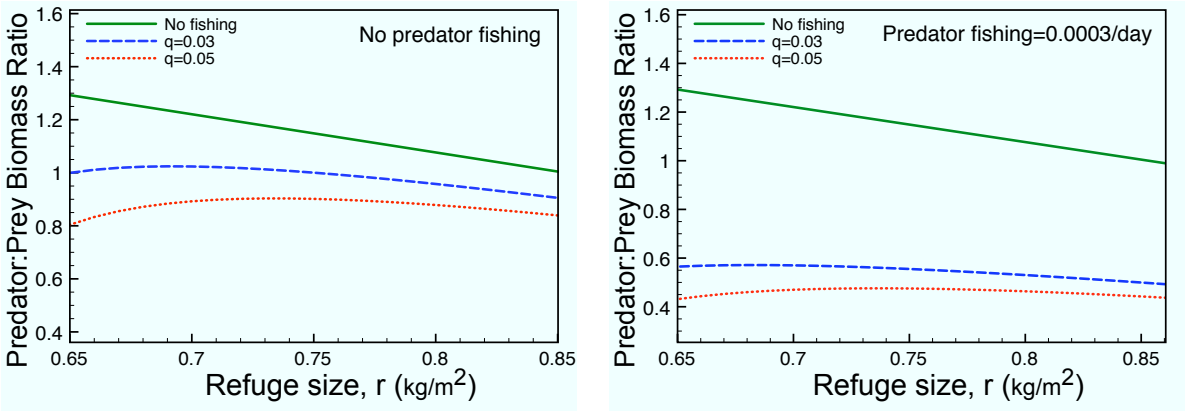

(a) (b)

Figure 4.3: Predator-prey biomass ratio as a function of refuge size with different rates of prey fishing (q). Parameters: $a = 0.0048, K = 1.0, b = 0.8, d = 0.0005$, predator fishing rate: (a) $l = 0$; (b) $l = 0.0003$.

We can now deduce the effect of fishing on the predator-prey biomass ratio by inspecting Figure 4.3 and comparing equation (4.12) with equation (4.6): *the predator-prey biomass ratio is a decreasing function of fishing pressure and the biomass pyramid becomes bottom heavy (ratio less than unity) at conventional coral reefs where high fishing pressure is experienced*. Figure 4.3(a) shows that the biomass ratio decreases even with prey fishing only and this makes the pyramid bottom heavy.

Our results are independent of the form of prey fishing. Let $p(x)$ be the general prey fishing rate. The modified equations are

$$\dot{x} = ax\left(1-\frac{x}{K}\right) - b\frac{y}{1+e^{-10(x-r)}} - p(x) \tag{4.14}$$

$$\dot{y} = cb\frac{y}{1+e^{-10(x-r)}} - dy - ly. \tag{4.15}$$

The predator-prey biomass ratio at the interior equilibrium point is

$$\frac{\tilde{y}(r,l)}{\tilde{x}(r,l)} = \frac{ac}{d+l}\left(1+\frac{1}{10K}\ln(\frac{bc}{d}-1)-\frac{r}{K}\right) - \frac{c}{d+l}\frac{p(\tilde{x})}{\tilde{x}} \tag{4.16}$$

$$\frac{\tilde{y}(r,l)}{\tilde{x}(r,l)} \leq \frac{ac}{d}\left(1+\frac{1}{10K}\ln(\frac{bc}{d}-1)-\frac{r}{K}\right) = \frac{y^*(r)}{x^*(r)}. \tag{4.17}$$

As a result of fishing, the predator-prey biomass ratio is less than the biomass ratio at reefs without fishing. This result is robust under different forms of fishing.

As another example of prey fishing, if the prey fishing rate is proportional to prey biomass, $p(x) = vx$, the predator-prey biomass ratio

$$\frac{\tilde{y}(r,l)}{\tilde{x}(r,l)} = \frac{ac}{d+l}\left(1-\frac{\tilde{x}}{K}\right) - \frac{c}{d+l}v. \tag{4.18}$$

This is less than the biomass ratio for the model without fishing in Equation (4.6) and high fishing pressure will destroy the inverted biomass pyramid.

4.5 Adaptive biomass conversion

When the investigators in [68] examined the stomaches of the predators, they were almost empty. This suggests that predators are usually hungry and have adapted to survive on low food supply. Reefs with greater refuge size provide more space for prey to hide and prey may be harder to catch at such reefs. Cushing [15] found copepod conversion efficiencies were higher in areas of low versus high food resources. Similarly, predators with higher biomass conversion efficiency should be evolutionarily favored at reefs with greater refuge size. The biomass conversion efficiency $c(r)$ would be small when no refuge exists, increase with refuge size and approach a constant for large refuge sizes. We use the simple function

$$c(r) = \left(0.1 + \frac{0.2r^{12}}{0.1 + r^{12}}\right) \tag{4.19}$$

shown in Figure 4.4.

The modified biomass equations describing the community are

$$\dot{x} = ax\left(1 - \frac{x}{K}\right) - b\frac{y}{1 + e^{-10(x-r)}} \tag{4.20}$$

$$\dot{y} = \left(0.1 + \frac{0.2r^{12}}{0.1 + r^{12}}\right) b\frac{y}{1 + e^{-10(x-r)}} - dy, \tag{4.21}$$

and the biomass ratio at the interior equilibrium is

$$\frac{y^*}{x^*} = \frac{a}{d}\left(0.1 + \frac{0.2r^{12}}{0.1 + r^{12}}\right)\left(1 + \frac{1}{10K}\ln(\frac{bc}{d} - 1) - \frac{r}{K}\right). \tag{4.22}$$

We plot the dependence of the predator-prey biomass ratio on the refuge size in Figure 4.5. The predator-prey biomass ratio is now an increasing function of refuge size, a prediction supported by data from Kingman and Palmyra. The coral cover at Kingman is more extensive than Palmyra. Predators constitute 85% of

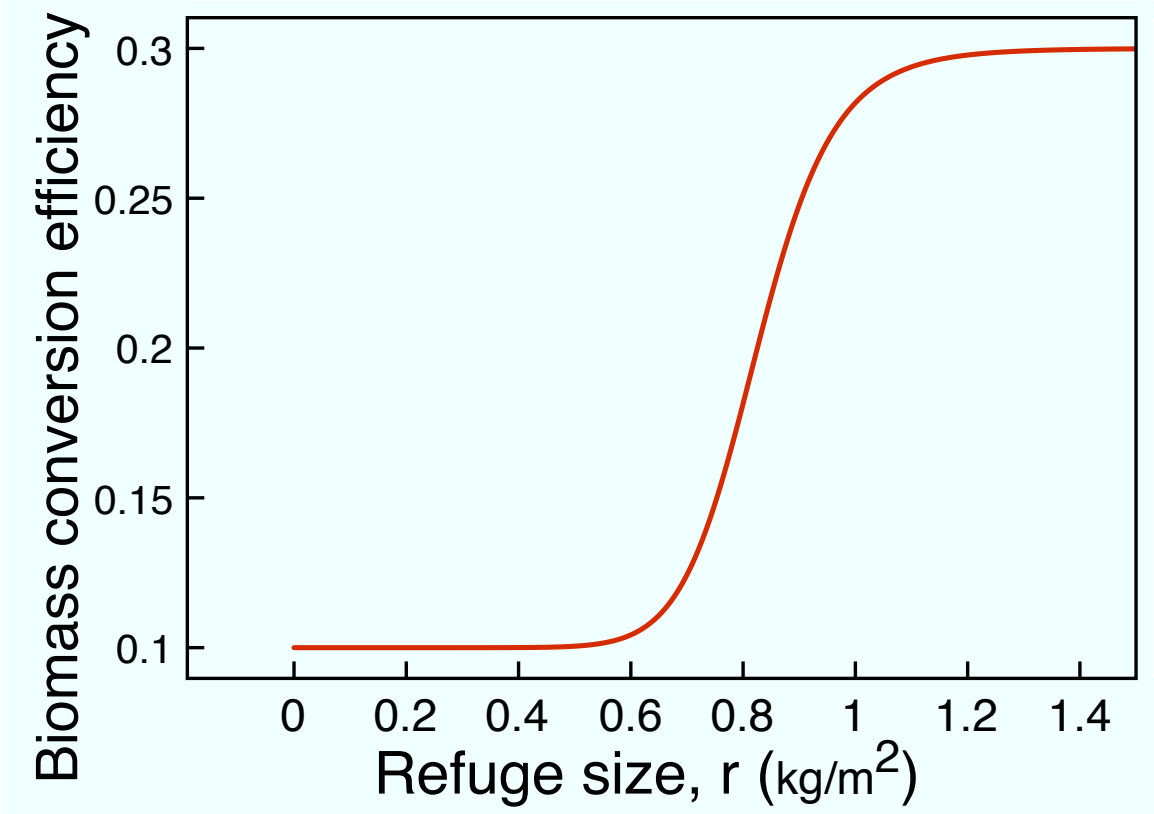

Figure 4.4: Monotonically increasing biomass conversion efficiency $c(r)$

the fish biomass at Kingman while they constitute only 66% of the fish biomass at Palmyra [68].

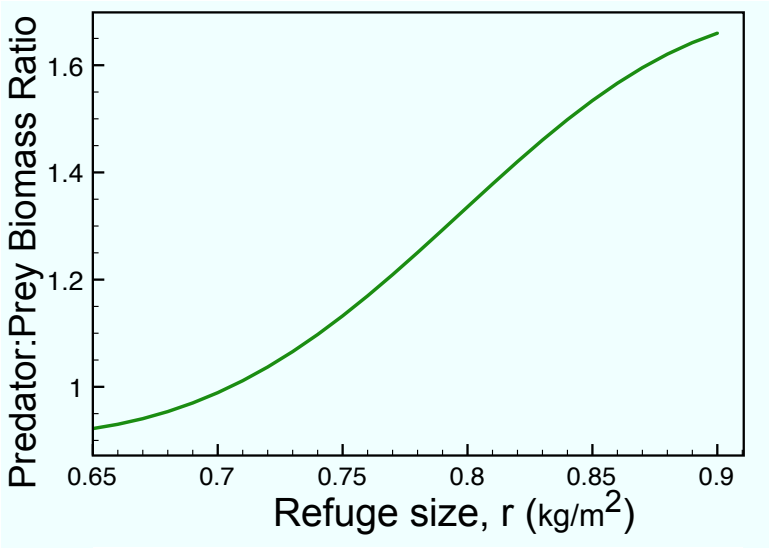

Figure 4.5: Predator-prey biomass ratio is an increasing function of refuge size when the biomass conversion efficiency c(r) is an increasing function of the refuge size.

It is easy to prove that the predator-prey biomass ratio cannot be an increasing function of the refuge size without the assumption that the biomass conversion efficiency is an increasing function of refuge size. To explain this, consider the predator-prey biomass ratio from Equation (4.6). It is a decreasing function of refuge size as long as the biomass conversion efficiency is constant.

We showed in Section 4 that the predator-prey biomass ratio is a decreasing function of fishing pressure. This result is robust and does not change if the biomass conversion efficiency of predators becomes a function of the refuge size. We plot the predator-prey biomass ratio as a function of fishing pressure in Figure 4.6. The predator-prey biomass ratio remains a decreasing function of fishing pressure and sufficiently high fishing pressure destroys the inverted biomass pyramid.

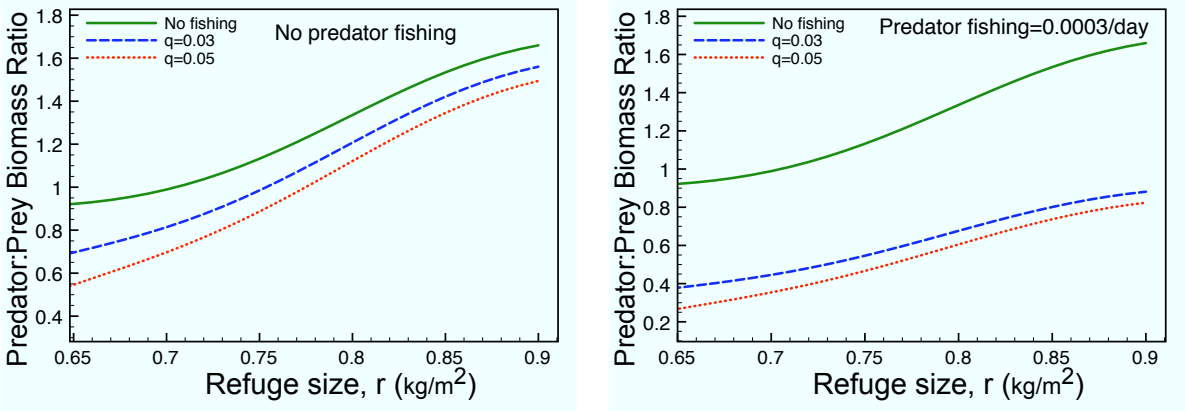

(a) (b)

Figure 4.6: Predator-prey biomass ratio as a function of refuge size with different rates of fishing. Parameters: $a = 0.0048, K = 1, b = 0.8, d = 0.0005$, predator fishing rate: (a) $l = 0$; (b) $l = 0.0003$. In both cases, the biomass ratio is a decreasing function of fishing pressure.

4.6 Discussion

In this chapter, we model the influence of coral cover on fish biomass dynamics. Our principal results are as follows. We provide a mechanistic explanation of the inverted biomass pyramid observed at Kingman and Palmyra [40, 59, 68]. We show that sufficiently high fishing pressure will destroy the inverted pyramid under general fishing conditions. We show that prey fishing alone will have this effect.

Coral holes are essential to our model as prey fish at pristine reefs take"refuge" in coral holes from predators and were rarely observed to leave the holes [68]. Prey fish also practiced "hot-bunking", i.e. if one prey fish left a hole, another immediately occupied that hole [59]. The predators' stomaches were usually found to be almost empty on spearing and the predators were observed to attack any available fish [68]. Our model assumes that the refuge size crucially affects predation response. However, no empirical evidence for the exact form of this influence currently exists. An increase in coral cover (greater refuge size) may make prey more difficult for predators

to catch, forcing only efficient predators to survive. Cushing [15] hypothesized a similar mechanism to explain the higher conversion efficiencies he measured in copepods with low food resources compared to copepods with abundant food. If we assume that predators with higher biomass conversion efficiency will be evolutionarily selected at reefs with greater refuge size, we find that the predator-prey biomass ratio is an increasing function of refuge size. This relationship is supported by data from [68] comparing Palmyra and Kingman, although this evolution assumption has not been tested experimentally.

There are two necessary conditions in our model to ensure inverted biomass pyramids. First, prey growth rate should be much higher than predator growth rate. Second, predator death rate should be low. Both conditions are satisfied at pristine reefs where apex predators such as sharks can live up to 20 years and reproduce rarely [77] and smaller prey fish can reproduce at least 3 times a year [78]. The importance of high prey productivity and predator longevity to inverted biomass pyramids has been noted before [18].

When the fishing pressure is high, the inverted biomass pyramid disappears (see Figure 4.6). This is consistent with field observations where reefs with fishing exhibit a non-inverted bottom heavy pyramid [68]. Our model shows that the biomass ratio decreases when either predator or prey fishing or a combination of both takes place. Our model shows that prey fishing alone will have the same effect.

CHAPTER V

BIFURCATIONS AT CORAL REEFS

5.1 Local bifurcation

The phase portrait of our model of coral reefs qualitatively changes three time as the refuge size changes from 0 kg/m^2 to 1 kg/m^2. We end the variation at 1 kg/m^2 as the prey carrying capacity of the prey has been set to 1 kg/m^2 and the refuge size cannot exceed the prey carrying capacity.

Our model of the biomass pyramid at coral reefs has three equilibrium points: $(0,0), (K,0)$ and $(\bar{x},\bar{y})$. The boundary equilibrium points $(0,0)$ and $(K,0)$ are always unstable (refer to Appendix A for a detailed local stability analysis). The interior equilibrium point $(\bar{x},\bar{y})$ exhibits a richer behavior, it is in turn unstable, a stable focus and a stable node. Figure 5.1 summarizes the changes in the stability of $(\bar{x},\bar{y})$.

The equilibrium point $(\bar{x},\bar{y})$ is unstable until the refuge is 0.639 kg/m^2 and then transitions to a stable focus. A quasi-bifurcation takes place when the refuge size is 0.695 kg/m^2 and $(\bar{x},\bar{y})$ becomes a stable node. The transition from an unstable focus to a stable focus suggests a Hopf bifurcation. Indeed, an unstable periodic orbit is born and Figure 5.2 shows the unstable periodic orbit when the refuge size is 0.64 kg/m^2. The region enclosed by the unstable periodic orbit is the attracting basin of the equilibrium point. The size of the attracting basin has an important ecological interpretation. If the coral reef is perturbed, say by fishing, such that the predator and prey biomass shifts to a point away from the equilibrium, but within the attracting basin, the reef will recover its equilibrium biomass ratio. But if a coral reef is rapidly fished such that predator and prey biomass shifts outside the attracting basin, *the reef will never recover its equilibrium biomass ratio.*

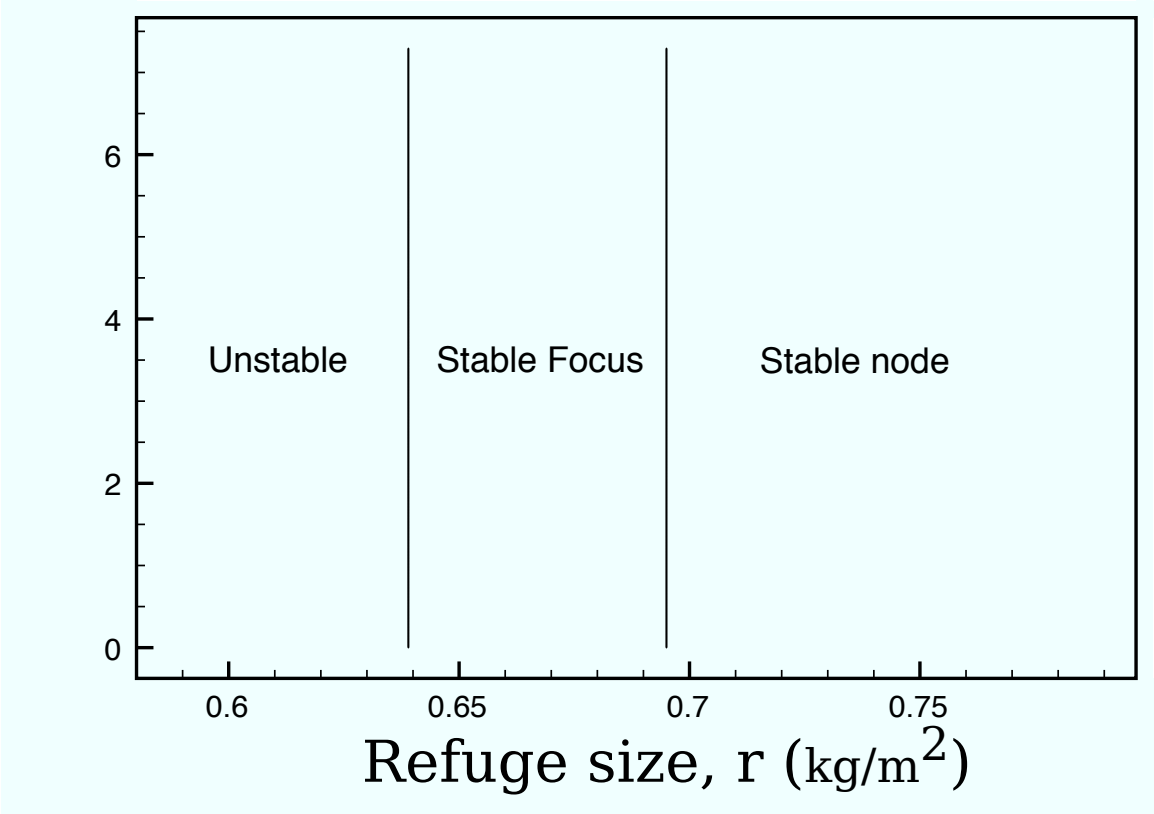

Figure 5.1: Stability of interior equilibrium point $(\bar{x}, \bar{y})$.

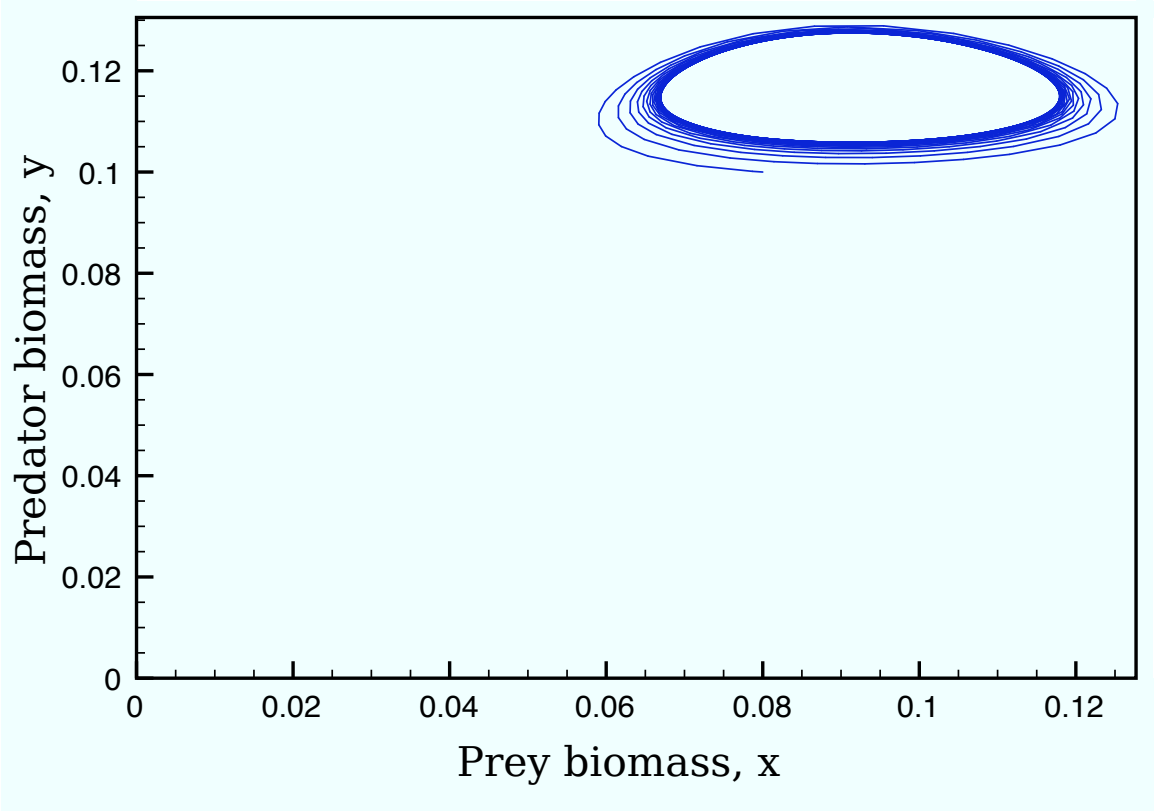

Figure 5.2: Backward trajectory starting from (0.08,0.1) for a refuge size 0.639 kg/m^2 approaches a limit cycle.

MATCONT computes the first Lyapunov co-efficient at the Hopf bifurcation; it is 0.124. Since the first Lyapunov co-efficient is positive, the Hopf bifurcation is subcritical. We no longer find the unstable periodic orbit when $(\bar{x}, \bar{y})$ becomes a stable node indicating a global change in the phase portrait.

5.2 Global bifurcation

A closer numerical investigation shows that the periodic orbit does not disappear during the transition from a focus to a node, it occurs much earlier when the equilibrium point is still a stable focus. Figure 5.2 shows the periodic orbit when the refuge size is 0.64 kg/m^2. The periodic orbit expands rapidly as the refuge size increases to 0.645 kg/m^2 (see Figure 5.3) and disappears completely at 0.653 kg/m^2.

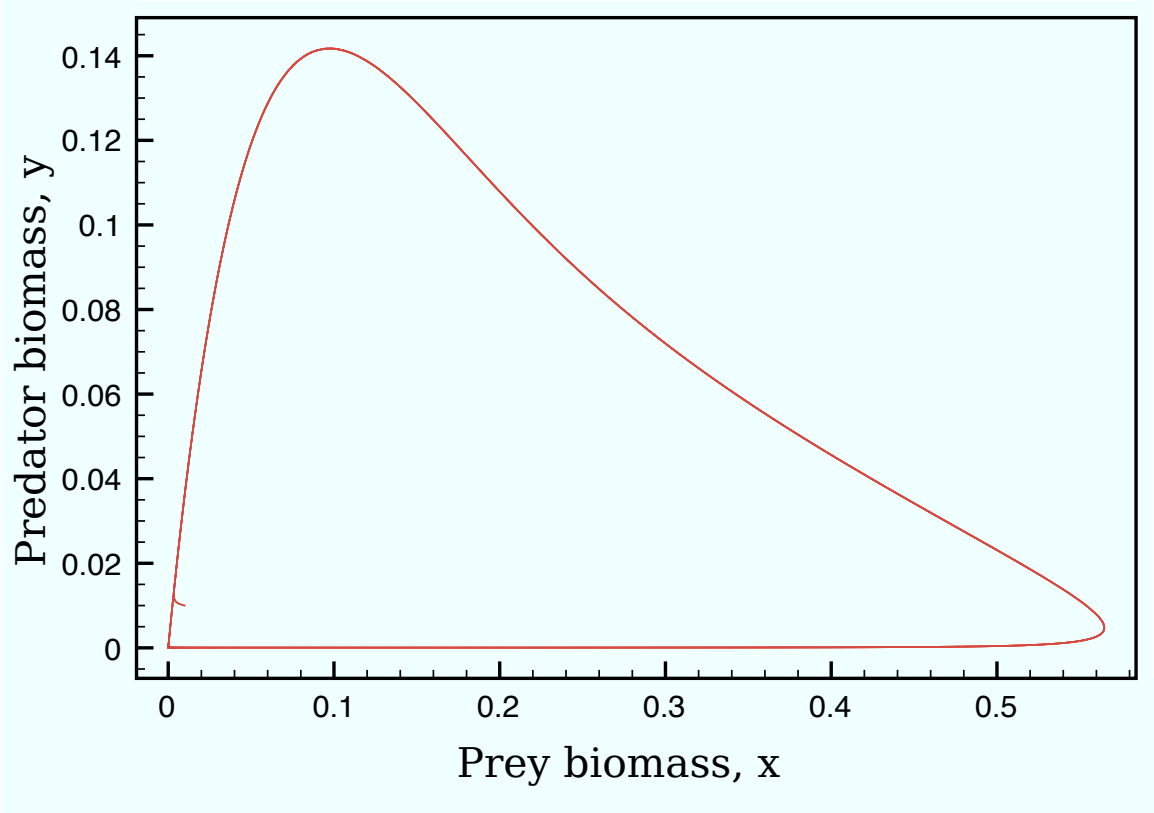

Figure 5.3: Backward trajectory starting from $(0.01, 0.01)$ for a refuge size 0.645 kg/m^2.

As the periodic orbit expands, it gets close to the boundary equilibrium points

$(0,0)$ and $(K,0)$ and the positive x-axis. The positive x-axis is a heteroclinic connection joining the unstable manifold of $(0,0)$ and the stable manifold of $(K,0)$. As long as the periodic orbit exists, the stable manifold of $(0,0)$ originates from the neighborhood of the unstable periodic orbit (see Figure 5.4) while the unstable manifold of $(K,0)$ approaches the negative x-axis asymptomatically. When the periodic orbit

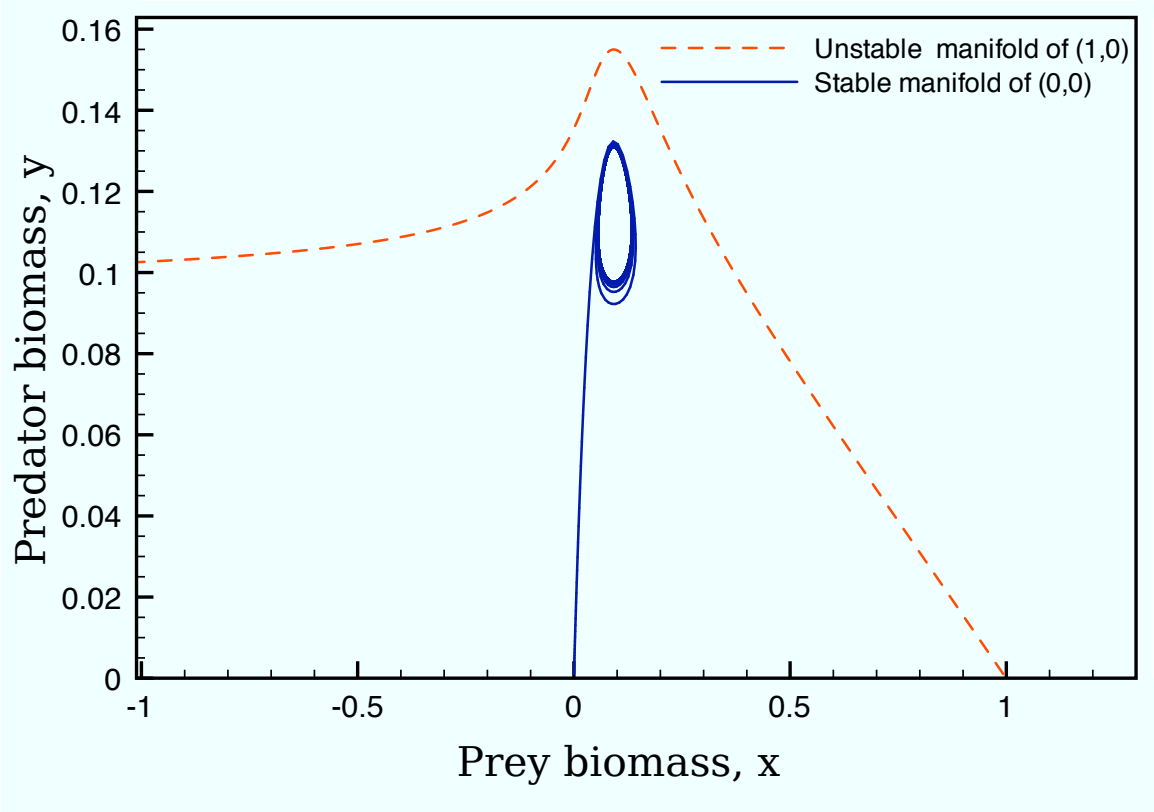

Figure 5.4: Unstable manifold of (1,0) and stable manifold of (0,0). Refuge size = 0.64 kg/m^2.

disappears the global portrait changes dramatically. The unstable manifold of $(K,0)$ now heads straight to the interior equilibrium point $(\bar{x},\bar{y})$ while the stable manifold of $(0,0)$ approaches the positive x-axis asymptomatically (see Figure 5.5). Numerical evidence suggests that when the global bifurcation occurs, another brief heteroclinic connection is made when the unstable manifold of $(K,0)$ and the stable manifold of $(0,0)$ merge.

The global bifurcation has an important ecological implication, the attracting

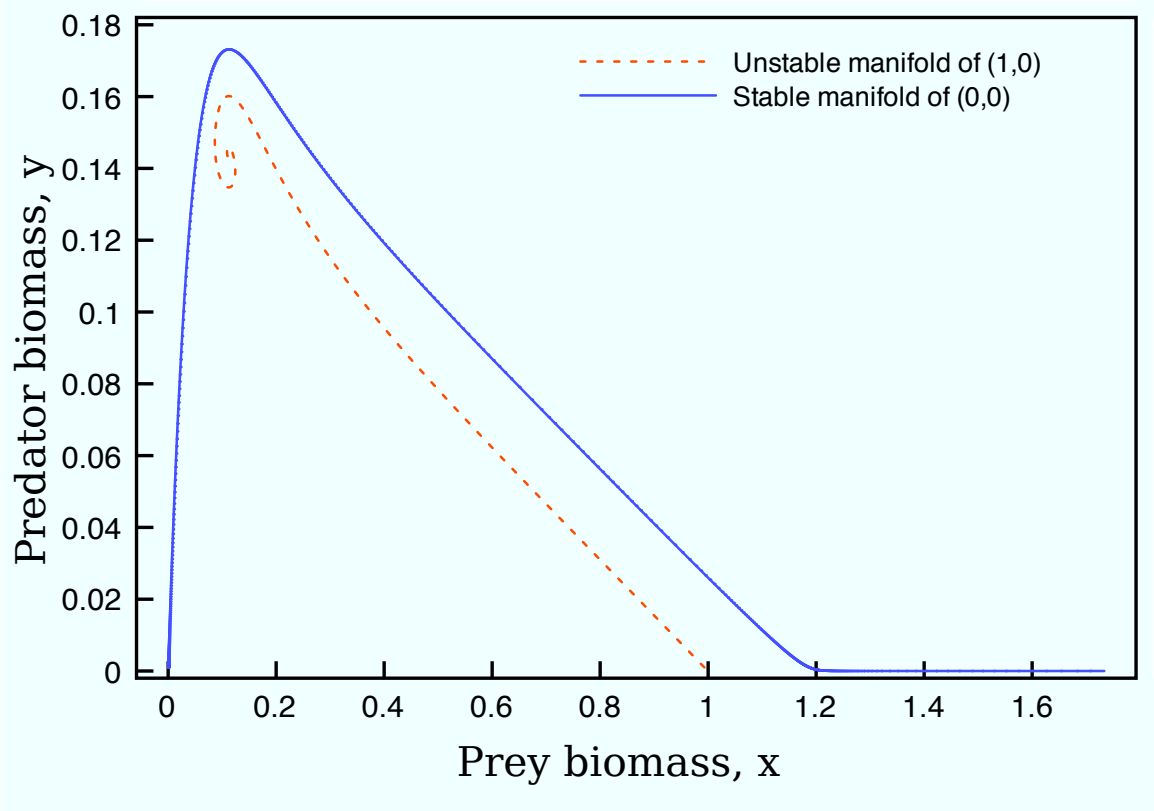

Figure 5.5: Unstable manifold of $(1, 0)$ and stable manifold of $(0, 0)$. Refuge size $= 0.66 \ \ kg/m^2$.

basin of the interior equilibrium point greatly expands making the biomass ratio at the equilibrium point much more robust to perturbations. However note that there still exist regions of state space which lie outside the attracting basin. If the coral reef is strongly perturbed, especially if the prey are strongly fished, the coral reef will never recover its equilibrium biomass ratio.

CHAPTER VI

CONCLUSION

In Chapter 1, we quantify the dependence of city aggregation in the Schelling model on city size, disparate neighbor comfortability threshold, and population density. We make two methodological innovations: we devise new measures to quantify the aggregation in the Schelling model and we develop new fast algorithms to simulate a large city in the model. We ran thousands of simulations for a large city, something which has never been done before and compile accurate statistics of aggregation in a large city based on these simulations. We find that the striking global aggregation Schelling observed for disparate neighbor comfortability threshold $T = 3$ for the 8×8 city is strictly a small city phenomenon, and higher values of T are necessary for more pronounced aggregation in large cities. We also find that aggregation in a large city is highly sensitive to the combination of the disparate neighbor comfortability threshold and the number of vacancies in a city, in particular that aggregation is an increasing function of vacancies when T=3 but is inversely correlated with vacancies when T=4. We also find a remarkable linear dependence of aggregation measures on the vacancy ratio in large cities.

We extend our analysis of the Schelling model in chapter 2 to cities where one type of agents is in a minority. Agents in a minority aggregated differently from agents in a majority. Minority agents exhibit two different kinds of behavior, they try and set up large compact segregated clusters, but can often also be found isolated and unhappy.

The Schelling model became influential because it is a simple rule based system. The happiness of an agent depends only its immediate neighborhood, an agent is

happy if it is surrounded by a minimum number of similar agents and it moves individually to a suitable location if it is not happy. The simplicity of the model by construction ignores the complexity of behavior of agents in a city. An agent is only happy or unhappy, there is no notion of 'happier'. Most conspicuously, we note the complete lack of collective behavior of agents in the Schelling city. Often, there are locations in a city where no agent would be happy if it were to move there individually, but a group of agents could be happy. As a next question, we must determine the qualitative and quantitative differences in aggregation when the rules of the Schelling model are modified.

The Schelling model is a prime example of a model in population dynamics where one focuses on the behavior of individuals at the expense of the collective. These models exhibit complex, rich patterns in simulations but do not allow us to attack them with generalized analytical techniques. Our study of biomass pyramids eschews the heterogeneity in the behavior of individuals and utilizes the traditional language of differential equations to track the dynamics of predators and prey in coral reefs and other ecosystems.

Biomass pyramids dominated by predators are rare in ecology and are very counterintuitive at first sight. Predators convert only a small fraction of the food that they consume into their own biomass, therefore, biomass is concentrated within prey species in most ecosystems. In the fall of 2007, a team of scientists led an expedition to the isolated coral reefs Kingman and Palmyra where they discovered that the fish biomass pyramid in the two isolated reefs was dominated by apex heavy predators like sharks and snappers. They also found that the coral cover at the two isolated reefs was extensive and provides a refuge for small prey fish from predators. We build a model in the framework of predator-prey dynamics which explicitly incorporates the role of the coral in mediating the interaction of predator and prey fish and recovers the inverted biomass pyramid.

We further develop a general quantitative theory of biomass pyramids. We focus on ecosystems where the assumption of well mixed predator and prey populations does not hold and refuges play an important role; coral reefs such as Kingman and Palmyra are prime examples of such a situation. We explicitly introduce refuges into predator-prey models by developing Refuge-modulated predator prey (RPP) models. Ecological evidence supports the hypothesis that refuges can have positive or negative effect on the feeding habits of predators. Correspondingly our RPP models show that the refuge size can facilitate or discourage inverted biomass pyramids. On the other hand, immigration of prey fish unequivocally promotes an inverted biomass pyramid. We find that high prey reproductive rate, high biomass conversion efficiency and long predator life are positively correlated with the inverted biomass pyramid.

Our current models of biomass pyramids focuses on the interactions of two species. Food webs usually involve multiple species interacting in complex ways; there are many more players in the ecosystem at coral reefs such as bacteria and the corals themselves. The next step is to consider the coral cover not as a static variable, but as an active dynamic variable. This is a vital step since an understanding of the interdependence of fish biomass structure and health of coral reefs is one of the main open questions in marine ecology.

APPENDIX A

STABILITY AND SENSITIVITY ANALYSIS AT CORAL REEFS

A.1 Local Stability of equilibrium points

The equations governing the dynamics of predator and prey biomass are described by

$$\dot{x} = ax\left(1 - \frac{x}{K}\right) - bf(x,r)y,$$
$$\dot{y} = cbf(x,r)y - dy.$$

x : prey biomass density (kg/m^2),

y : predator biomass density (kg/m^2),

a : prey growth rate (/day),

b : maximum predation rate: maximum prey biomass, hunted per kg of predator biomass (/day),

K : prey carrying capacity in absence of predators (kg/m^2),

r : refuge size (kg/m^2),

$f(x,r)$: predation response,

c : biomass conversion efficiency,

d : predator death rate (/day).

The equilibrium points are (0,0), (k,0) and $\left(x^* = r - \frac{1}{10}\ln(\frac{bc}{d} - 1),\ y^* = \frac{ac}{d}x^*(1 - \frac{x^*}{K})\right)$. We determine the local stability of the equilibrium points by computing the Jacobian at the equilibrium points. The Jacobian

$$J = \begin{bmatrix} a - 2a\frac{x}{K} - 10by\frac{(e^{-10(x-r)})}{(1+e^{-10(x-r)})^2} & -\frac{b}{1+e^{-10(x-r)}} \\ 4bc\frac{y(e^{-10(x-r)})}{(1+e^{-10(x-r)})^2} & \frac{bc}{1+e^{-10(x-r)}} - d \end{bmatrix}.$$

At (0,0)

$$J(0,0) = \begin{bmatrix} a & -\frac{b}{1+e^{10r}} \\ 0 & \frac{bc}{1+e^{10r}} - d \end{bmatrix}.$$

The eigenvalues of the Jacobian are a and $(bc/(1 + e^{10r}) - d)$. As $a \geq 0$, (0,0) is an unstable equilibrium point [79].

At (K,0),

$$J(K,0) = \begin{bmatrix} -a & -\frac{b}{1+e^{-10(K-r)}} \\ 0 & \frac{bc}{1+e^{-10(K-r)}} - d \end{bmatrix}$$

$$\text{and } \det(J(K,0)) = -a\left(\frac{bc}{1 + e^{-10(K-r)}} - d\right) < 0.$$

As $1 + e^{-10(K-r)} \leq 2$ and $bc > 2d$, $\det(J(K,0)) < 0$. Therefore, (K,0) is a saddle equilibrium point [79].

At (x^*, y^*),

$$x^*(r) = r - \frac{1}{10}\ln\left(\frac{bc}{d} - 1\right),$$
$$y^*(r) = \frac{ac}{d}x^*\left(1 - \frac{x^*}{K}\right),$$
$$J(x^*, y^*) = \begin{bmatrix} a - 2a\frac{x^*}{K} - 10by^*\frac{(e^{-10(x^*-r)})}{(1+e^{-10(x^*-r)})^2} & \frac{-b}{1+e^{-10(x^*-r)}} \\ 10bc\frac{y^*(e^{-10(x^*-r)})}{(1+e^{-10(x^*-r)})^2} & 0 \end{bmatrix},$$

$$\det J(x^*, y^*) = \frac{10acx^*(1 - x^*/K)(\frac{c}{d} - 1)}{b(\frac{c}{d})^2},$$
$$\mathrm{tr}(x^*, y^*) = a - 2a\frac{x^*}{K} - 10by^*\frac{(e^{-10(x^*-r)})}{(1 + e^{-10(x^*-r)})^2}.$$

The determinant and the trace of the Jacobian are complicated functions of the parameter values and equilibrium predator and prey biomass. Numerical analysis shows that $\det J(x^*, y^*) \geq 0$ and $\mathrm{tr}\, J(x^*, y^*) \leq 0$ when $0.65 \leq r \leq 0.85$. Therefore, (x^*, y^*) is an attractive equilibrium point when $0.65 \leq r \leq 0.85$.

A.2 Sensitivity analysis

We determine the sensitivity of the predator:prey biomass ratio to variation in the parameters of the equations (4.1), (4.2) and (4.6) by means of a sensitivity index. The normalized forward sensitivity index of a variable to a parameter is the ratio of the relative change in the variable to the relative change in the parameter [9]. As an example, the sensitivity of the biomass ratio to variation in prey growth rate (a) is given by

$$\gamma_a^{ratio} = \frac{\partial ratio}{\partial a}.\frac{a}{ratio} = \frac{c}{d}\left(1 - r + \frac{1}{10}\ln\left(\frac{bc}{d} - 1\right)\right)\frac{a}{ratio}.$$

The absolute value and the sign of the sensitivity index provide two separate pieces of information to us. The absolute value of the sensitivity index denotes the sensitivity of the variable to variation in the parameter, a low absolute value denotes robustness in the value of the variable to variation in the parameter and vice versa. In addition, a positive sensitive index for a parameter shows that the variable is an increasing function of the parameter.

Table A.1 shows the sensitivity index for each parameter and organizes them in decreasing order of influence on the biomass ratio.

Table A.1: Sensitivity indices for parameters in equations (4.1), (4.2) and (4.6). Baseline value for parameters:($a = 0.0048, b = 0.8, c = 0.15, d = 0.0005, K = 1.0, r = 0.7$, biomass ratio= 1.22).

Parameter	Sensitivity Index
a	1
r	-0.83
c	0.47
d	-0.47
b	0.12
K	-0.07

The predator:prey biomass ratio is most sensitive to variation in the prey growth rate (a) and least sensitive to variation in the predation response (b). The signs of the sensitivity indices tell us that the predator:prey biomass ratio is an increasing function of a (prey growth rate), b (maximum predation rate), c (biomass conversion efficiency), and a decreasing function of d (predator death rate), K (prey carrying capacity) and r (per unit area coral reef size).

APPENDIX B

PSEUDO-CODE FOR THE SCHELLING MODEL

B.1 Useful subroutines

The agent matrix or city matrix is the matrix representing the state of the city at any given point during the simulation. An R agent is represented by 1, a B agent by -1 and an empty location by 0. A useful matrix is the ones matrix. The ones matrix is an $N \times N$ matrix and each of its elements is 1.

B.1.1 Finding a random location

Consider a matrix filled with only 0's and 1's. One frequently requires in this program to pick a 1 randomly from the matrix. We do so through the steps given below.

1. Convert the matrix into a 1-D array.
2. Determine the number of 1's in the matrix by finding the sum of all the elements in the array.
3. Find a random integer less than the number of 1's in the array. Let us call α.
4. Create a 1-D array whose elements range from 0 to the number of elements in the given matrix.
5. Multiply the elements of the two 1-D arrays, elementwise. This produces a 1-D array which contains the address of the 1's in the array and is zero otherwise.
6. Start a loop and run it across the array of addresses. Keep a count of the number of 1's encountered and stop when it is equal to α.

B.1.2 Surrounding R neighbors

At many points in the program we need to determine the number of R agents in the neighborhood of each agent. We do so through the following steps

- Create 8 different matrices by by shifting the agent matrix in 8 different directions. These include 2 horizontal shifts, 2 vertical shifts and and 4 diagonal shifts. Keep in mind the periodic boundary conditions.
- Add these 8 matrices and call the resultant matrix M1.
- Create an absolute agent matrix whose elements are the absolute values of the elements in the agent matrix. Repeat the previous 2 steps for this new absolute agent matrix. Call the result matrix M2.
- Add M1 and M2. Divide each element by half.

The result is a matrix whose elements are the number of R agents in the neighborhood of an agent at each corresponding location. A similar procedure can be used to determine the number of B agents which I outline below.

B.1.3 Surrounding B neighbors

- Create 8 different matrices by by shifting the agent matrix in 8 different directions. These include 2 horizontal shifts, 2 vertical shifts and and 4 diagonal shifts. Keep in mind the periodic boundary conditions.
- Add these 8 matrices and call the result matrix M1.
- Create an absolute agent matrix whose elements are the absolute values of the elements in the agent matrix. Repeat the previous 2 steps for this new absolute agent matrix. Let us call the resultant matrix M2.
- Subtract M2 from M1. Divide Each element by half.

The result is a matrix whose elements are the number of B agents in the neighborhood of an agent at each corresponding location.

B.1.4 Determining happiness

Consider a matrix filled with -1, 0 and 1's. Each R is represented by 1 and each B by -1. 0 represents an empty location. We show we determine the happiness of all the R agents in the matrix. An analogous procedure can followed for the B agents.

- We first determine the number of red neighbors for each agent.
- We produce a matrix which has a value of 1 for each R and 0 for the Bs. Let us call it the Rlocator matrix.
- We then multiply these two matrices to produce a matrix which shows the neighbors for each R agent and is 0 otherwise, call it Rredneighbor matrix.
- We generate a threshold matrix which is a matrix whose elements are identically equal to the value of the neighbor comfort threshold T as desired for the simulation.
- We multiply the R locator matrix with the threshold matrix and call the resulting matrix as Rthreshold matrix.
- Subtract the Rthreshold matrix from Rredneighbor matrix and convert all negative numbers to 1 and the rest as 0. Each 1 now represents an unhappy R agent.

B.1.4.1 Perimeter

- Subtract the agent matrix from the ones matrix and multiply elementwise with the Rlocator matrix. This provides the contribution of all the R agents to the Lyapunov function.

- Add the agent matrix to the ones matrix and multiply elementwise with the Blocator matrix. This provides the contribution of all the B agents to the Lyapunov function.

- Define an absolute agent matrix whose elements are the absolute values of the elements in the agent matrix. Multiply the absolute agent matrix with the Elocator matrix and this provides the contribution of all the empty locations to the Lyapunov functiion.

- Add the three matrices and calculate the sum of all the elemts of the resulting matrix to generate the Lyapunov function.

B.2 Program Flow

B.2.1 Initial Conditions

We set up the initial condition for the array using all the variables in the given order

1. Choose to set up a checkerboard or distribute the agents randomly and fill the complete amtrix with agents

2. Perturb the system according to the number and specified size

3. Remove a fraction of the agents to create empty locations

B.2.2 Evolution

B.2.2.1 Generate useful matrices

- Create matrix with 1 corresponding to empty locations and 0 otherwise.

- Create matrix with 1 corresponding to R agents and 0 otherwise.

- Create matrix with 1 corresponding to B agents and 0 otherwise.

- Create matrix with 1 corresponding to all empty locations where an R agent can be happy and 0 otherwise.

- Create matrix with 1 corresponding to unhappy R agents and 0 otherwise.

B.2.2.2 Move

- Check if there is possibility of movement. If it is possible, choose a random unhappy R agent and move to a random suitable empty location.

- Repeat for B agent.

B.2.2.3 Halt

- If no movement possible for R and B agents, halt the program.

REFERENCES

[1] Barnes, R. and Hughes, R., *An introduction to marine ecology*. Blackwell Scientific Publications, 1999.

[2] Bellwood, D., Hughes, T., Folke, C., and Nystroem, M., "Confronting the coral reef crisis," *Nature*, vol. 429, no. 6994, pp. 827–833, 2004.

[3] Benenson, I., Or, E., Hatna, E., and Omer, I., "Residential Distribution in the City–Reexamined," 2008.

[4] Berger, J., "Pregnancy incentives, predation constraints and habitat shifts: Experimental and field evidence for wild bighorn sheep.," *Animal Behaviour*, vol. 41, no. 1, pp. 61–77, 1991.

[5] Bruch, E. and Mare, R., "Neighborhood Choice and Neighborhood Change 1," *American Journal of Sociology*, vol. 112, no. 3, pp. 667–709, 2006.

[6] Buck, K., Chavez, F., and Campbell, L., "Basin-wide distributions of living carbon components and the inverted trophic pyramid of the central gyre of the North Atlantic Ocean, summer 1993," *Aquatic Microbial Ecology*, vol. 10, no. 3, pp. 283–298, 1996.

[7] Caley, M. and St John, J., "Refuge availability structures assemblages of tropical reef fishes," *Journal of Animal Ecology*, vol. 65, no. 4, pp. 414–428, 1996.

[8] Cassini, M., "Foraging under predation risk in the wild guinea pig Cavia aperea," *Oikos*, pp. 20–24, 1991.

[9] Chitnis, N., Hyman, J., and Cushing, J., "Determining Important Parameters in the Spread of Malaria Through the Sensitivity Analysis of a Mathematical Model," *Bull Math Biol*, 2008.

[10] Cho, B. and Azam, F., "Biogeochemical significance of bacterial biomass in the ocean's euphotic zone.," *Marine ecology progress series. Oldendorf*, vol. 63, no. 2, pp. 253–259, 1990.

[11] Clark, W., "Residential Preferences and Neighborhood Racial Segregation: A Test of the Schelling Segregation Model," *Demography*, vol. 28, no. 1, pp. 1–19, 1991.

[12] Clark, W. and Fossett, M., "Understanding the social context of the Schelling segregation model," *Proceedings of the National Academy of Sciences*, vol. 105, no. 11, p. 4109, 2008.

[13] Clarke, M., da Silva, K., Lair, H., Pocklington, R., Kramer, D., and McLaughlin, R., "Site familiarity affects escape behaviour of the eastern chipmunk, Tamias striatus," *Oikos*, pp. 533–537, 1993.

[14] Cowlishaw, G., "Refuge use and predation risk in a desert baboon population," *Animal behaviour*, vol. 54, no. 2, pp. 241–253, 1997.

[15] Cushing, D., "Upwelling and the production of fish," *Adv. Mar. Biol*, vol. 9, pp. 255–334, 1971.

[16] Daily, G. and Ehrlich, P., "Population, Sustainability, and earth's Carrying Capacity," *Bioscience*, vol. 42, no. 10, pp. 761–771, 1992.

[17] Dash, M., *Fundamentals of ecology*. Tata McGraw-Hill, 2001.

[18] Del Giorgio, P., Cole, J., Caraco, N., and Peters, R., "Linking planktonic biomass and metabolism to net gas fluxes in northern temperate lakes," *Ecology*, vol. 80, no. 4, pp. 1422–1431, 1999.

[19] Del Giorgio, P., Cole, J., Caraco, N., and Peters, R., "Linking planktonic biomass and metabolism to net gas fluxes in northern temperate lakes," *Ecology*, vol. 80, no. 4, pp. 1422–1431, 1999.

[20] DeMartini, E., Friedlander, A., Sandin, S., and Sala, E., "Differences in fish-assemblage structure between fished and unfished atolls in the northern Line Islands, central Pacific," *Mar Ecol Prog Ser*, vol. 365, pp. 199–215, 2008.

[21] Dill, L. and Houtman, R., "The influence of distance to refuge on flight initiation distance in the gray squirrel (Sciurus carolinensis)," *Canadian Journal of Zoology*, vol. 67, no. 1, pp. 233–235, 1989.

[22] Duncan, O. and Duncan, B., "A Methodological Analysis of Segregation Indexes," *American Sociological Review*, vol. 20, no. 2, pp. 210–217, 1955.

[23] Elliott, J., "Prey switching in four species of carnivorous stoneflies," *Freshwater biology*, vol. 49, no. 6, pp. 709–720, 2004.

[24] Fossett, M., "Ethnic Preferences, Social Distance Dynamics, and Residential Segregation: Theoretical Explorations Using Simulation Analysis*," *The Journal of Mathematical Sociology*, vol. 30, no. 3, pp. 185–273, 2006.

[25] Friedlander, A. and DeMartini, E., "Contrasts in density, size, and biomass of reef fishes between the northwestern and the main Hawaiian islands: the effects of fishing down apex predators," *Marine Ecology Progress Series*, vol. 230, pp. 253–264, 2002.

[26] Froese, R. and Pauly, D., "FishBase. version (06/2008)," *World Wide Web electronic publication. www.fishbase.org*, 2008.

[27] Gasol, J., del Giorgio, P., and Duarte, C., "Biomass distribution in marine planktonic communities," *Limnology and Oceanography*, pp. 1353–1363, 1997.

[28] Gerhold, G., Glebsky, G., Schneider, C., Weiss, H., and Zimmermann, B., "Limit States for One-dimensional Schelling Segregation Models," 2008.

[29] Gonzalez-Olivares, E. and Ramos-Jiliberto, R., "Dynamic consequences of prey refuges in a simple model system: more prey, fewer predators and enhanced stability," *Ecological Modelling*, vol. 166, no. 1-2, pp. 135–146, 2003.

[30] Hausrath, A., "Analysis of a model predator-prey system with refuges," *Journal of mathematical analysis and applications*, vol. 181, no. 2, pp. 531–545, 1994.

[31] Hay, M., "Personal communication," 2008.

[32] Hixon, M. and Beets, J., "Predation, Prey Refuges, and the Structure of Coral-Reef Fish Assemblages," *Ecological Monographs*, vol. 63, no. 1, pp. 77–101, 1993.

[33] Hoegh-Guldberg, O., Mumby, P., Hooten, A., Steneck, R., Greenfield, P., Gomez, E., Harvell, C., Sale, P., Edwards, A., Caldeira, K., and others, "Coral Reefs Under Rapid Climate Change and Ocean Acidification," *Science*, vol. 318, no. 5857, p. 1737, 2007.

[34] Holling, C., "Some characteristics of simple types of predation and parasitism," *Canadian Entomologist*, vol. 91, no. 7, pp. 385–398, 1959.

[35] Holling, C., "The components of predation as revealed by a study of small-mammal predation of the European pine sawfly," *Canadian Entomologist*, vol. 91, pp. 293–320, 1959.

[36] Holmes, W., "Predator risk affects foraging behaviour of pikas: Observational and experimental evidence.," *Animal behaviour*, vol. 42, no. 1, pp. 111–119, 1991.

[37] Huang, Y., Chen, F., and Zhong, L., "Stability analysis of a prey–predator model with holling type III response function incorporating a prey refuge," *Applied Mathematics and Computation*, vol. 182, no. 1, pp. 672–683, 2006.

[38] Jameson, S., McManus, J., and Spalding, M., "State of the Reefs: Regional and Global Perspectives," *US Department of State, Washington, DC*, vol. 26, 1995.

[39] Kar, T., "Stability analysis of a prey–predator model incorporating a prey refuge," *Communications in Nonlinear Science and Numerical Simulation*, vol. 10, no. 6, pp. 681–691, 2005.

[40] Kennedy, W., "An Uneasy Eden," *National Geographic*, pp. 144–157, 2008.

[41] Kjellander, P. and Nordstrom, J., "Cyclic voles, prey switching in red fox, and roe deer dynamics-a test of the alternative prey hypothesis.," *Oikos*, vol. 101, no. 2, p. 338, 2003.

[42] Knowlton, N. and Jackson, J., "Shifting Baselines, Local Impacts, and Global Change on Coral Reefs," *PLoS Biol*, vol. 6, no. 2, p. e54, 2008.

[43] Ko, W. and Ryu, K., "Qualitative analysis of a predator–prey model with Holling type II functional response incorporating a prey refuge," *Journal of Differential Equations*, vol. 231, no. 2, pp. 534–550, 2006.

[44] Kritzer, J., "Stock Structure, Mortality and Growth of The Decorated Goby, Istigobius decoratus (Gobiidae), at Lizard Island, Great Barrier Reef," *Environmental Biology of Fishes*, vol. 63, no. 2, pp. 211–216, 2002.

[45] Kumar Kar, T., "Modelling and analysis of a harvested prey–predator system incorporating a prey refuge," *Journal of Computational and Applied Mathematics*, vol. 185, no. 1, pp. 19–33, 2006.

[46] Laurie, A. and Jaggi, N., "Role of'Vision'in Neighbourhood Racial Segregation: A Variant of the Schelling Segregation Model," *Urban Studies*, vol. 40, no. 13, p. 2687, 2003.

[47] Lotka, A., *Elements of physical biology*. Williams & Wilkins company, 1925.

[48] Lubow, B. and Smith, B., "Population dynamics of the Jackson elk herd," *Journal of Wildlife management*, vol. 68, no. 4, pp. 810–829, 2004.

[49] Massey, D., "American Apartheid: Segregation and the Making of the Underclass," *American Journal of Sociology*, vol. 96, no. 2, p. 329, 1990.

[50] Massey, D. and Denton, N., "Dimensions of Residential Segregation, The," *Social Forces*, vol. 67, p. 281, 1988.

[51] Massey, D., White, M., and Phua, V., "The Dimensions of Segregation Revisited," *Sociological Methods & Research*, vol. 25, no. 2, p. 172, 1996.

[52] McNair, J., "The effects of refuges on predator-prey interactions: A reconsideration.," *Theoretical Population Biology*, vol. 29, no. 1, pp. 38–63, 1986.

[53] Mollet, H. and Cailliet, G., "Comparative population demography of elasmobranchs using life history tables, Leslie matrices and stage-based matrix models," *Marine and Freshwater Research*, vol. 53, no. 2, pp. 503–516, 2002.

[54] Moustaka-Gouni, M., Vardaka, E., Michaloudi, E., Kormas, K., Tryfon, E., Mihalatou, H., Gkelis, S., and Lanaras, T., "Plankton food web structure in a eutrophic polymictic lake with a history in toxic cyanobacterial blooms," *Limnology and Oceanography*, vol. 51, no. 1, pp. 715–727, 2006.

[55] Murdoch, W. and Oaten, A., "Predation and population stability," *Advances in ecological research*, vol. 9, no. 1, p. 131, 1975.

[56] Odum, E. and Odum, H., "Fundamentals of ecology," 1971.

[57] Ohizumi, H., Kuramochi, T., Amano, M., and Miyazaki, N., "Prey switching of Dall's porpoise Phocoenoides dalli with population decline of Japanese pilchard Sardinops melanostictus around Hokkaido, Japan," *Marine Ecology Progress Series*, vol. 200, pp. 265–275, 2000.

[58] Oliphant, T. and Provo, U., *A Guide to NumPy*. Trelgol Publishing, 2006.

[59] Pala, C., "Reefs in Trouble: Life on the Mean Reefs," *Science*, vol. 318, no. 5857, p. 1719, 2007.

[60] Pandolfi, J., Bradbury, R., Sala, E., Hughes, T., Bjorndal, K., Cooke, R., McArdle, D., McClenachan, L., Newman, M., Paredes, G., and others, "Global Trajectories of the Long-Term Decline of Coral Reef Ecosystems," *Science*, vol. 301, no. 5635, p. 955, 2003.

[61] Pauly, D. and Christensen, V., "Primary production required to sustain global fisheries," *Nature*, vol. 374, no. 6519, pp. 255–257, 1995.

[62] Persson, L. and Eklöv, P., "Prey refuges affecting interactions between piscivorous perch and juvenile perch and roach," *Ecology*, pp. 70–81, 1995.

[63] Pollicott, M. and Weiss, H., "The Dynamics of Schelling-Type Segregation Models and a Nonlinear Graph Laplacian Variational Problem," *Advances in Applied Mathematics*, vol. 27, no. 1, pp. 17–40, 2001.

[64] Portugali, J., Benenson, I., and Omer, I., "Sociospatial residential dynamics: stability and instability within a self-organizing city," *Geographical Analysis*, vol. 26, no. 4, pp. 321–340, 1994.

[65] Reaney, L., "Foraging and mating opportunities influence refuge use in the fiddler crab, Uca mjoebergi," *Animal Behaviour*, vol. 73, no. 4, pp. 711–716, 2007.

[66] Reichle, D., *Dynamic properties of forest ecosystems*. Cambridge University Press, 1981.

[67] Sander, R., Schreiber, D., and Doherty, J., "Empirically Testing a Computational Model: The Example of Housing Segregation," *Proceedings of the Workshop on Simulation of Social Agents: Architectures and Institutions*, pp. 108–115, 2000.

[68] Sandin, S., Smith, J., DeMartini, E., Dinsdale, E., Donner, S., Friedlander, A., Konotchick, T., Malay, M., Maragos, J., Obura, D., and others, "Baselines and Degradation of Coral Reefs in the Northern Line Islands," *PLoS ONE*, vol. 3, no. 2, p. e1548, 2008.

[69] Sandin, S., Smith, J., DeMartini, E., Dinsdale, E., Donner, S., Friedlander, A., Konotchick, T., Malay, M., Maragos, J., Obura, D., and others, "Baselines and degradation of coral reefs in the northern Line Islands," *PLoS ONE*, vol. 3, no. 2, 2008.

[70] Schelling, T., "Models of segregation," *American Economic Review*, vol. 59, no. 2, pp. 488–493, 1969.

[71] Schelling, T., "Dynamic models of segregation," *Journal of Mathematical Sociology*, vol. 1, no. 1, pp. 143–186, 1971.

[72] Schelling, T., "On the ecology of micromotives," *The Public Interest*, vol. 25, pp. 61–98, 1971.

[73] Schelling, T., *Micromotives and macrobehavior*. WW Norton, New York, 2006.

[74] Sih, A., "Prey refuges and predator-prey stability," *Theoretical population biology*, vol. 31, no. 1, pp. 1–12, 1987.

[75] Sih, A., "To hide or not to hide? Refuge use in a fluctuating environment," *Trends in Ecology & Evolution*, vol. 12, no. 10, pp. 375–376, 1997.

[76] Smith, B., "Personal communication," 2008.

[77] Smith, S., Au, D., and Show, C., "Intrinsic rebound potentials of 26 species of Pacific sharks," *Marine & Freshwater Research*, vol. 49, no. 7, pp. 663–678, 1998.

[78] Srinivasan, M. and Jones, G., "Extended breeding and recruitment periods of fishes on a low latitude coral reef," *Coral Reefs*, vol. 25, no. 4, pp. 673–682, 2006.

[79] Strogatz, S., *Nonlinear dynamics and chaos*. Addison-Wesley Reading, MA, 1994.

[80] Sweatman, H., "A field study of the predatory behavior and feeding rate of a piscivorous coral reef fish, the lizardfish Synodus englemani," *Copeia*, no. 1, pp. 187–194, 1984.

[81] Volterra, V., *Variazioni e fluttuazioni del numero d'individui in specie animali conviventi*. C. Ferrari, 1927.

[82] Warburton, K., Retif, S., and Hume, D., "Generalists as sequential specialists: diets and prey switching in juvenile silver perch," *Environmental Biology of fishes*, vol. 51, no. 4, pp. 445–454, 1998.

[83] Weisbuch, G., Deffuant, G., Amblard, F., and Nadal, J., "Meet, discuss, and segregate!," *Complexity*, vol. 7, no. 3, pp. 55–63, 2002.

[84] Wilson, S., "Growth, mortality and turnover rates of a small detritivorous fish," *Marine Ecology Progress Series*, vol. 284, pp. 253–259, 2004.

[85] Young, H., *Individual Strategy and Social Structure: An Evolutionary Theory of Institutions*. Princeton University Press, 1998.

[86] Zhang, J., "Residential segregation in an all-integrationist world," *Journal of Economic Behavior and Organization*, vol. 54, no. 4, pp. 533–550, 2004.

VITA

Abhinav Singh was born in New Delhi, India. He attended schools in many different parts of the country and moved to Chennai for his undergraduate studies in electrical engineering. He moved to Atlanta in 2005 for graduate studies at Georgia Institute of Technology.